

CP Violation and Neutrino Oscillations

Hiroshi Nunokawa¹, Stephen Parke² and José W. F. Valle³

¹ Departamento de Física, Pontifícia Universidade Católica do Rio de Janeiro,
C. P. 38071, 22452-970, Rio de Janeiro, Brazil

² Theoretical Physics Department, Fermi National Accelerator Laboratory,
P.O. Box 500, Batavia, IL 60510, USA

³ AHEP Group, Instituto de Física Corpuscular, C.S.I.C. – Universitat de València
Edificio de Institutos de Paterna, Apartado 22085, E-46071 València, Spain

November 26, 2024

Abstract

We review the basic mechanisms of neutrino mass generation and the corresponding structure of the lepton mixing matrix. We summarize the status of three-neutrino oscillation parameters as determined from current observations, using state-of-the-art solar and atmospheric neutrino fluxes, as well as latest experimental data as of September 2007. We also comment on recent attempts to account for these results and to understand flavour from first principles. We discuss extensively the prospects for probing the strength of CP violation in two near term accelerator neutrino oscillation experiments, T2K and NO ν A, as well as possible extensions such as T2KK and a second large off-axis detector near the NO ν A detector. We also briefly discuss the possibility of probing the effect of Majorana phases in future neutrinoless double beta decay searches and discuss other implications of leptonic CP violation such as leptogenesis. Finally we comment on the issue of robustness of the current oscillation interpretation and possible ways of probing for non-standard neutrino interactions in precision oscillation studies.

Contents

1	Introduction	3
2	Kinematics of neutrino mass	4
2.1	Majorana and Dirac masses	4
2.2	Quantization	6
2.3	CP properties	7

3	The origin of neutrino mass	8
3.1	Seesaw-type neutrino masses	9
3.1.1	The majoron seesaw	9
3.1.2	Left-right symmetric seesaw	10
3.1.3	Double seesaw	11
3.1.4	Unconventional seesaw	12
3.2	Bottom-up neutrino masses	13
3.2.1	Radiative models	13
3.2.2	Supersymmetric neutrino masses	14
3.2.3	Inverse seesaw	15
3.3	Phenomenology of neutrino masses and mixings	15
4	The general structure of the lepton mixing matrix	19
4.1	Quark-like lepton mixing matrix	19
4.2	Majorana case: unitary approximation	21
4.3	General seesaw-type lepton mixing matrix	22
4.4	Leptonic CP violation and leptogenesis	23
5	Neutrino oscillations	26
5.1	The formalism	26
5.2	The current data	28
5.2.1	Solar and reactor data	28
5.2.2	Atmospheric and accelerator data	29
5.3	Status of three-neutrino oscillations	30
5.4	Predicting neutrino oscillation parameters	32
6	CP violation in neutrino oscillations	36
6.1	Preliminaries	36
6.2	The oscillation probability $\nu_\mu \rightarrow \nu_e$	39
6.2.1	Vacuum: $\nu_\mu \rightarrow \nu_e$	40
6.2.2	Matter: $\nu_\mu \rightarrow \nu_e$	43
7	Near Term Experiments	49
7.1	Dependence of probabilities on θ_{13} and δ	50
7.2	Bi-probability plots	52
7.3	Parameter Degeneracy	52
7.4	Beyond the First Oscillation Maximum:	57
7.5	Possible Experiments	58
8	CP violation and lepton number violation: $\beta\beta_{0\nu}$	60

9	Beyond neutrino oscillations	64
9.1	Solar magnetic fields	64
9.1.1	Radiative zone magnetic fields and density noise	64
9.1.2	Convective zone magnetic fields and spin flavour precession	64
9.1.3	Probing for neutrino magnetic moments	64
9.2	Non-standard neutrino interactions	65
10	Summary	67

1 Introduction

CP violation has been discussed phenomenologically since the sixties. Gauge theories naturally account for its presence, although leave its ultimate origin unanswered [1]. Understanding the origin of CP violation from first principles constitutes one of the central challenges of theoretical elementary particle physics. With the historic discovery of neutrino oscillations [2, 3, 4, 5, 6] the issue of leptonic CP violation has also come to the center of the agenda of the particle and nuclear physics communities. The existence of CP violation in the lepton sector is expected in gauge theories of neutrino mass. The main difference with respect to CP violation in the quark mixing matrix is the appearance of new phases associated to the Majorana nature of neutrinos and/or with the admixture of $SU(3) \otimes SU(2) \otimes U(1)$ singlet leptons in the charged current weak interaction [7, 8]. The latter also leads to the effective violation of unitarity in the lepton mixing matrix describing neutrino oscillations. Irrespective of what the underlying origin of neutrino mass may turn out to be, Majorana phases are a generic feature of gauge theories that account for the smallness of neutrino mass through the feebleness of lepton (or B-L) number violation. This includes two alternative classes of gauge theories, that differ by the scale at which L is broken and neutrino masses arise. In Sec. 3 we give a very sketchy summary of the various ways to endow neutrinos with mass, and in Sec. 4 we describe the basic structure of the lepton mixing matrix that follows from theory.

The analysis of current neutrino oscillation experiments is given in Sec. 5 within the simplest CP-conserving three-neutrino mixing pattern, leaving aside the LSND and Mini-Boone data [9, 10, 11]. We summarise the status of neutrino mass and mixing parameters [12] as determined from current neutrino oscillation data [2, 3, 4, 5, 6] [14, 15]. In addition to a determination of the solar angle θ_{12} , the atmospheric angle θ_{23} and the corresponding mass squared splittings, the data place a constraint on the last angle in the three-neutrino leptonic mixing matrix, θ_{13} . Necessary inputs of such interpretation are the solar and atmospheric neutrino fluxes [16, 17], the neutrino cross sections and response functions, as well as the accurate description of neutrino propagation in the Sun and the Earth, taking into account matter effects [18, 19].

It is well known that CP violation should manifest itself in neutrino oscillation experiments [20]. In Sec. 6 we review the basic theoretical features of CP violation in neutrino oscillation probabilities,

while in Sec. 7 we proceed to a summary of the prospects for probing θ_{13} and CP violation in neutrino oscillations. We focus on the case of accelerator neutrino experiments and give a detailed discussion of the potential of the T2K and NO ν A experiments and their possible extensions such as T2KK and a second large off-axis detector near the NO ν A detector.

Lepton number violating processes such as neutrinoless double beta decay [21, 22] are briefly discussed in Sec. 8. In particular, searching for $\beta\beta_{0\nu}$ constitutes a very important milestone for the future, as this will probe the fundamental nature of neutrinos, irrespective of the nature of the neutrino mass-generation mechanism [23]. Within the simplest mass mechanism the search for $\beta\beta_{0\nu}$ probes not only the absolute scale of neutrino mass but is also sensitive to CP violation induced by the so-called Majorana phases [7], inaccessible in conventional oscillations [24, 25, 26, 27].

In Sec. 9 we also briefly comment on the robustness of the current oscillation interpretation and point out the interest in probing for non-standard neutrino interactions in future precision oscillation studies.

2 Kinematics of neutrino mass

2.1 Majorana and Dirac masses

Massive fermions can either be Dirac or Majorana. If they carry electric charge, we have no choice, they must be Dirac. Electrically neutral fermions, like neutrinos (or supersymmetric “inos”), are expected to be Majorana-type on general grounds, irrespective of how they acquire their mass (see Sec. 3). Phenomenological differences between Dirac and Majorana neutrinos are tiny for most processes, such as neutrino oscillations: first because neutrinos are known to be light and, second, because the weak interaction is chiral, well described by the V-A form. Nevertheless it is basic, in particular, for the issue of CP violation and, for this reason, it will be reviewed here.

The most basic spin 1/2 fermion corresponding to the lowest representation of the Lorentz group is given in terms of a 2-component spinor ρ , with the following free Lagrangean [7]

$$\mathcal{L}_{\mathcal{M}} = -i\rho^\dagger \sigma_\mu \partial_\mu \rho - \frac{m}{2} \rho^T \sigma_2 \rho + H.C. \quad (1)$$

where we use the 2×2 σ matrices, with σ_i being the usual Pauli matrices and $\sigma_4 = -iI$, I being the identity matrix, in Pauli’s metric conventions, where $a.b \equiv a_\mu b_\mu \equiv \vec{a} \cdot \vec{b} + a_4 b_4$, $a_4 = ia_0$. Under a Lorentz transformation, $x \rightarrow \Lambda x$, the spinor ρ transforms as $\rho \rightarrow S(\Lambda)\rho(\Lambda^{-1}x)$ where S obeys

$$S^\dagger \sigma_\mu S = \Lambda_{\mu\nu} \sigma_\nu . \quad (2)$$

The kinetic term in Eq. (1) is clearly invariant, and so is the mass term, as a result of unimodular property $\det S = 1$. However, the mass term is not invariant under a phase transformation

$$\rho \rightarrow e^{i\alpha} \rho. \quad (3)$$

The equation of motion following from Eq. (1) is

$$-i\sigma_\mu\partial_\mu\rho = m\sigma_2\rho^*. \quad (4)$$

As a result of the conjugation and Clifford properties of the σ -matrices, one can verify that each component of the spinor ρ obeys the Klein-Gordon wave-equation.

In order to display clearly the relationship between our theory, Eq. (1) and the usual theory of a massive spin 1/2 Dirac fermion, defined by the familiar Lagrangean

$$\mathcal{L}_D = -\bar{\Psi}\gamma_\mu\partial_\mu\Psi - m\bar{\Psi}\Psi, \quad (5)$$

where by convenience we use the chiral representation of the Dirac algebra $\gamma_\mu\gamma_\nu + \gamma_\nu\gamma_\mu = 2\delta_{\mu\nu}$ in which γ_5 is diagonal,

$$\gamma_i = \begin{pmatrix} 0 & -i\sigma_i \\ i\sigma_i & 0 \end{pmatrix}, \quad \gamma_4 = \begin{pmatrix} 0 & I \\ I & 0 \end{pmatrix}, \quad \gamma_5 = \begin{pmatrix} I & 0 \\ 0 & -I \end{pmatrix}. \quad (6)$$

In this representation the charge conjugation matrix C obeying

$$C^T = -C \quad (7)$$

$$C^\dagger = C^{-1} \quad (8)$$

$$C^{-1}\gamma_\mu C = -\gamma_\mu^T \quad (9)$$

$$(10)$$

is simply given in terms of the basic conjugation matrix σ_2 as

$$C = \begin{pmatrix} -\sigma_2 & 0 \\ 0 & \sigma_2 \end{pmatrix}. \quad (11)$$

A Dirac spinor can then be written as

$$\Psi_D = \begin{pmatrix} \chi \\ \sigma_2\phi^* \end{pmatrix}, \quad (12)$$

so that the corresponding charge-conjugate spinor $\Psi_D^c = C\bar{\Psi}_D^T$ is the same as Ψ_D but exchanging ϕ and χ , i. e.

$$\Psi_D^c = \begin{pmatrix} \phi \\ \sigma_2\chi^* \end{pmatrix}. \quad (13)$$

A 4-component spinor is said to be Majorana or self-conjugate if $\Psi = C\bar{\Psi}^T$ which amounts to setting $\chi = \phi$. Using Eq. (12) we can rewrite Eq. (5) as

$$\mathcal{L}_D = -i\sum_{\alpha=1}^2\rho_\alpha^\dagger\sigma_\mu\partial_\mu\rho_\alpha - \frac{m}{2}\sum_{\alpha=1}^2\rho_\alpha^T\sigma_2\rho_\alpha + H.C. \quad (14)$$

where

$$\begin{aligned}\chi &= \frac{1}{\sqrt{2}}(\rho_2 + i\rho_1), \\ \phi &= \frac{1}{\sqrt{2}}(\rho_2 - i\rho_1),\end{aligned}\tag{15}$$

are the left handed components of Ψ_D and of the charge-conjugate field Ψ_D^c , respectively. In this way the Dirac fermion is shown to be equivalent to two Majorana fermions of equal mass. The $U(1)$ symmetry of the theory described by Eq. (5) under $\Psi_D \rightarrow e^{i\alpha}\Psi_D$ corresponds to continuous rotation symmetry between ρ_1 and ρ_2

$$\begin{aligned}\rho_1 &\rightarrow \cos\theta\rho_1 + \sin\theta\rho_2 \\ \rho_2 &\rightarrow -\sin\theta\rho_1 + \cos\theta\rho_2\end{aligned}$$

which result from the mass degeneracy between the ρ 's, showing that, indeed, the concept of fermion number is not basic.

2.2 Quantization

The mass term in Eq. (1) vanishes unless ρ and ρ^* are anti-commuting, so we consider the Majorana fermion, right from the start, as a quantized field. The solutions to Eq. (1) can easily be obtained in terms of those of Eq. (5), which are well known. The answer is

$$\Psi_M = (2\pi)^{-3/2} \int d^3k \sum_{r=1}^2 \left(\frac{m}{E}\right)^{1/2} [e^{ik \cdot x} A_r(k) u_{Lr}(k) + e^{-ik \cdot x} A_r^\dagger(k) v_{Lr}(k)],\tag{16}$$

where $u = C \bar{v}^T$ and $E(k) = (\vec{k}^2 + m^2)^{1/2}$ is the mass-shell condition. The creation and annihilation operators obey canonical anti-commutation rules and, like the u 's and v 's, depend on the momentum k and helicity label r . The expression in Eq. (16) describes the basic Fourier expansion of a massive Majorana fermion. It differs from the usual Fourier expansion for the Dirac spinor in Eq. (17) in two ways,

- the spinor is two-component, as there is a chiral projection acting of the u 's and v 's
- there is only one Fock space, particle and anti-particle coincide, showing that a massive Majorana fermion corresponds to one half of a conventional massive Dirac fermion.

The u 's and v 's are the same wave functions that appear in the Fourier decomposition the Dirac field

$$\Psi_D = (2\pi)^{-3/2} \int d^3k \sum_{r=1}^2 \left(\frac{m}{E}\right)^{1/2} [e^{ik \cdot x} a_r(k) u_r(k) + e^{-ik \cdot x} b_r^\dagger(k) v_r(k)].\tag{17}$$

Using the helicity eigenstate wave-functions,

$$\vec{\sigma} \cdot \vec{k} u_L^\pm(k) = \pm |\vec{k}| u_L^\pm(k),\tag{18}$$

$$\vec{\sigma} \cdot \vec{k} v_L^\pm(k) = \mp |\vec{k}| v_L^\pm(k),\tag{19}$$

one can show that, out of the 4 linearly independent wave functions $u_L^\pm(k)$ and $v_L^\pm(k)$, only two survive as the mass approaches zero, namely, $u_L^-(k)$ and $v_L^+(k)$ [28]. This way the Lee-Yang two-component massless neutrino theory is recovered as the massless limit of the Majorana theory.

Two independent propagators follow from Eq. (1),

$$\langle 0 | \rho(x) \rho^*(y) | 0 \rangle = i \sigma_\mu \partial_\mu \Delta_F(x - y; m), \quad (20)$$

$$\langle 0 | \rho(x) \rho(y) | 0 \rangle = m \sigma_2 \Delta_F(x - y; m), \quad (21)$$

where $\Delta_F(x - y; m)$ is the usual Feynman function. The first one is the “normal” propagator that intervenes in total lepton number conserving ($\Delta L = 0$) processes, while the one in Eq. (21) describes the virtual propagation of Majorana neutrinos in $\Delta L = 2$ processes such as neutrinoless double-beta decay.

2.3 CP properties

The Lagrangean in Eq. (1) can be easily generalized for a system of an arbitrary number of Majorana neutrinos, giving

$$\mathcal{L}_{\mathcal{M}} = -i \sum_{\alpha=1}^n \rho_\alpha^\dagger \sigma_\mu \partial_\mu \rho_\alpha - \frac{1}{2} \sum_{\alpha, \beta=1}^n M_{\alpha\beta} \rho_\alpha^T \sigma_2 \rho_\beta + H.C. \quad (22)$$

where the sum runs over the “neutrino-type” indices α and β . By Fermi statistics the mass coefficients $M_{\alpha\beta}$ must form a symmetric matrix, in general complex. This matrix can always be diagonalized by a complex $n \times n$ unitary matrix U [7]

$$M_{diag} = U^T M U. \quad (23)$$

When M is real (CP conserving) its diagonalizing matrix U may be chosen to be orthogonal and, in general, the mass eigenvalues can have different signs. These may be assembled as a signature matrix

$$\eta = diag(+, +, \dots, -, -, \dots) \quad (24)$$

For two neutrino types there are two classes of models, one with $\eta = diag(+, -)$ and another characterized by $\eta = diag(+, +)$. The class with $\eta = diag(+, -)$ contains as a limit the case where the two fermions make up a Dirac neutrino. Depending on whether the two neutrinos are active-sterile or active-active the limit is called quasi- [29, 30] or pseudo-Dirac neutrino [31]. Oscillations between the quasi-Dirac neutrino components potentially change the predictions of Big Bang Nucleosynthesis while oscillations between the components of a pseudo-Dirac neutrino do not.

Note that one can always make all masses positive by introducing appropriate phase factors in the wave functions, such as the factors of i in Eq. (15). When interactions are added (see Sec. 4) these signs become physical. As emphasized by Wolfenstein, these signs and the corresponding CP phases play an important role in the discussion of neutrinoless double beta decay [32].

	$SU(3) \otimes SU(2) \otimes U(1)$
$\ell_a = (\nu_a, l_a)^T$	$(1, 2, -1)$
e_a^c	$(1, 1, 2)$
$Q_a = (u_a, d_a)^T$	$(3, 2, 1/3)$
u_a^c	$(\bar{3}, 1, -4/3)$
d_a^c	$(\bar{3}, 1, 2/3)$
Φ	$(1, 2, 1)$

Table 1: Matter and scalar multiplets of the Standard Model

3 The origin of neutrino mass

The fifteen basic building blocks of matter listed in Table 1 are all 2-component sequential “left-handed” chiral fermions, one set for each generation. Parity violation in the weak interaction is accounted for “effectively” by having “left” and “right” fermions which behave differently with respect to the $SU(3) \otimes SU(2) \otimes U(1)$ gauge group. In contrast to charged fermions, neutrinos come only in one chiral species. It has been long noted by Weinberg [33] that one can add to the Standard $SU(3) \otimes SU(2) \otimes U(1)$ Model (SM) an effective dimension-five operator $\mathcal{O} = \lambda \ell \ell \Phi \Phi$, where ℓ denotes a lepton doublet for each generation and Φ is the SM scalar doublet.

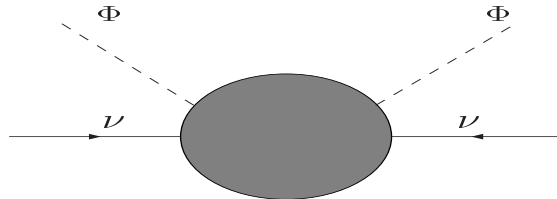


Figure 1: Dimension five operator responsible for neutrino mass.

Once the electroweak symmetry breaks through the nonzero vacuum expectation value (vev) $\langle \Phi \rangle$ Majorana neutrino masses $\propto \langle \Phi \rangle^2$ are induced, in contrast to the masses of the charged fermions which are linear in $\langle \Phi \rangle$. This constitutes the most basic definition of neutrino mass, in which its smallness relative to the masses of the SM charged fermions is ascribed to the fact that \mathcal{O} violates lepton number by two units ($\Delta L = 2$) whereas the other fermion masses do not. Note that this argument is totally general and holds irrespective of the underlying origin of neutrino mass. From such general point of view the emergence of Dirac neutrinos would be a surprise, an “accident”, justified only in the presence of a fundamental lepton number symmetry, in general absent. For example, neutrinos could naturally get very small Dirac masses via mixing with a bulk fermion in models involving extra dimensions [34, 35, 36]. Barring such very special circumstances, gauge theories expect neutrinos to be Majorana.

Little more can be said from first principles about the *mechanism* giving rise to the operator in Fig. 1, its associated mass *scale* or its *flavour structure*. For example, the strength λ of the operator \mathcal{O}

may be suppressed by a large scale M_X in the denominator (top-down) scenario, leading to

$$m_\nu = \lambda_0 \frac{\langle \Phi \rangle^2}{M_X},$$

where λ_0 is some unknown dimensionless constant. Gravity, which in a sense "belongs" to the SM, could induce the dimension-five operator \mathcal{O} , providing the first example of a top-down scenario with $M_X = M_P$, the Planck scale. In this case the magnitude of the resulting Majorana neutrino masses are too small to be relevant in current searches.

Alternatively, the strength λ of the operator \mathcal{O} may be suppressed by small parameters (e.g. scales, Yukawa couplings) in the numerator and/or loop-factors (bottom-up scenario). Both classes of scenarios are viable and allow for many natural realizations. While models of the top-down type are closer to the idea of unification, bottom-up schemes are closer to experimental verification.

Models of neutrino mass may also be classified according to whether or not additional neutral heavy states are present, in addition to the three isodoublet neutrinos. As an example, such leptons could be $SU(3) \otimes SU(2) \otimes U(1)$ singlet "right-handed" neutrinos. In what follows we classify models according to the mass scale at which \mathcal{O} is induced, namely bottom-up and top-down scenarios.

3.1 Seesaw-type neutrino masses

The most popular top-down scenario is the seesaw. The idea is to generate the operator \mathcal{O} by the exchange of heavy states. The smallness of its strength is understood by ascribing it to the violation of lepton number at a high mass scale, namely the scale at which the heavy states acquire masses.

3.1.1 The majoron seesaw

The simplest possibility for the seesaw is to have ungauged lepton number [8]. It is also the most general, as it can be studied in the framework of just the $SU(3) \otimes SU(2) \otimes U(1)$ gauge group. Such "1-2-3" scheme is characterized by $SU(3) \otimes SU(2) \otimes U(1)$ singlet, doublet and triplet mass terms, described by the matrix [7, 8]

$$\mathcal{M}_\nu = \begin{pmatrix} Y_3 v_3 & Y_\nu \langle \Phi \rangle \\ Y_\nu^T \langle \Phi \rangle & Y_1 v_1 \end{pmatrix} \quad (25)$$

in the basis ν_L, ν_L^c , corresponding to the three "left" and three "right" neutrinos, respectively. Note that, though symmetric, by the Pauli principle, \mathcal{M}_ν is complex, so that its Yukawa coupling sub-matrices Y_ν as well as Y_3 and Y_1 are complex matrices denoting the relevant Yukawa couplings, the last two symmetric.

Such $SU(3) \otimes SU(2) \otimes U(1)$ seesaw contains singlet, doublet and triplet scalar multiplets, obeying a simple "1-2-3" vev seesaw relation of the type

$$v_3 v_1 \sim v_2^2 \quad \text{with} \quad v_1 \gg v_2 \gg v_3 \quad (26)$$

This follows simply from the minimization condition of the $SU(3) \otimes SU(2) \otimes U(1)$ invariant scalar potential and arises in a wide variety of seesaw type models, as reviewed in [37, 38]. It implies that the

triplet vev $v_3 \rightarrow 0$ as the singlet vev v_1 grows. Here $v_2 \equiv \langle \Phi \rangle$ denotes the SM Higgs doublet vev. Small neutrino masses are induced either by heavy $SU(3) \otimes SU(2) \otimes U(1)$ singlet “right-handed” neutrino exchange (type I) or the smallness of the induced triplet vev that follows from heavy scalar exchange (type II), as illustrated in Fig. 2. The matrix \mathcal{M}_ν is diagonalized by a unitary mixing matrix U_ν ,

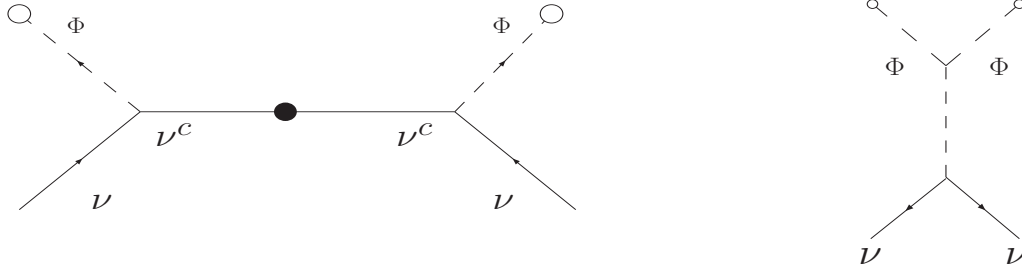


Figure 2: Two types of seesaw mechanism. Left: right-handed neutrino exchange (type-I), right: heavy $SU(3) \otimes SU(2) \otimes U(1)$ triplet exchange (type-II).

$$U_\nu^T \mathcal{M}_\nu U_\nu = \text{diag}(m_i, M_i), \quad (27)$$

yielding 6 mass eigenstates, including the three light neutrinos with masses m_i , and three two-component leptons. The light neutrino mass states ν_i are given in terms of the flavour eigenstates via the unitary matrix U_ν [7, 8]

$$\nu_i = \sum_{a=1}^6 (U_\nu)_{ia} n_a. \quad (28)$$

The effective light neutrino mass, obtained this way is of the form

$$m_\nu \simeq Y_3 v_3 - Y_\nu Y_1^{-1} Y_\nu^T \frac{\langle \Phi \rangle^2}{v_1} \quad (29)$$

The diagonalization matrices can be worked out explicitly as a perturbation series, see Ref. [8].

There is an important feature of such “1-2-3” seesaw namely, that since lepton number is ungauged, there is a physical Goldstone boson associated with its spontaneous breakdown, the Majoron [39]. It is often argued that, due to quantum gravity effects the associated majoron will pick up a mass. It has been shown that, a massive majoron with mass in the fraction of keV range can provide the observed dark matter of the Universe [40]. Such majoron decaying dark matter offers an alternative to the supersymmetric dark matter scenario and may lead to interesting phenomenological implications.

3.1.2 Left-right symmetric seesaw

A more elegant setting for the seesaw is a gauge theory containing B-L as a generator, such as $SU(3) \otimes SU(2)_L \otimes SU(2)_R \otimes U(1)_{B-L}$ or the unified models based on $SO(10)$ or $E(6)$ [41, 37, 42]. For example in $SO(10)$ each matter generation is naturally assigned to a **16** (spinorial in $SO(10)$) so that there are

$\mathbf{16} \cdot \mathbf{16} \cdot \mathbf{10}$ as well as $\mathbf{16} \cdot \overline{\mathbf{126}} \cdot \mathbf{16}$ terms generating Dirac and Majorana neutrino mass terms, respectively, leading to the neutrino mass matrix

$$\mathcal{M}_\nu = \begin{pmatrix} Y_L \langle \Delta_L \rangle & Y_\nu \langle \Phi \rangle \\ Y_\nu^T \langle \Phi \rangle & Y_R \langle \Delta_R \rangle \end{pmatrix} \quad (30)$$

in the basis ν_L, ν_L^c , corresponding to the “left” and “right” neutrinos, respectively, where Y_L and Y_R denote the Yukawas of the $\mathbf{126}$ of $SO(10)$, whose vevs $\langle \Delta_{L,R} \rangle$ give rise to the Majorana terms, while Y_ν is the Dirac Yukawa coupling in $\mathbf{16} \cdot \mathbf{16} \cdot \mathbf{10}$. The matrix Y_ν is an arbitrary complex matrix in flavour space, while Y_L and Y_R are complex symmetric 3×3 matrices that correspond to Y_1 and Y_3 of the simplest $SU(3) \otimes SU(2) \otimes U(1)$ model. Small neutrino masses are induced either by heavy $SU(3) \otimes SU(2) \otimes U(1)$ singlet “right-handed” neutrino exchange (type I) or heavy scalar boson exchange (type II) as illustrated in Fig. 2. The matrix \mathcal{M}_ν is diagonalized by a unitary mixing matrix U_ν as before. The diagonalization matrices can be worked out explicitly as a perturbation series, using the same method of Ref. [8]. This means that the explicit formulas for the 6×6 unitary diagonalizing matrix U given explicitly in Ref. [8] also hold in the left-right case, provided one takes into account that $v_1 \rightarrow \langle \Delta_R \rangle$ and $v_3 \rightarrow \langle \Delta_L \rangle$. The effective light neutrino mass, obtained this way is of the form

$$m_\nu \approx Y_L \langle \Delta_L \rangle - Y_\nu Y_R^{-1} Y_\nu^T \frac{\langle \Phi \rangle^2}{\langle \Delta_R \rangle}. \quad (31)$$

We have the new vev seesaw relation

$$\langle \Delta_L \rangle \langle \Delta_R \rangle \sim \langle \Phi \rangle^2, \quad (32)$$

which naturally follows from minimization of the left-right symmetric scalar potential, together with the vev hierarchy [37]

$$\langle \Delta_L \rangle \ll \langle \Phi \rangle \ll \langle \Delta_R \rangle. \quad (33)$$

This implies that both type I and type II contributions vanish as $\langle \Delta_R \rangle \rightarrow \infty$. The structure of the seesaw is exactly the same as before, enabling one to employ the same perturbative diagonalization method in [8].

The new insight that is obtained this way is that now one can arrange for the breakdown of parity invariance to be spontaneous, so that smallness of neutrino masses gets correlated to the observed maximality of parity violation in low-energy weak interactions, as stressed by Mohapatra and Senjanovic [37]. However this is hardly relevant phenomenologically in view of the large value of the B-L scale needed both to fit the neutrino masses, as well as unify the gauge couplings. Another important difference with the $SU(3) \otimes SU(2) \otimes U(1)$ seesaw case is the absence of the Majoron, now absorbed as the longitudinal mode of the gauge boson corresponding to the B-L generator.

3.1.3 Double seesaw

Nothing is sacred about the number of (anomaly-free) gauge singlet leptons S_i in the SM [7] or of singlets outside the $\mathbf{16}$ in $SO(10)$ or the $\mathbf{27}$ in $E(6)$ [43]. New important features may emerge when the

seesaw is realized with non-minimal lepton content. Here we mention the seesaw scheme suggested in Ref. [43] with $E(6)$ motivations [44]. The model extends minimally the particle content of the SM by the sequential addition of a pair of two-component $SU(3) \otimes SU(2) \otimes U(1)$ singlet leptons, ν_i^c, S_i , with i a generation index running over 1, 2, 3. In the ν, ν^c, S basis, the 9×9 neutral leptons mass matrix \mathcal{M}_ν is given as

$$\mathcal{M}_\nu = \begin{pmatrix} 0 & Y_\nu^T \langle \Phi \rangle & 0 \\ Y_\nu \langle \Phi \rangle & 0 & M^T \\ 0 & M & \mu \end{pmatrix}, \quad (34)$$

in the basis ν_L, ν_L^c, S_L , where Y_ν is an arbitrary 3×3 complex Yukawa matrix, M and μ are $SU(3) \otimes SU(2) \otimes U(1)$ singlet complex mass matrices, μ being symmetric. Notice that it has zeros in the ν_L - ν_L and ν_L^c - ν_L^c entries, a feature of several string models [44].

For $\mu \gg M$ one has to first approximation that the S_i decouple leaving the simpler seesaw at scales below that. In such a “double” seesaw scheme the three light neutrino masses are determined from

$$m_\nu \approx \langle \Phi \rangle^2 Y_\nu^T M^{T-1} \mu M^{-1} Y_\nu. \quad (35)$$

The mass generation is illustrated in Fig. 3. This formula can be readily derived from the method given

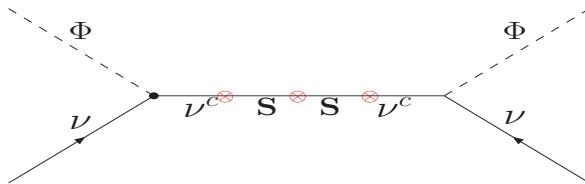


Figure 3: “Double” and “inverse” seesaw mechanism.

in Ref. [8] and decoupling the heavy states in two steps, first S then ν^c since $\mu \gg M$. A new feature is that there are two independent scales, μ and M , with the B-L symmetry broken only by the largest scale μ . It is completely natural also to consider the case where μ instead of large is very small [43], even smaller than the electroweak vev. This low μ case will be considered in Sec. 3.2.3, and opens new phenomenological possibilities, discussed in Sec. 3.3.

Irrespective of what sets its scale, the entry μ may be proportional to the vev of an $SU(3) \otimes SU(2) \otimes U(1)$ singlet scalar, in which case the model contains a singlet majoron.

3.1.4 Unconventional seesaw

There are many types of seesaw. More important than keeping track of the taxonomy of schemes (type I [41, 37, 42], type II [7, 8], type III [45, 46, 47], etc.) is understanding that the seesaw is not a theory but a mechanism that allows for many possible realizations. Schemes leading to the same pattern of neutrino masses may differ in many other respects.

As an example of extended seesaw models, let us consider one that has recently been suggested [48]. It belongs to the class of supersymmetric $SO(10)$ models with broken D-parity. In addition to the three right-handed neutrinos of the standard seesaw model, it contains three sequential gauge singlets S_{iL} with the following mass matrix

$$\mathcal{M}_\nu = \begin{pmatrix} 0 & Y_\nu \langle \Phi \rangle & F \langle \chi_L \rangle \\ Y_\nu^T \langle \Phi \rangle & 0 & \tilde{F} \langle \chi_R \rangle \\ F^T \langle \chi_L \rangle & \tilde{F}^T \langle \chi_R \rangle & 0 \end{pmatrix} \quad (36)$$

in the basis ν_L, ν_L^c, S_L . Notice that it has zeros along the diagonal, specially in the ν_L - ν_L and ν_L^c - ν_L^c entries, thanks to the fact that there is no **126**, a feature of several string-inspired models [44, 43]. The resulting neutrino mass is

$$m_\nu \simeq \frac{\langle \Phi \rangle^2}{M_{\text{unif}}} \left[Y_\nu (F \tilde{F}^{-1})^T + (F \tilde{F}^{-1}) Y_\nu^T \right], \quad (37)$$

where M_{unif} is the unification scale, F and \tilde{F} denote independent combinations of Yukawa couplings of the S_{iL} . One can see that the neutrino mass is suppressed by the unification scale M_{unif} *irrespective of how low is the B-L breaking scale*. In contrast to all familiar seesaws, see e.g. Eq. (31), this new seesaw mechanism is *linear* in the Dirac Yukawa couplings Y_ν , as illustrated in Fig. 4. It is rather remarkable

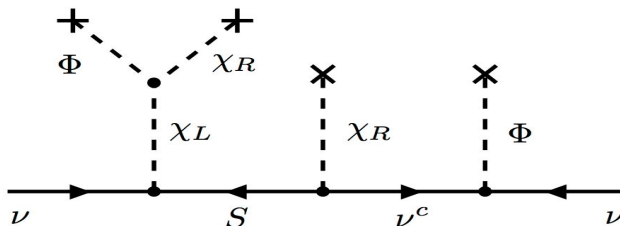


Figure 4: Unconventional seesaw mechanism.

that one can indeed take the B-L scale as low as TeV without generating inconsistencies with gauge coupling unification [48].

3.2 Bottom-up neutrino masses

There is a variety of models of neutrino mass where the operator \mathcal{O} is induced from physics at accessible scales, TeV or less. The smallness of its strength is naturally achieved due to loop and Yukawa couplings suppression. Note also that lepton number violating parameters may appear in the numerator instead of the denominator of \mathcal{O} with the smallness of its strength natural in t'Hofft's sense [49]. For example, in the inverse seesaw scheme of Sec. 3.2.3, one can consistently take μ to be small as the symmetry of the theory increases in the limit of vanishing μ , namely B-L is restored.

3.2.1 Radiative models

The first possibility is that neutrino masses are induced by calculable radiative corrections [50]. For example, they may arise at the two-loop level [51] as illustrated in Fig. 5. Up to a logarithmic factor

one has, schematically,

$$\mathcal{M}_\nu \sim \lambda_0 \left(\frac{1}{16\pi^2} \right)^2 f Y_l h Y_l f^T \frac{\langle \Phi \rangle^2}{(m_k)^2} \langle \sigma \rangle \quad (38)$$

in the limit where the doubly-charged scalar k is much heavier than the singly charged one. Here l denotes a charged lepton, f and h are their Yukawa coupling matrices and Y_l denotes the SM Higgs Yukawa couplings to charged leptons and $\langle \sigma \rangle$ is an $SU(3) \otimes SU(2) \otimes U(1)$ singlet vev introduced in Ref. [52]. Clearly, even if the proportionality factor λ_0 is large, the neutrino mass can be made naturally small by the presence of a product of five small Yukawas and the appearance of the two-loop factor. A remarkable feature of the model is that, thanks to the anti-symmetry of the f Yukawa coupling matrix, one of the neutrinos is massless.

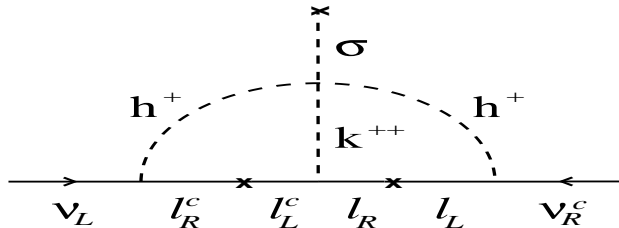


Figure 5: Two-loop origin for neutrino mass.

3.2.2 Supersymmetric neutrino masses

Another very interesting alternative are models where low energy supersymmetry is the origin of neutrino mass [53]. The intrinsically supersymmetric way to break lepton number is to break the so-called R parity. This could happen spontaneously, driven by a nonzero vev of an $SU(3) \otimes SU(2) \otimes U(1)$ singlet sneutrino [54, 55, 56]. This way one is led to a very simple reference model which can be regarded as the minimal way to include neutrino masses into the MSSM. In this model R parity is violated only through an effective bilinear term [57]. Neutrino mass generation takes place in a hybrid scenario, with one scale generated at tree level by the mixing of neutralinos and neutrinos, induced by the sneutrino vevs, and the other induced by “calculable” radiative corrections [58]. Here the two blobs in each graph

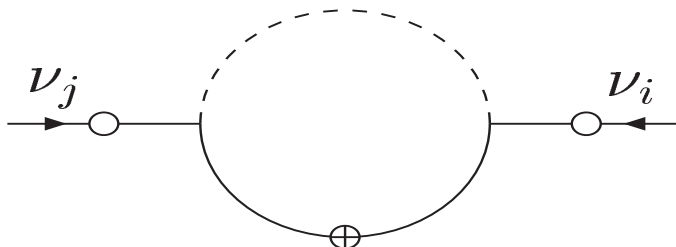


Figure 6: Loop origin of solar mass scale. Atmospheric scale arises from a type-I weak-scale seesaw-like graph involving exchange of sleptons and squarks.

denote $\Delta L = 1$ insertions, while the crossed blob accounts for chirality flipping. The general form of

the expression is quite involved but the approximation

$$\mathcal{M}_\nu \sim \left(\frac{1}{16\pi^2} \right) \langle \Phi \rangle^2 \frac{A}{m_0} Y_d Y_d \quad (39)$$

holds in some regions of parameters. Here A denotes the trilinear soft supersymmetry breaking coupling (not shown in the diagram), m_0 the scalar supersymmetry breaking mass, and Y_d the suitable Yukawa coupling. The neutrino mass spectrum naturally follows a normal hierarchy, with the atmospheric scale generated at the tree level and the solar mass scale arising from calculable loops.

3.2.3 Inverse seesaw

Before closing this section we mention that there are also tree level neutrino mass schemes with naturally light neutrinos. One is the inverse seesaw scheme suggested in Ref. [44] from heterotic string motivations which led to the $E(6)$ gauge group. The model extends minimally the particle content of the SM by the sequential addition of a pair of two-component $SU(3) \otimes SU(2) \otimes U(1)$ singlet leptons, ν_i^c, S_i , with i denoting a generation index running over 1, 2, 3.

In the ν, ν^c, S basis, the 9×9 neutral leptons mass matrix \mathcal{M}_ν is the formally exactly the same as given in Eq. (34) [43]. Again the diagonalization follows the method in Ref. [8] but, in contrast to what is done for the large μ regime, now one separates the full heavy sector consisting of three Quasi-Dirac states (six two-component leptons) at once. One obtains exactly the same light neutrino mass formula despite the important difference that now the entry μ is taken very small, e. g. $\mu \ll Y_\nu \langle \Phi \rangle \ll M$.

As before Y_ν and M are arbitrary 3×3 complex Yukawa matrices, μ being symmetric due to the Pauli principle. Notice that for small μ neutrino masses vanish with μ , as we saw in Eq. (35), illustrated in Fig. 3. The fact that the neutrino mass vanishes as $\mu \rightarrow 0$ is just the opposite of the behaviour of the seesaw formulas in Eqs. (29) and (31) with respect to v_3 and $\langle \Delta_R \rangle$, respectively; thus this is sometimes called inverse seesaw model of neutrino masses. The entry μ may be proportional to the vev of an $SU(3) \otimes SU(2) \otimes U(1)$ singlet scalar, in which case spontaneous B-L violation leads to the existence of a majoron [59]. This would be characterized by a relatively low scale, so that the corresponding phase transition could take place after the electroweak transition [52]. The naturalness of the model stems from the fact that the limit when $\mu \rightarrow 0$ increases the symmetry of the theory. One possible phenomenological implication would be the phenomenon of invisibly decaying Higgs boson [60, 61, 62]. In such schemes it will be crucial to take into account the existence of sizeable invisible Higgs boson decay channels in the analysis of experimental data on Higgs searches [63, 64]. Another possible implication is the existence of novel neutrino decay and annihilation processes that may be relevant in dense supernova media [65]. Other aspects of the phenomenology are mentioned in Sec. 3.3.

3.3 Phenomenology of neutrino masses and mixings

Clearly the first phenomenological implication of neutrino mass models is the phenomenon of neutrino oscillations, required to account for the current data. Before turning to the prospects for probing

neutrino oscillations with high precision at the future generation of long baseline oscillation experiments discussed in Sec. 6, let us comment on other manifestations of neutrino mass.

First comes the issue of the absolute scale of neutrino masses. This will be tested directly in searches for tritium beta decay [66, 67] and cosmology [68, 69]. Some models do indeed suggest a lower bound on the absolute neutrino mass. For example the model in Ref. [70] gives $m_\nu \gtrsim 0.3$ eV and therefore will be tested soon. Lastly, the nature (Dirac or Majorana) of neutrinos and the new sources of CP violation associated to its Majorana character can be scrutinized in neutrinoless double beta decay searches and other lepton number violation processes (see Sec. 8). What else is there?

If neutrino masses arise *a la* seesaw this may be all. The simplest $SO(10)$ seesaw has a drawback that the dynamics responsible for generating the small neutrino masses seems most likely untestable. In other words, beyond neutrino masses and oscillations, the model can not be probed phenomenologically at low energies, due to the large scale involved.

However, in the presence of supersymmetry, the phenomenology of the seesaw mechanism can be richer. A generic feature of supersymmetric seesaw models is the existence lepton flavour violation decays like $\mu^- \rightarrow e^- \gamma$, flavour violating tau decays (Fig. 7) and nuclear $\mu^- - e^-$ conversion (Fig. 8). These can have accessible rates (Figs. 9 and 10) which depend not only on the seesaw mechanism, but also on the details of supersymmetry breaking and on a possible theory of flavour. The way these LFV processes arise through supersymmetry [71] is illustrated in Fig. 7. The existence of such loop effects leads to enhanced rates for flavour violating processes [72, 73, 74, 75, 76, 77] [78, 79]. We note that such LFV and/or CP violating effects may arise at the one-loop level from the exchange of relatively light neutral heavy leptons, even in the absence of supersymmetry [80, 81, 82, 83, 84].

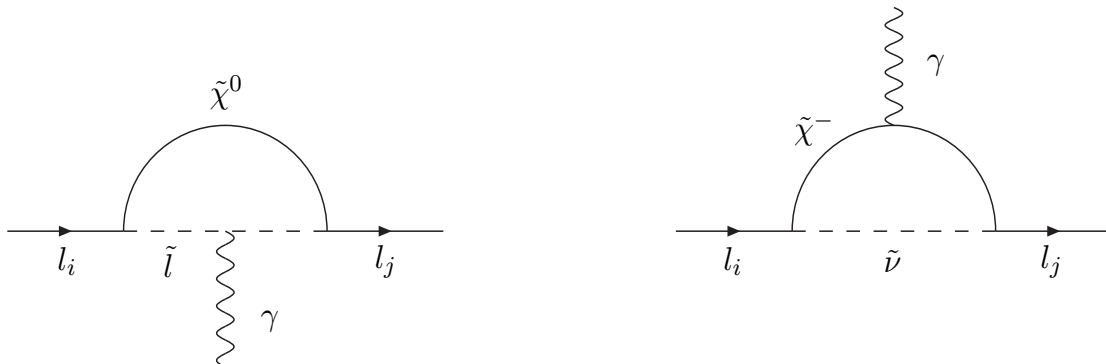


Figure 7: Supersymmetric Feynman diagrams for $l_i^- \rightarrow l_j^- \gamma$. They involve the exchange of charginos(neutralinos) and sneutrinos (charged sleptons).

As an illustration of the interplay of supersymmetry with heavy lepton exchange in engendering lepton flavour violation processes we consider the rates for the $\mu^- \rightarrow e^- \gamma$ decay in the framework of the supersymmetric inverse seesaw model [78, 79]. Fig. 9 displays the dependence of the branching ratios for $\mu^- - e^-$ conversion in Ti (left) and $\mu^- \rightarrow e^- \gamma$ (right) with the small neutrino mixing angle θ_{13} , for different values of θ_{12} (black curve: θ_{12} best fit value, blue bands denote 2σ , 3σ , 4σ confidence intervals for the solar mixing angle θ_{12}). The inverse seesaw parameters are given by: $M = 1$ TeV and

$\mu = 30$ eV. The light neutrino parameters used are from [12], except for θ_{13} which is varied as shown in the plots. The vertical coloured bands denote the exclusion areas from the 2σ , 3σ and 4σ limits on $\sin^2\theta_{13}$, respectively. These lepton flavour violation rates may be testable in the new generation of upcoming experiments. For large M the estimates are similar to those of the standard supersymmetric seesaw.

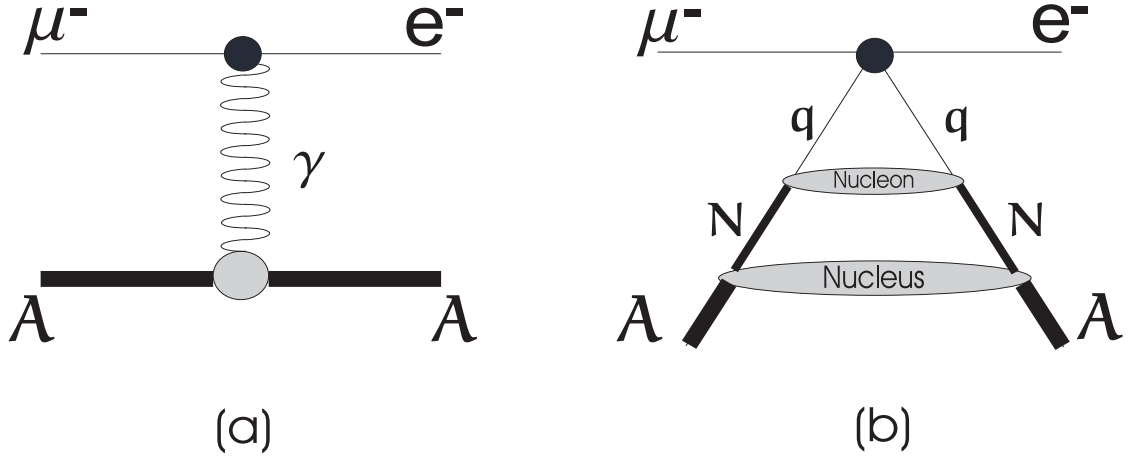


Figure 8: Contributions to the nuclear $\mu^- - e^-$ conversion: (a) long-distance and (b) short-distance.

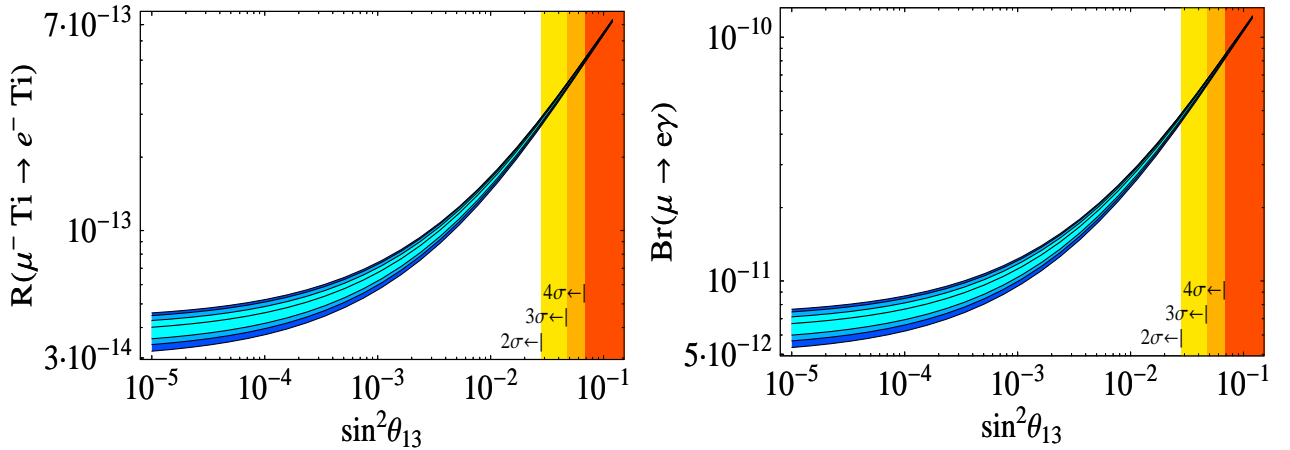


Figure 9: LFV branching ratios in the supersymmetric inverse seesaw model of neutrino mass (see text).

The novel feature present in this model and not in the minimal seesaw is the possibility of enhancing $Br(\mu \rightarrow e\gamma)$ and other tau decays with lepton flavour violation even in the *absence* of supersymmetry in the case where M is low, around TeV or so. In this region of parameters the model also gives rise to large estimates for the nuclear $\mu^- - e^-$ conversion, depicted in Fig. 8. The latter fall within the sensitivity of future experiments such as PRISM [85]. Note that LFV happens even in the absence of supersymmetry and even in the massless neutrino limit. The allowed rates are hence unsuppressed by the smallness of neutrino masses [80, 81, 82, 83, 84]. Finally, for low enough M the corresponding quasi-Dirac heavy leptons could be searched directly at accelerators [86, 87].

Supersymmetric neutrino mass and collider tests

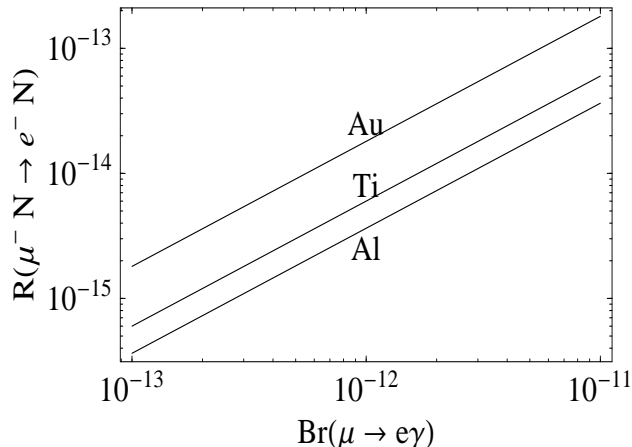


Figure 10: Correlation between $Br(\mu \rightarrow e\gamma)$ and muon-electron conversion in nuclei from Ref. [79].

We now turn to the case of low-scale models of neutrino mass, considered in Sec. 3.2. As an example we consider the case of models where supersymmetry is the origin of neutrino mass [53, 58], considered in Sec. 3.2.2. A general feature of these models is that, unprotected by any symmetry, the lightest supersymmetric particle (LSP) is unstable. In order to reproduce the masses indicated by current neutrino oscillation data, typically the LSP is expected to decay inside the detector. More strikingly, its decay properties correlate with neutrino mixing angles. For example, if the LSP is the lightest neutralino, it is expected to have the same decay rate into muons and taus, since the observed atmospheric angle, as we will see below, is close to $\pi/4$ [88, 89, 90]. This opens the tantalizing possibility

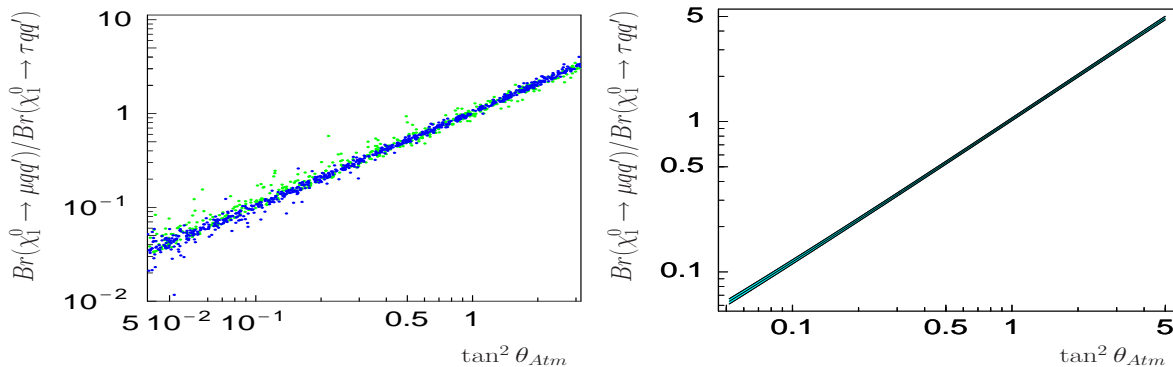


Figure 11: LSP decays trace the atmospheric mixing angle [88].

of testing neutrino mixing at high energy accelerators, like the "Large Hadron Collider" (LHC) and the "International Linear Collider" (ILC) and constitutes a smoking gun signature of this proposal that for sure will be tested. This possibility also illustrates the complementarity of accelerator and non-accelerator approaches in elementary particle physics.

Majorons and B-L gauge bosons

Before closing let us also mention that there could be a dynamical "tracer" of the mass-generation mechanism. In the case of the "1-2-3" majoron seesaw considered in Sec. 3.1.1 the existence of the Goldstone boson brings new interactions of neutrinos with majoron, but the rates are probably too

small to be cosmologically relevant. There can also be a new neutrino decay mode, $\nu_3 \rightarrow \nu + J$, involving the emission of the majoron, denoted J [8]. However, the strong suppression of the majoron emitting decay rates obtained in Ref. [8] and the smallness of neutrino masses that follows from current laboratory experiments, as well as cosmology, indicates that such neutrino decays are purely academic. However, there is an important exception. In models with family-dependent lepton numbers the decay is enhanced even in vacuum [91, 92]. Alternatively, if the neutrino decays in high density media, like supernovae, characterized by huge matter effects, then they could lead to detectable signals in underground water Cerenkov experiments [65] even in the simplest majoron schemes. Conversely, in the case of seesaw mechanisms with gauged B-L symmetry, if the corresponding B-L scale is low, as in the model discussed in Sec. 3.1.4, there will exist a light new neutral gauge boson, Z' that could be detected in searches for Drell-Yan processes at the LHC.

4 The general structure of the lepton mixing matrix

In any gauge theory in order to identify physical particles one must diagonalize all relevant mass matrices, which typically result from gauge symmetry breaking. Mechanisms giving mass to neutrinos generally imply the need for new interactions whose Yukawa couplings (like Y_ν) will coexist with that of the charged leptons, Y_l . The lepton mixing matrix V follows from a mismatch between the diagonalization of the charged lepton mass matrix and that of the neutrino mass matrix, which involve these Yukawas. This is similar to the way the Cabibbo-Kobayashi-Maskawa matrix arises in the quark sector, namely from a mismatch between up and down-type Yukawa couplings. Hence, like quarks, massive neutrinos will generally mix. The structure of this mixing is not generally predicted from first principles. Whatever the ultimate high energy gauge theory may be it must be broken to the SM at low scales, so one should characterize the structure of the lepton mixing matrix in terms of the $SU(3) \otimes SU(2) \otimes U(1)$ structure.

4.1 Quark-like lepton mixing matrix

From the start, in the absence of a fundamental theory of flavour, the lepton mixing matrix of massive Dirac neutrinos is a unitary matrix V which can always be parametrized as

$$V = \omega_0(\gamma) \prod_{i < j}^n \omega_{ij}(\eta_{ij}) \quad (40)$$

where

$$\omega_0(\gamma) = \exp i \left(\sum_{a=1}^n \gamma_a A_a^a \right)$$

is a diagonal unitary matrix described by $n - 1$ real parameters γ_a . (By choosing an overall relative phase between charged leptons and Dirac neutrinos we can take V as unimodular, i. e. $\det V = 1$, so

that the phases in the ‘‘Cartan’’ matrix ω_0 obey $\sum_{a=1}^n \gamma_a = 1$). On the other hand

$$\omega_{ab}(\eta_{ab}) = \exp \sum_{a=1}^n (\eta_{ab} A_a^b - \eta_{ab}^* A_b^a)$$

is a complex rotation in ab with parameter $\eta_{ab} = |\eta_{ab}| \exp i\theta_{ab}$. For example,

$$\omega_{12}(\eta_{12}) = \begin{pmatrix} c_{12} & e^{i\phi_{12}} s_{12} & 0 \dots \\ -e^{-i\phi_{12}} s_{12} & c_{12} & 0 \dots \\ 0 & 0 & 1 \dots \\ \dots & \dots & \dots \dots \dots \end{pmatrix} \quad (41)$$

However, in order to obtain the parametrization of this matrix, as presented in Ref. [7], one must take into account that its structure can be further simplified by taking into account that, once the charged leptons and Dirac neutrino mass matrices are diagonal, one can still rephase the corresponding fields by $\omega_0(\alpha)$ and $\omega_0(\gamma - \alpha)$, respectively, keeping invariant the form of the free Lagrangean. This results in the form

$$V = \omega_0(\alpha) \prod_{i < j}^n \omega_{ij}(\eta_{ij}) \omega_0^\dagger(\alpha). \quad (42)$$

There are $n - 1$ α -values associated to Dirac neutrino phase redefinitions which we are still free to choose. Using the conjugation property

$$\omega_0(\alpha) \omega_{ab}(|\eta_{ab}| \exp i\theta_{ab}) \omega_0^\dagger(\alpha) = \omega_{ab}[|\eta_{ab}| \exp i(\alpha_a + \theta_{ab} - \alpha_b)] \quad (43)$$

we arrive at the final Dirac lepton mixing matrix which is, of course, identical in form to that describing quark mixing. It involves a set of

$$n(n - 1)/2 \text{ mixing angles } \theta_{ij} \text{ and } n(n - 1)/2 - (n - 1) \text{ CP phases.} \quad (44)$$

One sees that $(n - 1)$ phases were eliminated by rephasing, a possibility that would be absent in the case of Majorana neutrinos. This is the parametrization as originally given in [7], with unspecified factor ordering. It needs to be supplemented only by an ordering prescription, for this we refer the reader to the PDG choice [93].

In summary, if neutrinos masses were added *a la Dirac* their charged current weak interaction would have exactly the same structure as that of quarks. From Eq. (44) for the case $n = 3$ there are 3 angles and precisely one leptonic CP violating phase, just as in the Kobayashi-Maskawa matrix describing quark mixing.

However the imposition of lepton number conservation is *ad hoc* in a gauge theory and hence neutrinos are expected to be Majorana¹. Note that the argument in favour of neutrinos being Majorana has nothing to do with the neutrino mass generation mechanism, it is much more basic.

¹The same happens for electrically neutral supersymmetric fermions such as the gravitino, gluino and neutralinos.

4.2 Majorana case: unitary approximation

Here we consider the form of the lepton mixing matrix in models where neutrino masses arise in the absence of right-handed neutrinos. These include, for example, the models in Sec. 3.2.1 and constitute a good approximation for high-scale seesaw models in Sec. 3.1.

For n generations of Majorana neutrinos the lepton mixing matrix has exactly the same form given in Eq. (42). The difference insofar as the structure of lepton mixing is concerned come about since in the case of Majorana neutrinos the mass terms are manifestly not invariant under rephasings of the neutrino fields. As a result, the parameters α in Eq. (42) can not be used to eliminate $n - 1$ Majorana phases as we just did in Sec. 4.1. Consequently these are additional sources of CP violation in the currents of gauge theories with Majorana neutrinos. They are sometimes called ‘‘Majorana phases’’. They already exist in a theory with just two generations of Majorana neutrinos, $n = 2$, which is described by

$$\omega_{13} = \begin{pmatrix} c_{12} & e^{i\phi_{12}} s_{12} \\ -e^{-i\phi_{12}} s_{12} & c_{12} \end{pmatrix}, \quad (45)$$

where ϕ_{12} is the Majorana phase. Such ‘‘Majorana’’-type CP phase is, in a sense, mathematically more ‘‘fundamental’’ than the Dirac phase whose existence, as we just saw, requires three generations at least.

For the case of three neutrinos the lepton mixing matrix can be parametrized as ($n = 3$) [7]

$$K = \omega_{23}\omega_{13}\omega_{12}, \quad (46)$$

where each factor in the product of the ω 's is effectively 2×2 , characterized by an angle and a CP phase. Two of the three angles are involved in solar and atmospheric oscillations, so we set $\theta_{12} \equiv \theta_{\text{SOL}}$ and $\theta_{23} \equiv \theta_{\text{ATM}}$. The last angle in the three-neutrino leptonic mixing matrix is θ_{13} ,

$$\omega_{13} = \begin{pmatrix} c_{13} & 0 & e^{i\phi_{13}} s_{13} \\ 0 & 1 & 0 \\ -e^{-i\phi_{13}} s_{13} & 0 & c_{13} \end{pmatrix}. \quad (47)$$

Such symmetrical parametrization of the lepton mixing matrix, K can be written as:

$$K = \begin{bmatrix} c_{12}c_{13} & s_{12}c_{13}e^{i\phi_{12}} & s_{13}e^{i\phi_{13}} \\ -s_{12}c_{23}e^{-i\phi_{12}} - c_{12}s_{13}s_{23}e^{i(\phi_{23}-\phi_{13})} & c_{12}c_{23} - s_{12}s_{13}s_{23}e^{i(\phi_{12}+\phi_{23}-\phi_{13})} & c_{13}s_{23}e^{i\phi_{23}} \\ s_{12}s_{23}e^{-i(\phi_{12}+\phi_{23})} - c_{12}s_{13}c_{23}e^{-i\phi_{13}} & -c_{12}s_{23}e^{-i\phi_{23}} - s_{12}s_{13}c_{23}e^{i(\phi_{12}-\phi_{13})} & c_{13}c_{23} \end{bmatrix}. \quad (48)$$

All three CP violating phases are physical [25]: ϕ_{12} , ϕ_{23} and ϕ_{13} . Even though the parametrization is fully ‘‘symmetric’’ there is a basic difference between Dirac and Majorana phases. The ‘‘invariant’’ combination $\delta \equiv \phi_{12} + \phi_{23} - \phi_{13}$ corresponding to the ‘‘Dirac phase’’ exists only beyond $n = 3$. At $n = 3$ a single phase (say ϕ_{13}) may be taken to be non-zero. This is the phase that corresponds to the Dirac phase present in the quark sector, and affects neutrino oscillations involving three neutrinos. The other two phases are associated to the Majorana nature of neutrinos. These already exist for $n = 2$ but show up only in lepton-number violating processes, like neutrinoless double beta decay. They

do not affect conventional neutrino oscillations [25, 26, 27] but do enter in the “neutrino oscillation thought-experiment” described in [25]. Needless to say the latter process is of conceptual interest, only.

An important subtlety arises regarding the conditions for CP conservation in gauge theories of massive Majorana neutrinos. Unlike the case of Dirac fermions, where CP invariance implies that the mixing matrix should be real, in the Majorana case the condition one needs is

$$K^* = K\eta$$

where $\eta = \text{diag}(+, +, \dots, , \dots)$ is the signature matrix describing the relative signs of the neutrino mass eigenvalues that follow from diagonalizing the relevant Majorana mass matrix, if one insists in using real diagonalizing matrices, like Wolfenstein [32]. Consequently the value $\phi_{12} = \pi/2$ and $\phi_{12} = 0$ are both CP conserving. These important signs determine the CP properties of the neutrinos and play a crucial role in $\beta\beta_{0\nu}$.

Before concluding let us mention that the above parametrization of the lepton mixing matrix was originally given in [7], but with unspecified factor ordering. In what follows we tacitly employ the ordering prescription now adopted by the PDG [93]. Further discussion on the advantages of this “symmetrical parametrization” and additional references can be found in Ref. [94].

4.3 General seesaw-type lepton mixing matrix

What we now present is a brief summary of the original systematic study of the effective form of the lepton mixing matrix originally given in [7], applicable to any scheme of Majorana neutrino masses where isosinglet and isodoublet mass terms coexist. In addition to the existence of Majorana phases, which do not require the existence of $SU(3) \otimes SU(2) \otimes U(1)$ singlets, one has doublet-singlet mixing parameters, in general complex. As a result one finds that leptonic mixing as well as CP violation may take place even in the massless neutrino limit [81, 82].

The most general effective model is described by (n, m) , n being the number of $SU(3) \otimes SU(2) \otimes U(1)$ isodoublet and m the number of $SU(3) \otimes SU(2) \otimes U(1)$ isosinglet leptons. In this Section we assume $m \neq 0$, the $(n, 0)$ has just been considered in Sec. 4.2. The two-component $SU(3) \otimes SU(2) \otimes U(1)$ singlet leptons present in the theory have in general a gauge and Lorentz invariant Majorana mass term, breaking total lepton number symmetry. Their number, m , is completely arbitrary, as $SU(3) \otimes SU(2) \otimes U(1)$ singlets carry no anomaly.

The resulting structure of the weak currents can be substantially more complex, since the heavy isosinglets will now mix with the ordinary $SU(2)$ doublet neutrinos in the charged current weak interaction. As a result, the mixing matrix describing the charged leptonic weak interaction is a rectangular matrix, called K .

Typically the charged weak interactions of the light (mass-eigenstate) neutrinos in (n, m) models are effectively described by a mixing matrix which is non-unitary. For example, one sees that the coupling of a given light neutrino to the corresponding charged lepton is decreased by a certain factor. The existence of these neutral heavy leptons could therefore be inferred from low energy weak decay

processes, where the neutrinos that can be kinematically produced are only the light ones. There are constraints on the strength of the such mixing matrix elements that follow from low energy weak decay measurements as well as from LEP.

An explicit parametrization of the weak charged current mixing matrix K that covers the most general situation present in these (n, m) models has also been given in Ref. [7] so that here we only highlight the main points. It involves in general

$$n(n + 2m - 1)/2 \tag{49}$$

mixing angles θ_{ij} and

$$n(n + 2m - 1)/2 \tag{50}$$

CP violating phases ϕ_{ij} .

This number far exceeds the corresponding number of parameters describing the charged current weak interaction of quarks Eq. (42). The reason is twofold: (i) neutrinos are Majorana particles, their mass terms are not invariant under rephasings, and (ii) the isodoublet neutrinos in general mix with the $SU(3) \otimes SU(2) \otimes U(1)$ singlets and, in addition, so CP may also be violated in this mixing. As a result, there are far less CP phases that can be eliminated by field redefinitions. They may play a role in leptogenesis as well as neutrino oscillations.

Another important feature which arises in any theory based on $SU(3) \otimes SU(2) \otimes U(1)$ where isosinglet and isodoublet lepton mass terms coexist is that the leptonic neutral current is non-trivial [7]: there are non diagonal couplings of the Z to the mass-eigenstate neutrinos. They are expressed as a projective Hermitian matrix

$$P = K^\dagger K$$

This contrasts with the neutral current couplings of mass-eigenstate neutrinos in theories where there are no isosinglet neutrinos, i.e., $m = 0$. In that case, just as in the case of Dirac neutrinos, the neutral current couplings of mass-eigenstate neutrinos is diagonal.

Before closing this section we mention explicitly that the $(3, 3)$ seesaw model is characterized, from Eqs. (49) and (50) by 12 mixing angles and 12 CP phases (both Dirac and Majorana-type) [7].

Before we close, note that, in a scheme with $m < n$, $n - m$ neutrinos will remain massless, while $2m$ neutrinos will acquire Majorana masses, m light and m heavy. For example, in a model with $n = 3$ and $m = 1$ one has one light and one heavy Majorana neutrino, in addition to the two massless ones. In this case clearly there will be less parameters than present in a model with $m = n$. Note also that for $m > n$, the case $m = 2n$ corresponds to the models considered in Secs. 3.1.4 and 3.2.3.

4.4 Leptonic CP violation and leptogenesis

An interesting cosmological implication of leptonic CP violation is that it opens an attractive possibility of accounting for the matter-antimatter asymmetry in the Universe within the so-called thermal leptogenesis mechanism [95, 96]. In this picture the heavy “right-handed” neutrinos of the seesaw mechanism

play a crucial role. They decay out of equilibrium generating a lepton asymmetry, through diagrams in Fig. 12. This lepton (or B-L) asymmetry gets converted, through sphaleron processes, into a baryon

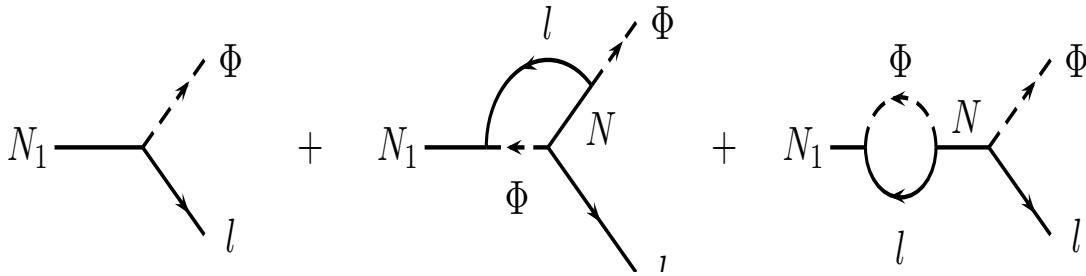


Figure 12: Diagrams contributing to heavy neutrino decays whose interference leads to leptogenesis.

asymmetry [97]. One of the crucial ingredients is CP violation in the lepton sector.

In the framework of a supersymmetric seesaw scheme the high temperature needed for leptogenesis leads to an overproduction of gravitinos, which destroys the standard predictions of Big Bang Nucleosynthesis (BBN). In minimal supergravity models, with $m_{3/2} \sim 100$ GeV to 10 TeV gravitinos are not stable, decaying during or after BBN. Their rate of production can be so large that subsequent gravitino decays completely change the standard BBN scenario. To prevent such “gravitino crisis” one requires an upper bound on the reheating temperature T_R after inflation, since the abundance of gravitinos is proportional to the reheating temperature. A recent detailed analysis derived a stringent upper bound $T_R \lesssim 10^6$ GeV when the gravitino decay has hadronic modes [98]. This upper bound is in conflict with the temperature required for leptogenesis, $T_R > 2 \times 10^9$ GeV [99]. Therefore, thermal leptogenesis in the usual hierarchical case seems difficult to reconcile with low energy supersymmetry if gravitino masses lie in the range suggested by the simplest minimal supergravity models. Their required mass is typically too large in order for them to be produced after inflation, implying that the minimal type I supersymmetric seesaw schemes may be in trouble ².

One way to cure this inconsistency has been suggested in Ref. [101] is to add a singlet Σ to the supersymmetric $SO(10)$ seesaw model discussed in [48]. Leptogenesis can occur at the TeV scale through the decay of Σ , thereby avoiding the gravitino crisis. Washout of the asymmetry is suppressed by the absence of direct couplings of Σ to leptons. The leptogenesis parameter region is illustrated in Fig. 13 and the reader is addressed to the original paper for details. Here we simply comment that in this model successful leptogenesis can occur for $M_\Sigma = 1$ TeV and low $v_R = 10$ TeV. As an example we consider the Σ decay asymmetries ϵ_1 that can be generated in this way. The contours of the maximum ϵ_1 values obtained in this model using the Fritzsch texture for the quark masses are illustrated in Fig. 14. The left and right panels correspond to two alternative choices of the relevant model parameters, explained in Ref. [102]. Taking into account washout effects, acceptable values of the baryon asymmetry $\mathcal{O}(10^{-10})$ require ϵ_1 above $\mathcal{O}(10^{-7})$ or so. From Fig. 14 one sees that this is clearly possible to achieve within this model even if the only source of CP violation is that provided by the three-flavour Dirac phase that enters in neutrino oscillations.

²A loophole is the possibility of resonant leptogenesis [100].

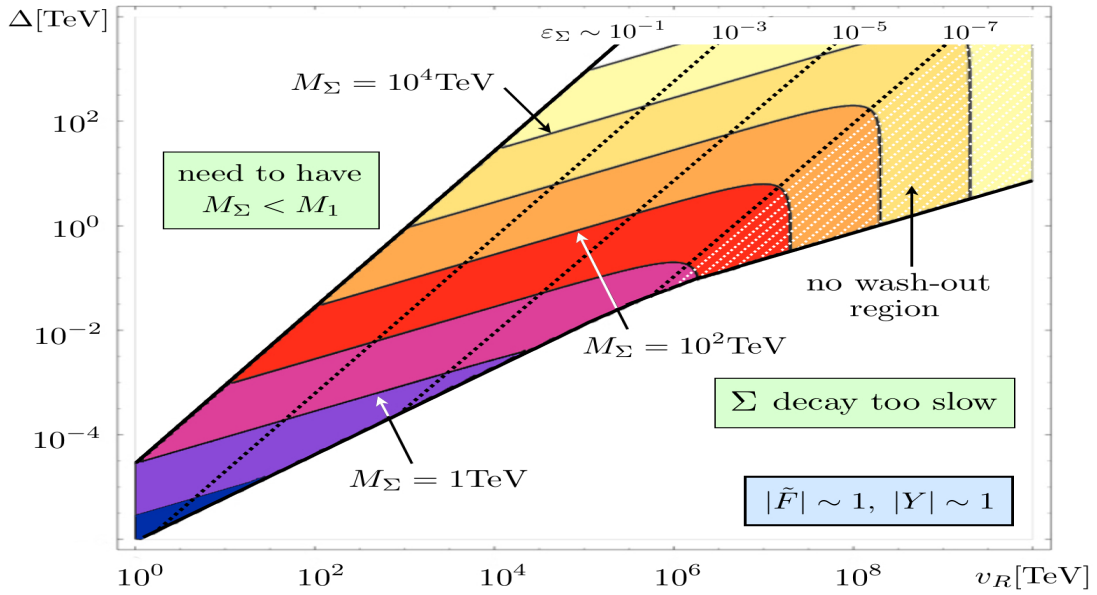


Figure 13: Parameter space in low-scale leptogenesis model of Ref. [101].

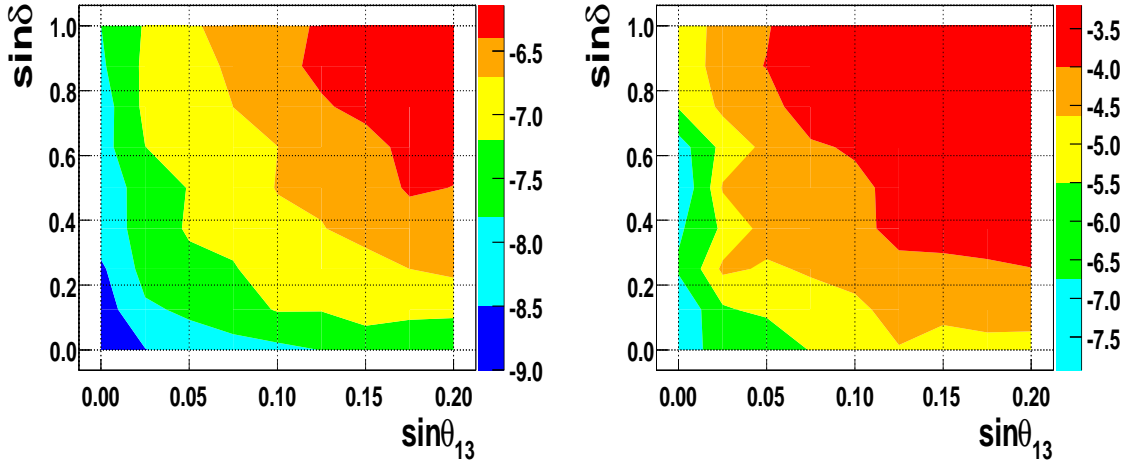


Figure 14: Contours of the maximum value of the asymmetry ϵ_1 obtained using the Fritzsch texture [102].

An alternative viable leptogenesis mechanism based on a modified type-I seesaw was suggested in Ref. [103]. It consists in adding a small R-parity violating $\lambda_i \hat{\nu}^c_i \hat{H}_u \hat{H}_d$ term in the superpotential, where $\hat{\nu}^c_i$ are right-handed neutrino supermultiplets. One can show that in the presence of this term, the produced lepton-antilepton asymmetry can be enhanced.

Last, but not least, leptogenesis may also be induced by the type-II seesaw mechanism, with or without supersymmetry. In the non-supersymmetric case this requires the addition of two heavy Higgs scalar triplets [104], while in supersymmetry even with a minimal triplet content, leptogenesis can be naturally accommodated thanks to the resonant interference between superpotential and soft supersymmetry breaking terms [105].

5 Neutrino oscillations

5.1 The formalism

We start with a very general discussion aimed at fixing the notation used in this review. As we have already seen in Sec. 4.3, in general models of neutrino mass the lepton mixing matrix K contain both Dirac and Majorana-type CP phases and is in general rectangular as it couples the charged leptons also to the heavy (mainly isosinglet) neutrinos postulated, e. g. in type-I seesaw models, in order to produce neutrino masses [7]. Such states are too heavy to participate in neutrino oscillations which are effectively described by a non-unitary mixing matrix. Such deviations from unitarity are the origin of gauge-induced neutrino non-standard interactions and may, in some cases, be sizeable, see Sec. 9. In the discussion of neutrino oscillations that we give in Secs. 5, 6 and 7 we will tacitly assume that K is strictly unitary, so that the three active neutrinos are mixed as follows,

$$\nu_{\alpha L} = \sum_{i=1}^3 U_{\alpha i} \nu_{iL}, \quad (\alpha = e, \mu, \tau), \quad (51)$$

where we have now denoted K by U , to highlight that $U^\dagger U = U U^\dagger = 1$. Here $\nu_{\alpha L}$ ($\alpha = e, \mu, \tau$) describe the left handed neutrino fields with definite flavor whereas ν_{iL} ($i = 1, 2, 3$) describe the fields with definite masses. Here, the matrix U is the leptonic analogue of the quark mixing matrix [1]. In this review, whenever it is necessary to use the explicit parametrization, we use the following standard parametrization [93],

$$\begin{aligned} U &= \begin{bmatrix} 1 & 0 & 0 \\ 0 & c_{23} & s_{23} \\ 0 & -s_{23} & c_{23} \end{bmatrix} \begin{bmatrix} c_{13} & 0 & s_{13}e^{-i\delta} \\ 0 & 1 & 0 \\ -s_{13}e^{i\delta} & 0 & c_{13} \end{bmatrix} \begin{bmatrix} c_{12} & s_{12} & 0 \\ -s_{12} & c_{12} & 0 \\ 0 & 0 & 1 \end{bmatrix} \\ &= \begin{bmatrix} c_{12}c_{13} & s_{12}c_{13} & s_{13}e^{-i\delta} \\ -s_{12}c_{23} - c_{12}s_{23}s_{13}e^{i\delta} & c_{12}c_{23} - s_{12}s_{23}s_{13}e^{i\delta} & s_{23}c_{13} \\ s_{12}s_{23} - c_{12}c_{23}s_{13}e^{i\delta} & -c_{12}s_{23} - s_{12}c_{23}s_{13}e^{i\delta} & c_{23}c_{13} \end{bmatrix} \end{aligned} \quad (52)$$

where $c_{ij} \equiv \cos \theta_{ij}$, $s_{ij} \equiv \sin \theta_{ij}$ and δ is the CP violating phase. This form is the same as Eq. (46) [7], taking $\phi_{12} = 0 = \phi_{23}$ in the ‘‘invariant’’ combination $\delta \equiv \phi_{12} + \phi_{23} - \phi_{13}$ that corresponds to the ‘‘Dirac phase’’ relevant for neutrino oscillations.

Eq. (51) implies that in terms of state vectors $|\nu_\alpha\rangle$ ($\alpha = e, \mu, \tau$) for flavor and $|\nu_i\rangle$ ($i = 1, 2, 3$) for mass eigenstates, they are related by U^* instead of U as (see e.g. [106]),

$$|\nu_\alpha\rangle = \sum_{i=1}^3 U_{\alpha i}^* |\nu_i\rangle, \quad (\alpha = e, \mu, \tau), \quad (54)$$

where for simplicity, we omitted the indices L which indicates the left handed chirality. Then it is straightforward to compute the $\nu_\alpha \rightarrow \nu_\beta$ oscillation probability, which is given, for ultra-relativistic

neutrinos, by,

$$\begin{aligned}
P(\nu_\alpha \rightarrow \nu_\beta) &= \left| \sum_j U_{\alpha j}^* U_{\beta j} e^{-i \frac{m_j^2}{2E} L} \right|^2 \\
&= \delta_{\alpha\beta} - 4 \sum_{i>j} \Re(U_{\alpha i}^* U_{\alpha j} U_{\beta i} U_{\beta j}^*) \sin^2 \left(\frac{\Delta m_{ij}^2}{4E} L \right) \\
&\quad + 2 \sum_{i>j} \Im(U_{\alpha i}^* U_{\alpha j} U_{\beta i} U_{\beta j}^*) \sin \left(\frac{\Delta m_{ij}^2}{2E} L \right), \tag{55}
\end{aligned}$$

where E is the neutrino energy, L is the distance traveled by neutrino, and $\Delta m_{ij} \equiv m_i^2 - m_j^2$ (m_i being mass eigenvalues) are the mass squared differences. Here \Re and \Im denote real and imaginary parts.

Let us now describe the neutrino evolution equation in matter. It is given in terms of flavor eigenstates as,

$$i \frac{d}{dx} \begin{bmatrix} \nu_e \\ \nu_\mu \\ \nu_\tau \end{bmatrix} = H(x) \begin{bmatrix} \nu_e \\ \nu_\mu \\ \nu_\tau \end{bmatrix}, \tag{56}$$

where ν_α ($\alpha = e, \mu, \tau$) is the amplitude for the α -flavor. The Hamiltonian matrix H is given by

$$H(x) = U \begin{bmatrix} \frac{m_1^2}{2E} & 0 & 0 \\ 0 & \frac{m_2^2}{2E} & 0 \\ 0 & 0 & \frac{m_3^2}{2E} \end{bmatrix} U^\dagger + \begin{bmatrix} V(x) & 0 & 0 \\ 0 & 0 & 0 \\ 0 & 0 & 0 \end{bmatrix}, \tag{57}$$

where x is the position along the neutrino trajectory and $V(x)$ is the matter potential which is given, for unpolarized medium ³, as

$$V(x) = \sqrt{2} G_F N_e(x), \tag{58}$$

where G_F is the Fermi constant, $N_e(x)$ is the electron number density at x . The Hamiltonian matrix in Eq. (57) can be replaced by,

$$H(x) = U \text{diag} \left[0, \frac{\Delta m_{21}^2}{2E}, \frac{\Delta m_{31}^2}{2E} \right] U^\dagger + \text{diag}[V(x), 0, 0], \tag{59}$$

by re-phasing all of the neutrino flavors by $\exp[-im_1^2 x/(2E)]$. For anti-neutrinos, the same Eq. holds with the change $V(x) \rightarrow -V(x)$ and $U \rightarrow U^*$ (or equivalently $\delta \rightarrow -\delta$).

For a given x , Hamiltonian can be diagonalized by using the effective mixing matrix in matter $U(N)$,

$$H(x) = U(N) \text{diag} \left[0, \frac{\Delta m_{21}^2(N)}{2E}, \frac{\Delta m_{31}^2(N)}{2E} \right] U^\dagger(N), \tag{60}$$

where $\Delta m_{ij}^2(N)$ are the effective mass squared differences in matter (see Eq. 88).

³Neutrino evolution in polarized media was treated in [107].

5.2 The current data

Current neutrino oscillation data have no sensitivity to CP violation. Thus we neglect all phases in the analysis and take, moreover, the simplest unitary 3-by-3 form of the lepton mixing matrix in Eq. (46). In this approximation oscillations depend on the three mixing parameters $\sin^2 \theta_{12}$, $\sin^2 \theta_{23}$, $\sin^2 \theta_{13}$ and on the two mass-squared splittings $\Delta m_{\text{SOL}}^2 \equiv \Delta m_{21}^2 \equiv m_2^2 - m_1^2$ and $\Delta m_{\text{ATM}}^2 \equiv \Delta m_{31}^2 \equiv m_3^2 - m_1^2$ characterizing solar and atmospheric neutrinos. The hierarchy $\Delta m_{\text{SOL}}^2 \ll \Delta m_{\text{ATM}}^2$ implies that one can set $\Delta m_{\text{SOL}}^2 = 0$, to a good approximation, in the analysis of atmospheric and accelerator data. Similarly, one can set Δm_{ATM}^2 to infinity in the analysis of solar and KamLAND data. Apart from the data already mentioned, the analysis also includes the constraints from "negative" searches at reactor experiments.

5.2.1 Solar and reactor data

The solar neutrino data includes the rates of the chlorine experiment ($2.56 \pm 0.16 \pm 0.16$ SNU), the gallium results of SAGE ($66.9_{-3.8}^{+3.9} {}_{-3.2}^{+3.6}$ SNU) and GALLEX/GNO ($69.3 \pm 4.1 \pm 3.6$ SNU), as well as the 1496-day Super-K data (44 bins: 8 energy bins, 6 of which are further divided into 7 zenith angle bins). The SNO sample includes the 2002 spectral day/night data (17 energy bins for each day and night period) [3] and the most recent data (391-day data) from the salt phase in the form of the neutral current (NC), charged current (CC) and elastic scattering (ES) fluxes [108]. The analysis includes both statistical errors, as well as systematic uncertainties such as those of the eight solar neutrino fluxes. Taking into account new radiative opacities, Bahcall et al (for references see Appendix C in hep-ph/0405172-v5) obtain new solar neutrino fluxes, neutrino production distributions and solar density profile, included in the analysis.

Reactor anti-neutrinos from a network of power stations in Japan are detected by the KamLAND collaboration at the Kamiokande site through the process $\bar{\nu}_e + p \rightarrow e^+ + n$, where the delayed coincidence of the prompt energy from the positron and a characteristic gamma from the neutron capture allows an efficient reduction of backgrounds. Most of the incident $\bar{\nu}_e$'s come from nuclear plants at distances of 80 – 350 km from the detector, far enough to probe large mixing angle (LMA) oscillations. To avoid large uncertainties associated with geo-neutrinos an energy cut at 2.6 MeV prompt energy is applied for the oscillation analysis.

The first KamLAND data corresponding to a 162 ton-year exposure gave 54 anti-neutrino events in the final sample, after cuts, whereas 86.8 ± 5.6 events are predicted for no oscillations with 0.95 ± 0.99 background events [109]. This is consistent with the no-disappearance hypothesis at less than 0.05% probability, giving the first terrestrial confirmation of oscillations with Δm_{SOL}^2 . Additional KamLAND data with a larger fiducial volume of the detector corresponding to an 766.3 ton-year exposure have been presented in [4]. In total 258 events have been observed, versus 356.2 ± 23.7 reactor neutrino events expected in the case of no disappearance and 7.5 ± 1.3 background events. This leads to a confidence level of 99.995% for $\bar{\nu}_e$ disappearance, in addition to evidence for spectral distortion consistent with oscillations.

Finally, recent data from the KamLAND experiment have been presented at the 10th International Conference on Topics in Astroparticle and Underground Physics, TAUP 2007 [110]. These data correspond to a total exposure of 2881 ton-year. They provide a better measurement of the solar neutrino oscillation parameters, especially the “solar” mass-squared splitting. This is due to the reduction of systematic uncertainties thanks to the full volume calibration. These data correspond to a total exposure of 2881 ton-year, almost 4 times larger than 2004 data. They provide a very precise measurement of the solar neutrino oscillation parameters, mainly the mass splitting. This is due to the reduction of systematic uncertainties thanks to the full volume calibration.

Various systematic errors associated to the neutrino fluxes, backgrounds, reactor fuel composition and individual reactor powers, small matter effects, and improved $\bar{\nu}_e$ flux parametrization are included in the analysis [12]. Assuming CPT invariance one can directly compare the information obtained from solar neutrino experiments with the KamLAND reactor results.

One finds that a strong evidence for spectral distortion in the KamLAND data, leading to a much improved Δm_{SOL}^2 determination, substantially reducing the allowed region of oscillation parameters. Altogether the KamLAND data single out the LMA solution from the previous “zoo” of alternatives [111]. As discussed in Sec. 9, more than just cornering the oscillation parameters [112], KamLAND has eliminated all previously viable non-oscillation solutions [113] playing a key role in the resolution of the solar neutrino problem.

Last, but not least, the Borexino collaboration has also recently presented their first data [114]. While they provide the first real time detection of ${}^7\text{Be}$ solar neutrinos, and an important confirmation of the Standard solar model and the large mixing oscillations, these data currently do not affect the determination of neutrino oscillation parameters.

5.2.2 Atmospheric and accelerator data

The first evidence for neutrino conversions was the zenith angle dependence of the μ -like atmospheric neutrino data from the Super-K experiment in 1998, an effect also seen in other atmospheric neutrino experiments. At that time there were equally good non-oscillation solutions, involving non-standard neutrino interactions [115]. Thanks to the accumulation of up-going muon data, and the observation of the dip in the L/E distribution of the atmospheric ν_μ survival probability, the signature for atmospheric neutrino oscillations has now become convincing. We have used the Super-K charged-current atmospheric neutrino events, with the e -like and μ -like data samples of sub- and multi-GeV contained events grouped into 10 zenith-angle bins, with 5 angular bins of stopping muons and 10 through-going bins of up-going muons [5]. Multi-ring μ and neutral-current events and ν_τ appearance are not used, since an efficient Monte-Carlo simulation of these data would require further details of the Super-K experiment, in particular of the way the neutral-current signal is extracted from the data. As far as atmospheric neutrino fluxes are concerned, the analysis of [12] employs state-of-the-art three-dimensional calculations given in [17].

The disappearance of ν_μ 's over a long-baseline probing the same Δm^2 region relevant for atmospheric neutrinos is now available from accelerator neutrino oscillation experiments, such as the KEK to Kamioka (K2K) neutrino oscillation experiment and the MINOS Experiment using the NuMI Beamline facility at Fermilab.

Neutrinos produced by a 12 GeV proton beam from the KEK proton synchrotron consist of 98% muon neutrinos with a mean energy of 1.3 GeV. The beam is controlled by a near detector 300 m away from the proton target. Comparing these near detector data with the ν_μ content of the beam observed by the Super-K detector at a distance of 250 km gives information on neutrino oscillations.

The K2K collaboration has published details of the analysis of their full data sample (K2K-I and K2K-II) [119]. The data have been taken in the period from June 1999 to November 2004 and correspond to 0.922×10^{20} p.o.t. Without oscillations $158_{-8.6}^{+9.2}$ events are expected whereas only 112 events have been observed. Out of these, 58 events are single-ring events where the reconstruction of the neutrino energy is possible. These events have been used in order to perform a spectral analysis of the K2K data, as described in Ref. [12].

The first MINOS results were released in 2006. MINOS is a long-baseline experiment that searches for ν_μ disappearance in a neutrino beam with a mean energy of 3 GeV produced at Fermilab. It consists of a near detector, located at 1 km from the neutrino source and a far detector located at the Soudan Mine, at 735 km from Fermilab. First data corresponding to 0.93×10^{20} p.o.t. [117], have comparable weight as the final K2K data sample. In the absence of oscillations 177 ± 11 ν_μ events with $E < 10$ GeV are expected, whereas 92 have been observed, which provides a 5.0σ evidence for disappearance. New experimental data have been released by the MINOS Collaboration. These have been collected from June 2006 to July 2007 (Run-IIa), and they have been analyzed together with the first data sample (Run-I), with a total exposure of 2.5×10^{20} p.o.t. In total, 563 ν_μ events have been observed at the far detector, while 738 ± 30 events were expected for no oscillation.

One finds that the values of the oscillation parameters from the ν_μ disappearance results at MINOS are consistent with the ones from K2K, as well as from Super-K atmospheric data, providing strong terrestrial confirmation of oscillations with Δm_{ATM}^2 with accelerator neutrinos. Statistics of the current data sample still does not strongly constrain the mixing angle. However, although the determination of $\sin^2 \theta_{\text{ATM}}$ is completely dominated by atmospheric data, K2K and MINOS data give an important restriction on the allowed Δm_{ATM}^2 values [12]. They constrain Δm_{ATM}^2 from below, which is important for further future long-baseline experiments, since their sensitivities are drastically affected if Δm_{ATM}^2 lies in the lower part of the 3σ range indicated by current atmospheric data. Note that there is currently no sensitivity to the sign of the atmospheric mass-squared splitting, this being one of the challenges for upcoming experiments.

5.3 Status of three-neutrino oscillations

The three-neutrino oscillation parameters that follow from the global analysis of neutrino oscillation data have been reviewed by Maltoni et al in Ref. [12]. An update of the results of this analysis

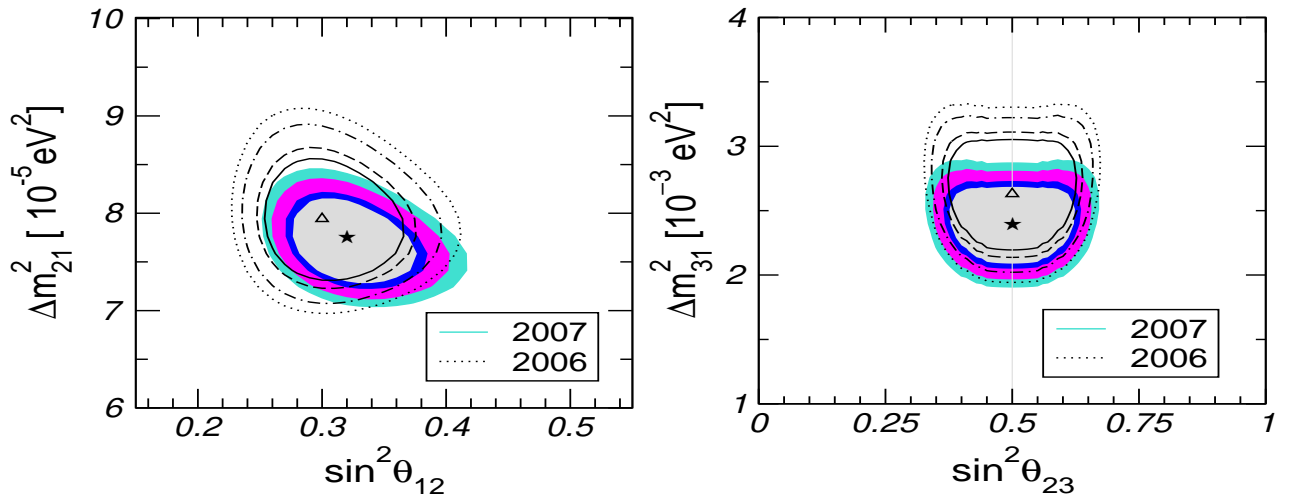


Figure 15: Current regions of neutrino oscillation parameters allowed by the world’s neutrino oscillation data at 90%, 95%, 99%, and 3σ C.L. for 2 d.o.f. from Ref. [12]. Shaded regions include 2007 data, while the empty regions correspond to results before the latest update.

can be found in the arXiv as version 6 of hep-ph/0405172. This update includes the latest relevant experimental data, as well as the latest update of the SSM of Bahcall et al (for references see Appendix C in hep-ph/0405172-v6). The results are summarized in Figs. 15 and 16 as well as in the Table.

The plots shown in Fig. 15 are two-dimensional projections of the allowed regions in the five-dimensional parameter space. The left panel in Fig. 15 gives the allowed regions of the “solar” neutrino oscillation parameters ($\sin^2\theta_{12}, \Delta m_{21}^2$). One sees the important role of the 2007 KamLAND data in providing an improved determination of both parameters, especially the mass squared splitting, now displayed on a linear scale. In the right panel of Fig. 15 we give the allowed regions of the “atmospheric” parameters ($\sin^2\theta_{23}, \Delta m_{31}^2$) also on a linear scale. In addition to a confirmation of oscillations with Δm_{ATM}^2 with accelerator neutrinos, these data provide a better determination of Δm_{ATM}^2 with little impact on the other parameters. Indeed, one can see from the figure that the inclusion of the MINOS data is crucial in the determination of Δm_{ATM}^2 . We see how accelerator data are starting to play the main role in the determination of the “atmospheric” splitting, a trend which will become stronger in the future. The best fit values and the allowed 3σ ranges of the oscillation parameters from the global data are summarized in the Table.

The left panel in Fig. 16 gives the parameter α , namely the ratio of solar over atmospheric splittings, as determined from the global χ^2 analysis. The right panel in Fig. 16 illustrates how the bound on $\sin^2\theta_{13}$ emerges from the interplay of different data samples. The plot shows the upper bound on $\sin^2\theta_{13}$ as a function of Δm_{ATM}^2 from CHOOZ data alone and compares to the bound obtained from an analysis including also solar and reactor neutrino data. One sees that, although for larger Δm_{ATM}^2 values the bound on $\sin^2\theta_{13}$ is dominated by CHOOZ, this bound deteriorates quickly as Δm_{ATM}^2 decreases, so that for $\Delta m_{\text{ATM}}^2 \lesssim 2 \times 10^{-3} \text{eV}^2$ the solar and KamLAND data become relevant.

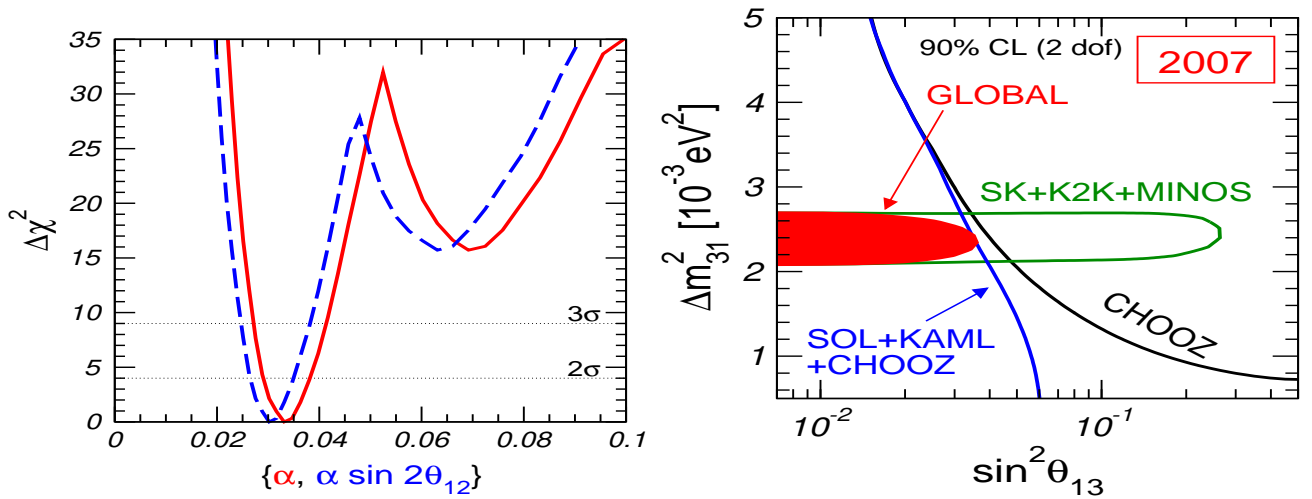


Figure 16: Current determination of $\alpha \equiv \Delta m_{\text{SOL}}^2 / \Delta m_{\text{ATM}}^2$ and bound on $\sin^2 \theta_{13}$ from the world's neutrino oscillation data, from Ref. [12].

parameter	best fit	2σ	3σ
$\Delta m_{21}^2 [10^{-5} \text{eV}^2]$	7.6	7.3–8.1	7.1–8.3
$\Delta m_{31}^2 [10^{-3} \text{eV}^2]$	2.4	2.1–2.7	2.0–2.8
$\sin^2 \theta_{12}$	0.32	0.28–0.37	0.26–0.40
$\sin^2 \theta_{23}$	0.50	0.38–0.63	0.34–0.67
$\sin^2 \theta_{13}$	0.007	≤ 0.033	≤ 0.050

Table I: Best-fit values, 2σ and 3σ intervals (1 d.o.f.) for the three-flavour neutrino oscillation parameters from global data including solar, atmospheric, reactor (KamLAND and CHOOZ) and accelerator (K2K and MINOS) experiments.

In summary, we find the following bounds at 90% C.L. (3σ) for 1 d.o.f.:

$$\sin^2 \theta_{13} \leq \begin{cases} 0.051 (0.084) & (\text{solar+KamLAND}) \\ 0.028 (0.059) & (\text{CHOOZ+atmospheric+K2K+MINOS}) \\ 0.028 (0.050) & (\text{global data}) \end{cases} \quad (61)$$

5.4 Predicting neutrino oscillation parameters

As we saw in Sec. 5 only five of the basic parameters of the lepton sector are currently probed in neutrino oscillation studies [2, 3, 4, 5, 6] [14, 15]: the angle θ_{12} and the splitting Δm_{SOL}^2 , which are determined from solar and KamLAND data, together with the angle θ_{23} and the corresponding mass squared splitting Δm_{ATM}^2 determined by atmospheric and accelerator data.

Out of the five neutrino oscillation parameters in the three–neutrino leptonic mixing matrix, two play a key role for future CP violation studies in neutrino oscillation experiments: the third “small” angle θ_{13} , together with the ratio of solar to atmospheric splittings, derived from the oscillation analysis. These are given in Fig. 16.

As we have seen, current neutrino data point towards a well defined pattern of neutrino mixing angles, quite distinct from that of quarks. The data seem to indicate an intriguing complementarity between the angles that characterize the quark and lepton mixing matrices [120, 121, 122, 123]. It is not clear whether this numerical coincidence has a deeper meaning.

Some “flavour–blind” gauge models have the interesting feature of “accidentally” predicting a zero neutrino mass. For example, due to the anti-symmetry of the one of the Yukawa coupling matrices, the radiative models [50, 51] considered in Sec. 3.2.1 predict that one of the neutrinos is massless. Similarly for the model considered in Ref. [30]. These are rather exceptional examples and the predictions obtained are incomplete and/or problematic, such as those of the simplest Zee model [50] which also include a nearly maximal solar mixing angle, now in conflict with observation. This illustrates that, typically, gauge symmetry by itself is not sufficient to predict masses and mixings, neither for quarks, nor for leptons.

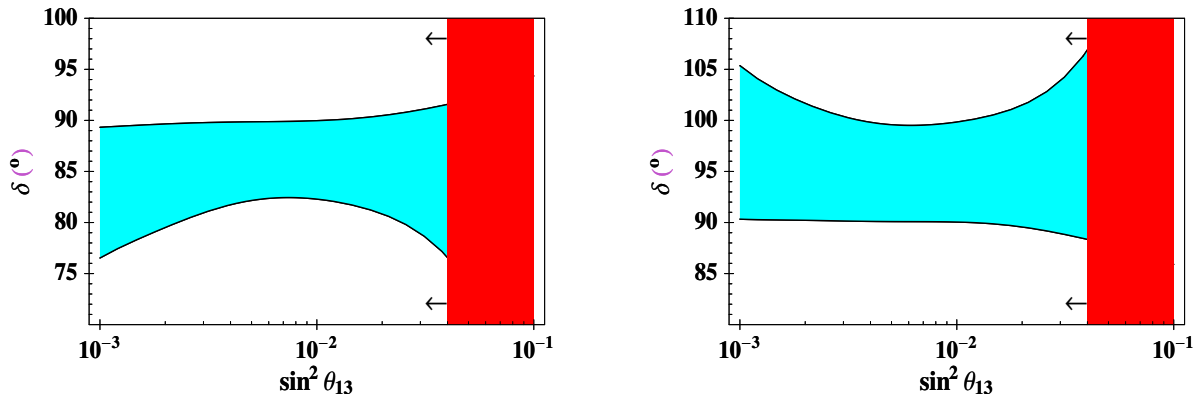


Figure 17: Near maximal CP violation in neutrino oscillations, as predicted in Ref. [133].

There has been a rush of papers attempting to understand the values of the leptonic mixing angles from underlying symmetries at a fundamental level. For example one can account for the maximum mixing in atmospheric neutrino oscillation, as well as vanishing of the θ_{13}

$$\theta_{23} = \pi/4 \quad \text{and} \quad \theta_{13} = 0 \tag{62}$$

in terms of a mu-tau symmetry, under which the neutrino mass matrix is invariant under the interchange of second and third generation neutrinos [124]. Other models with Z_2 symmetries have been considered [125]. For example, in [126] one such symmetry has been considered leading to a maximal atmospheric mixing angle θ_{23} , its breaking inducing a nonzero value of θ_{13} in a way that strongly depends on the neutrino mass hierarchy.

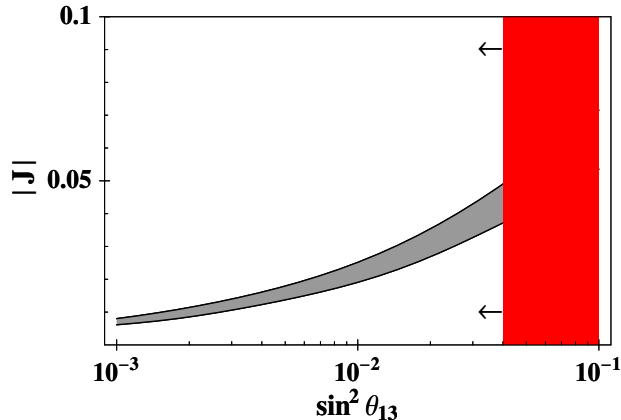


Figure 18: Magnitude of CP violation invariant in neutrino oscillations, as predicted in Ref. [133].

More generally, it has been argued that the form of the mixing at high energies could be [127]

$$\begin{aligned}
 \tan^2 \theta_{\text{ATM}} &= \tan^2 \theta_{23}^0 = 1 \\
 \sin^2 \theta_{\text{Chooz}} &= \sin^2 \theta_{13}^0 = 0 \\
 \tan^2 \theta_{\text{SOL}} &= \tan^2 \theta_{12}^0 = 0.5
 \end{aligned}
 \tag{63}$$

Such Harrison-Perkins-Scott pattern of lepton mixing [128] could result from some kind of flavour symmetry, valid at a very high energy scale where the dimension-five neutrino mass operator arises.

One idea is that neutrino masses arise from a common seed at some “neutrino mass unification” scale M_X [129], very similar the merging of the gauge coupling constants at high energies due to supersymmetry [130]. Unfortunately in its simplest (CP conserving) form this very simple theoretical ansatz is inconsistent with the significantly non-maximal value of the solar mixing angle θ_{12} inferred from current data [12].

A more satisfactory and fully viable alternative realization of the “neutrino mass unification” idea employs an A_4 flavour symmetry in the context of a seesaw scheme [70]. Starting from three-fold degeneracy of the neutrino masses at a high energy scale, a viable low energy neutrino mass matrix can indeed be obtained. The model predicts maximal atmospheric angle and vanishing θ_{13} , as in Eq. (62). Moreover, if CP is violated θ_{13} becomes arbitrary but the Dirac CP violation phase is maximal [131]. The solar angle θ_{12} is unpredicted. However, one expects it to be large,

$$\theta_{12} = \mathcal{O}(1).$$

(There have been variant realizations of the A_4 symmetry that enable one to predict the solar angle, see, for example Ref. [132]). Within such A_4 flavour symmetry seesaw scheme one can show that the lepton and slepton mixings are intimately related. It was shown that the resulting slepton spectrum must necessarily include at least one mass eigenstate below 200 GeV, which can be produced at the LHC. The prediction for the absolute Majorana neutrino mass scale

$$m_0 \geq 0.3\text{eV}$$

ensures that the model will be tested by future cosmological tests and $\beta\beta_{0\nu}$ searches. Rates for lepton flavour violating processes $\ell_j \rightarrow \ell_i + \gamma$ in the range of sensitivity of current experiments are typical in the model, with $\text{BR}(\mu \rightarrow e\gamma) \gtrsim 10^{-15}$ and the lower bound $\text{BR}(\tau \rightarrow \mu\gamma) > 10^{-9}$.

A variant A_4 flavour symmetry seesaw model has been suggested [133] which predicts a direct correlation between the expected magnitude of CP violation in neutrino oscillations and the value of $\sin^2 \theta_{13}$. The model leads to nearly maximal leptonic CP violation in neutrino oscillations through the CP phase δ . These predictions are illustrated in Figs. 17 and 18. For a discussion of various schemes to derive the neutrino mixing matrix using the tetrahedral group A_4 was given in Ref. [134].

Also discrete flavour groups of the D_n series have been used. For example, seesaw models for the lepton sector using D_4 and S_3 family symmetries have been suggested in [135]. The model predicts a normal hierarchy neutrino mass spectrum with the mixing angle $\theta_{13} = 0$ and an unpredicted solar mixing angle θ_{12} . It employs an enlarged Higgs scalar sector, so that the atmospheric mixing angle θ_{23} is given as a ratio of Higgs scalar vevs, and it is maximal if the full Lagrangian is D_4 -invariant. The deviation of θ_{23} from $\pi/4$ is governed by the strength of the soft breaking of the D_4 symmetry.

Other non-Abelian finite subgroups of $SU(3)$ have also been used as family symmetries and shown to generate tri-bimaximal mixing in the neutrino sector, while allowing for quark and charged lepton hierarchies [136]. Many attempts at predicting lepton mixing angles employ the Harrison-Perkins-Scott mixing pattern in Eq. (63) at some high energy scale [137]. Typically one must correct predictions made at a high scale by renormalization group evolution [138]. In this connection the idea of tri-bimaximal neutrino mixing has also been considered in the context of discrete symmetries in models with extra dimensions [139].

In short, progress made in the experimental determination of neutrino parameters has already ruled out many of the proposed models. For example, many interesting attempts have failed simply because the solar mixing angle has been shown to be large but significantly non-maximal [12].

Note that understanding the observed pattern of masses and mixings in the quark and lepton sector separately in the context of a non-unified model by appealing to suitable flavour symmetries is a relatively feasible challenge. However, in a unified model where quarks and leptons sit in the same multiplets, there is a tendency to correlate the corresponding mixing angles. In a “generic” flavour-blind unified model the lepton and quark mixing angles can always be reconciled thanks to the large number of parameters involved. For example, we have seen how in general seesaw-type models the leptonic mass matrices involves couplings which are absent for the quarks. Even in the simplest type-I seesaw mechanism discussed in Sec. 3.1 the B-L violating terms bring in their own independent flavor structure, distinct from that of the Dirac mass term which is restricted by the quark sector. Acceptable mixing patterns can certainly be accommodated, but not predicted. To achieve some degree of predictivity one must appeal to additional symmetries, beyond the gauge symmetry, realized at the unified level and suitably chosen so as to restrict the flavour “textures”. This constitutes a rather demanding challenge, so far not achieved with full success. Despite some progress on how to obtain successful unified models of flavour [140] using discrete non-abelian groups, we currently lack a fully satisfactory unified theory

of flavour, and it is likely that the “flavour problem” will indeed remain with us for a while.

6 CP violation in neutrino oscillations

In gauge theories of neutrino masses, the lepton mixing matrix typically contains a number of CP violating phases that may affect neutrino oscillations [7]. In this section, we discuss theoretical aspects of CP violation in neutrino oscillations and the possibility of probing it experimentally at future searches.

It has been recognized for a long time that the Dirac CP violating phase present in the simplest three-neutrino model could in principle be observed in neutrino oscillation experiments [20]. These are likely to be the most promising way to probe directly the Dirac CP phase present in the neutrino mixing matrix, unless θ_{13} is too small. If CPT is conserved violation of CP implies that of T. In this review, we do not consider the possible violation of CPT in the neutrino sector ⁴. Earlier works around 1980 on CP and/or T violation can be found in Refs. [7], [24, 25, 26] and [143, 144]. It has now been understood that the difference between oscillation probabilities for neutrino and anti-neutrino is proportional to the leptonic analogue of the CP-invariant factor of the quark sector [145]. In the last decade, CP violation in neutrino oscillation has received enormous amount of attention in the community [146, 147, 148, 149, 150, 151, 152, 153, 154, 155, 156, 157]. Here we consider three active neutrinos without sterile neutrino [158, 159, 160] which have been invoked in connection with LSND and MiniBoone data [10, 11].

In this review, in order keep the discussion as much general as possible, we do not show any kind of sensitivity plots for specific planned experiment or project, but try to keep the discussion at the level of neutrino oscillation probabilities.

6.1 Preliminaries

The simplest measure of CP violation, which is equivalent to T violation if CPT is conserved, would be the difference of oscillation probabilities between neutrinos and anti-neutrinos, $P(\nu_\alpha \rightarrow \nu_\beta)$ and $P(\bar{\nu}_\alpha \rightarrow \bar{\nu}_\beta)$, which is given by [143, 144],

$$\Delta P_{\nu\bar{\nu}\alpha\beta} \equiv P(\nu_\alpha \rightarrow \nu_\beta) - P(\bar{\nu}_\alpha \rightarrow \bar{\nu}_\beta) = -16J_{\alpha\beta} \sin \Delta_{12} \sin \Delta_{23} \sin \Delta_{31}, \quad (64)$$

where we used the notation, $\Delta_{ij} \equiv \Delta m_{ij}^2 L/4E$ and

$$J_{\alpha\beta} \equiv \Im(U_{\alpha 1} U_{\alpha 2}^* U_{\beta 1}^* U_{\beta 2}) = \pm J, \quad J \equiv s_{12} c_{12} s_{23} c_{23} s_{13} c_{13}^2 \sin \delta \quad (65)$$

with positive (negative) sign for (anti-)cyclic permutation of the flavor indices e , μ and τ . The parameter J is the leptonic analogue of the CP-invariant factor for quarks, the unique and phase-convention-independent measure for CP violation [145].

⁴See e.g. [141, 142] for such a possibility.

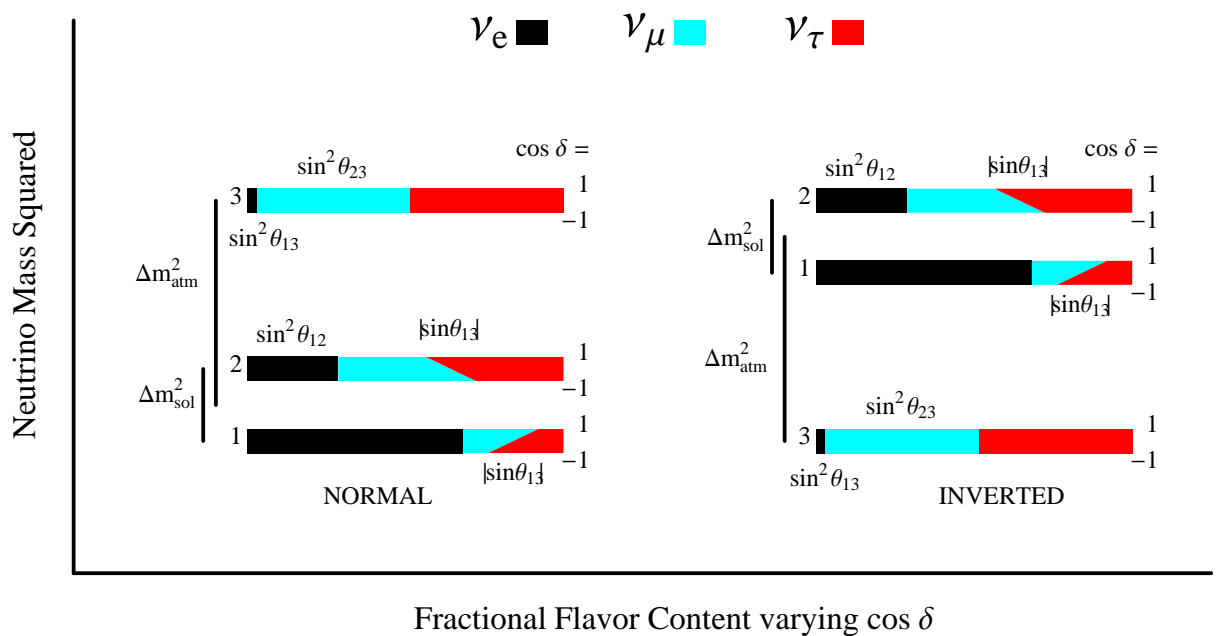


Figure 19: The range of probability of finding the α -flavor in the i -th mass eigenstate as indicated for the two different mass hierarchies for the best fit values of the solar and atmospheric mixing parameters, $\sin^2 2\theta_{13} = 0.1$ as the CP-violating phase, δ is varied, extracted from [161].

Since we do not yet know the value of δ and θ_{13} , the current neutrino data give only an upper bound on this quantity, as $J \lesssim 0.04$. Although we do not yet know whether the mass hierarchy is normal or inverted this will not cause an ambiguity in the vacuum ΔP , as it does not depend on the hierarchy ⁵.

Where we can expect to observe the effect of CP violation? In contrast with CP violation induced by Majorana phases, which occurs even for two generations of neutrinos [7], CP violation in neutrino oscillations is a genuine three (or more) flavor effect, so it can be observed only when there is an interference between flavor oscillations involving at least two different Δm^2 and three mixing angles, as we will see below. We observe that the accelerator based neutrino oscillation experiments will provide the most promising opportunities to observe such CP violation. This will be extensively discussed in what follows.

From the expression in Eq. (64), it is clear that there is no CP (or T) violation for three generation neutrino mixing in vacuum if $\delta = 0$ or π and

- one (or more) of the mixing angles is zero,
- two or more of the masses are degenerate.

Moreover, note that it is impossible to observe CP violation in the disappearance channels ($\alpha = \beta$) since $\nu_\alpha \rightarrow \nu_\alpha$ is related to $\bar{\nu}_\alpha \rightarrow \bar{\nu}_\alpha$ by CPT. Finally, there is no CP violation if the solar oscillations are averaged out.

⁵Strictly speaking, even in vacuum, the oscillation probability for normal and inverted hierarchy differ and give a tiny effect, but we do not consider such a effect in this review, see [162].

While ΔP defined in Eq.(64) vanishes for the disappearance channels,

$$\begin{aligned} P(\nu_\alpha \rightarrow \nu_\alpha) &= P(\bar{\nu}_\alpha \rightarrow \bar{\nu}_\alpha) \\ &= 1 - 4|U_{\alpha 1}|^2|U_{\alpha 2}|^2 \sin^2 \Delta_{21} - 4|U_{\alpha 2}|^2|U_{\alpha 3}|^2 \sin^2 \Delta_{32} - 4|U_{\alpha 3}|^2|U_{\alpha 1}|^2 \sin^2 \Delta_{31}, \end{aligned} \quad (66)$$

by CPT (hence no direct CP violation), the $\nu_\mu \rightarrow \nu_\mu$ and $\nu_\tau \rightarrow \nu_\tau$ disappearance probabilities depends on $\cos \delta$, using our parametrization of the mixing matrix⁶. Given that if one knows $\cos \delta$ one also knows the magnitude of $\sin \delta$ up to a sign, can this be used to say anything about leptonic CP violation? In principle, the answer is yes. However it requires precision measurements in two out of the three disappearance channels so that one can determine precisely the magnitude of four independent elements of the mixing matrix.

Suppose that one has measured $|U_{e2}|, |U_{e3}|, |U_{\mu 2}|$ and $|U_{\mu 3}|$ precisely, then from unitarity one knows the moduli of all the elements of the mixing matrix. Construct the triangle which has sides with length $|U_{e1}||U_{\mu 1}|, |U_{e2}||U_{\mu 2}|$ and $|U_{e3}||U_{\mu 3}|$, as shown in Fig. 20. This triangle must close due to the following unitarity relation

$$U_{e1}^* U_{\mu 1} + U_{e2}^* U_{\mu 2} + U_{e3}^* U_{\mu 3} = 0. \quad (67)$$

Now, twice the area of this triangle is the absolute value of the CP-invariant factor⁷. Using the rule relating the length of the sides to the area of the triangle, we have

$$\begin{aligned} J^2 &= \frac{1}{4} [|U_{e1}||U_{\mu 1}| + |U_{e2}||U_{\mu 2}| + |U_{e3}||U_{\mu 3}|] \times [-|U_{e1}||U_{\mu 1}| + |U_{e2}||U_{\mu 2}| + |U_{e3}||U_{\mu 3}|] \\ &\quad \times [|U_{e1}||U_{\mu 1}| - |U_{e2}||U_{\mu 2}| + |U_{e3}||U_{\mu 3}|] \times [|U_{e1}||U_{\mu 1}| + |U_{e2}||U_{\mu 2}| - |U_{e3}||U_{\mu 3}|]. \end{aligned} \quad (68)$$

The maximum possible difference in the lengths of the two sides, $|U_{e1}||U_{\mu 1}|$ and $|U_{e2}||U_{\mu 2}|$ is $|U_{e3}||U_{\mu 3}|$. At these extrema, the triangle fits on a line and has zero area and CP is conserved. Thus, to claim CP violation one must show at the required confidence level that $||U_{e1}||U_{\mu 1}| - |U_{e2}||U_{\mu 2}|| < |U_{e3}||U_{\mu 3}|$. Given that $|U_{e3}|$ is known to be small [12] and is yet unobserved, this will be a formidable challenge. The sign of J or equivalently the sign of CP violation cannot be determined from vacuum disappearance measurements.

Note that the center of the circle in the triangle diagram bi-sects the $|U_{e3}||U_{\mu 3}|$ side in the ratio of $|U_{e2}|^2 : |U_{e1}|^2$ from left to right. (This is equivalent to holding the “(1,2)” vertex fixed and rotating the “3” side about the same point.) Using the PDG parametrization of the lepton mixing matrix, the base of this triangle is $s_{13}c_{13}s_2$ and the height $c_{13}s_{12}c_{12}c_{23}|\sin \delta|$. The angle ω equals δ or $2\pi - \delta$.

The CP-invariant factor for any density matter is given by $J(N) \equiv (s_{12}c_{12}s_{23}c_{23}s_{13}c_{13}^2 \sin \delta)_N$, where the mixing angles and CP phase are their values in matter, obtained by writing $U(N)$ in the form of Eq. (53). The matter value of the CP-invariant factor is related to the vacuum value as follows [163]:

$$J(N) = \frac{\Delta m_{21}^2 \Delta m_{32}^2 \Delta m_{31}^2}{\Delta m_{21}^2(N) \Delta m_{32}^2(N) \Delta m_{31}^2(N)} J. \quad (69)$$

⁶Since $|U_{\mu 1}|^2, |U_{\mu 2}|^2, |U_{\tau 1}|^2$ and $|U_{\tau 2}|^2$ depend on $\cos \delta$, e.g. $|U_{\mu 2}|^2 = c_{23}^2 c_{12}^2 + s_{13}^2 s_{23}^2 s_{12}^2 - 2c_{12}s_{12}c_{23}s_{23}s_{13}c_{13} \cos \delta$.

⁷All other unitarity triangles have the same area.

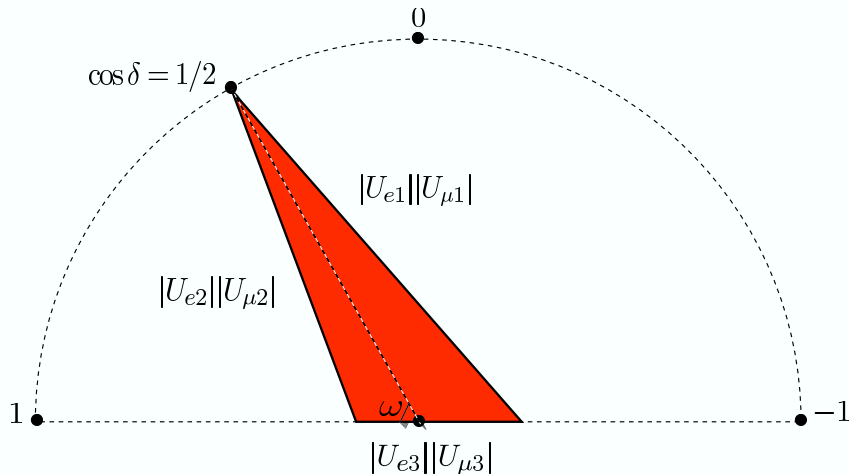


Figure 20: The unitarity triangle using the first and second rows of the mixing matrix. The lengths of each side are as labeled and twice the area of this triangle is the absolute value of the CP-invariant factor, $|J|$. The $|U_{e1}||U_{\mu1}|$ and $|U_{e2}||U_{\mu2}|$ vertex moves in a circle as the CP violating phase is changed.

This identity guarantees that the ΔP in Eq.(64) is the same in matter as in vacuum for distances smaller than any of the matter or vacuum oscillation lengths.

6.2 The oscillation probability $\nu_\mu \rightarrow \nu_e$

In this review, we mainly focus on the oscillation channel between electron and muon neutrinos because it is easier to create and detect these neutrinos compared to tau neutrinos. The drawing below shows schematically the relation among four possible channels.

$$\begin{array}{ccccc}
 & & & & \text{CP} \\
 & & & & \\
 \nu_\mu \rightarrow \nu_e & \iff & \bar{\nu}_\mu \rightarrow \bar{\nu}_e & & \\
 \text{T} & \iff & & \iff & \text{T} \\
 \nu_e \rightarrow \nu_\mu & \iff & \bar{\nu}_e \rightarrow \bar{\nu}_\mu & & \\
 & & & & \text{CP}
 \end{array}$$

The horizontal (vertical) processes are related by CP (T) whereas the processes across the diagonals are related by CPT. The first row will be explored in very powerful conventional beams, Superbeams, whereas the second row could be explored in Neutrino Factories or Beta Beams.

6.2.1 Vacuum: $\nu_\mu \rightarrow \nu_e$

Let us first consider oscillation in vacuum ignoring matter effect. The transition probability $\nu_\mu \rightarrow \nu_e$ can be simply written as the square of a sum of three amplitudes, one associated with each neutrino mass eigenstate, as follows [164],

$$\begin{aligned} P(\nu_\mu \rightarrow \nu_e) &= |U_{\mu 3}^* e^{-im_3^2 L/2E} U_{e3} + U_{\mu 2}^* e^{-im_2^2 L/2E} U_{e2} + U_{\mu 1}^* e^{-im_1^2 L/2E} U_{e1}|^2 \\ &= |2U_{\mu 3}^* U_{e3} \sin \Delta_{31} e^{-i\Delta_{32}} + 2U_{\mu 2}^* U_{e2} \sin \Delta_{21}|^2, \end{aligned} \quad (70)$$

where the unitarity of the lepton mixing matrix [1] has been used to eliminate the $U_{\mu 1}^* U_{e1}$ term and Δ_{jk} is used as a shorthand for the kinematic phase, $\Delta m_{jk}^2 L/4E$. It is convenient to rewrite this expression as follows

$$\begin{aligned} P(\nu_\mu \rightarrow \nu_e) &\approx |\sqrt{P_{\text{atm}}} e^{-i(\Delta_{32} + \delta)} + \sqrt{P_{\text{sol}}}|^2 \\ &= P_{\text{atm}} + 2\sqrt{P_{\text{atm}}}\sqrt{P_{\text{sol}}}\cos(\Delta_{32} + \delta) + P_{\text{sol}}, \end{aligned} \quad (71)$$

where as the notation suggests the amplitude $\sqrt{P_{\text{atm}}}$ depends only on Δm_{31}^2 and $\sqrt{P_{\text{sol}}}$ depends only on Δm_{21}^2 . For propagation in the vacuum, these amplitudes are simply given by

$$\begin{aligned} \sqrt{P_{\text{atm}}} &\equiv \sin \theta_{23} \sin 2\theta_{13} \sin \Delta_{31} \\ \sqrt{P_{\text{sol}}} &\equiv \cos \theta_{23} \cos \theta_{13} \sin 2\theta_{12} \sin \Delta_{21} \approx \cos \theta_{23} \cos \theta_{13} \sin 2\theta_{12} \Delta_{21}, \end{aligned} \quad (72)$$

where θ_{13} and Δ_{21} are assumed to be small. In the amplitude $\sqrt{P_{\text{sol}}}$, terms proportional to $\sin \theta_{13} \sin \Delta_{21} e^{-i\delta}$ have been neglected since they are of second order in the small quantities $\sin \theta_{13}$ and Δ_{21} .

For anti-neutrinos $\delta \rightarrow -\delta$. Thus the phase between $\sqrt{P_{\text{atm}}}$ and $\sqrt{P_{\text{sol}}}$ changes from $(\Delta_{32} + \delta)$ to $(\Delta_{32} - \delta)$. This changes the interference term from

$$2\sqrt{P_{\text{atm}}}\sqrt{P_{\text{sol}}}\cos(\Delta_{32} + \delta) \rightarrow 2\sqrt{P_{\text{atm}}}\sqrt{P_{\text{sol}}}\cos(\Delta_{32} - \delta). \quad (73)$$

Expanding $\cos(\Delta_{32} \pm \delta)$, one has a CP conserving part,

$$2\sqrt{P_{\text{atm}}}\sqrt{P_{\text{sol}}}\cos \Delta_{32} \cos \delta, \quad (74)$$

and the CP violating part,

$$\mp 2\sqrt{P_{\text{atm}}}\sqrt{P_{\text{sol}}}\sin \Delta_{32} \sin \delta, \quad (75)$$

where - (+) sign is for neutrino (anti-neutrino). This implies that ΔP given in Eq. (64) can be rewritten as

$$\Delta P_{\nu\bar{\nu}} \equiv P(\nu_\mu \rightarrow \nu_e) - P(\bar{\nu}_\mu \rightarrow \bar{\nu}_e) = -4\sqrt{P_{\text{atm}}}\sqrt{P_{\text{sol}}}\sin \Delta_{32} \sin \delta. \quad (76)$$

Note that this expression coincides with the exact formula in Eq. (64) because terms we neglected in Eqs. (71) and (72) do not contribute to the CP violating term.

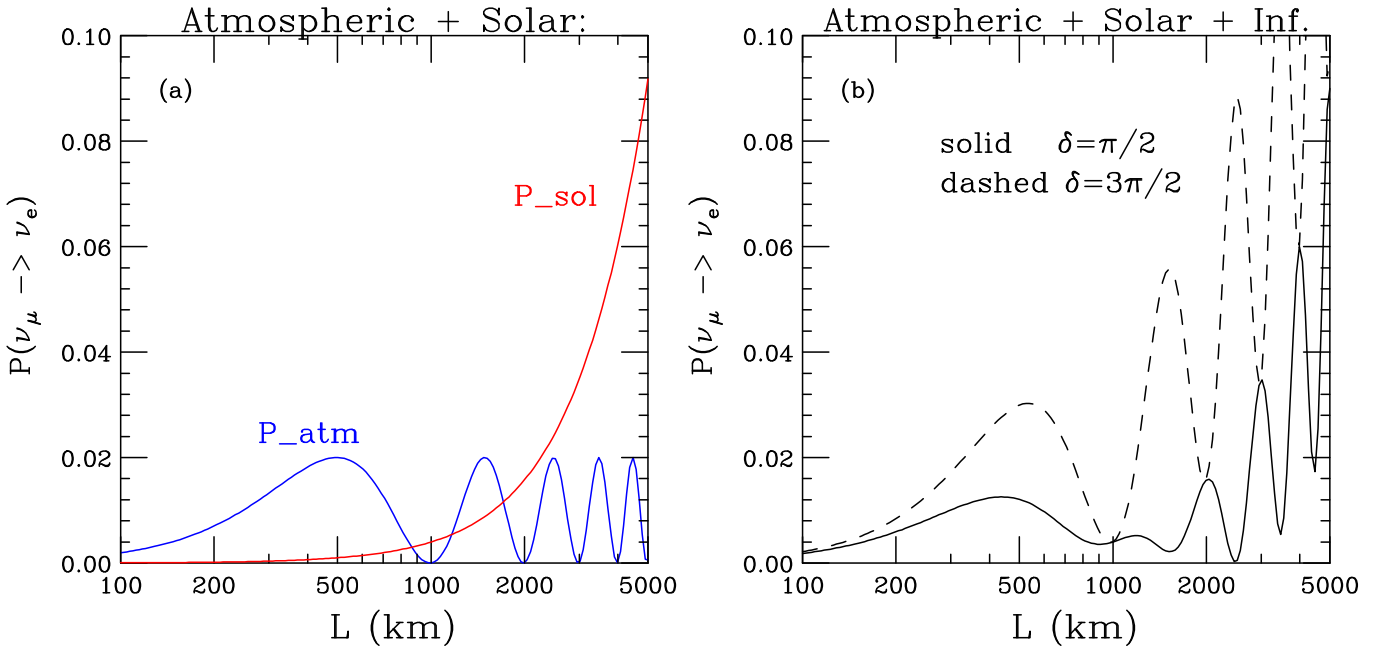


Figure 21: The probability $P(\nu_\mu \rightarrow \nu_e)$: (a) The components P_{atm} and P_{sol} , (b) The full probability including the interference term for $\delta = \frac{\pi}{2}$ and $\frac{3\pi}{2}$, solid and dashed respectively. Since $\frac{3\pi}{2} = -\frac{\pi}{2} + 2\pi$ we have $P(\nu_\mu \rightarrow \nu_e, \delta = \frac{3\pi}{2}) = P(\bar{\nu}_\mu \rightarrow \bar{\nu}_e, \delta = \frac{\pi}{2})$ so that these two probabilities can be considered to be $P(\nu_\mu \rightarrow \nu_e, \delta = \frac{\pi}{2})$ (solid) and $P(\bar{\nu}_\mu \rightarrow \bar{\nu}_e, \delta = \frac{\pi}{2})$ (dashed). The difference between these two curves demonstrates CP violation for this process.

Therefore CP violation is maximum when $\Delta_{32} = (2n + 1)\frac{\pi}{2}$ and grows with n since $\sin \Delta_{21}$ grows with n . Notice also that, as expected, for CP violating term to be non-zero the kinematical phase Δ_{32} cannot be $n\pi$. This is the neutrino counter part to the non-zero strong phase requirement for CP violation in the quark sector.

Fig. 21 shows the components of $P(\nu_\mu \rightarrow \nu_e)$ as well as the full probability for selected values of the CP phase δ for neutrino energy $E = 1$ GeV. Unless otherwise stated, we fix the absolute value of Δm_{31}^2 to be 2.5×10^{-3} eV², $\Delta m_{21}^2 = 8.0 \times 10^{-5}$ eV², $\sin^2 \theta_{12} = 0.31$ [12]. Since we can use CP and T to relate all the processes discussed earlier in section we have

$$P(\nu_\mu \rightarrow \nu_e, \delta) = P(\bar{\nu}_\mu \rightarrow \bar{\nu}_e, -\delta) = P(\nu_e \rightarrow \nu_\mu, -\delta) = P(\bar{\nu}_e \rightarrow \bar{\nu}_\mu, \delta), \quad (77)$$

all given from Eq. (71).

In the left panel of Fig. 22 we show $\Delta P_{\nu\bar{\nu}}$ in vacuum as a function of L for $\delta = 0, \pi/2, \pi$ and $3\pi/2$ for $\sin^2 2\theta_{13} = 0.05$. As mentioned before, peak of $|\Delta P_{\nu\bar{\nu}}|$ occurs at $\Delta_{32} = (2n + 1)\frac{\pi}{2}$ growing linearly as n or L increases.

For a fixed value of δ , as θ_{13} becomes smaller, the absolute value of ΔP become smaller but this does not means that CP violation gets smaller. Consider the neutrino-anti-neutrino asymmetry, defined as

$$\mathcal{A} \equiv \frac{P - \bar{P}}{P + \bar{P}} = \frac{2\sqrt{P_{\text{atm}}}\sqrt{P_{\text{sol}}}\sin \Delta_{32}\sin \delta}{P_{\text{atm}} + 2\sqrt{P_{\text{atm}}}\sqrt{P_{\text{sol}}}\cos \Delta_{32}\cos \delta + P_{\text{sol}}}, \quad (78)$$

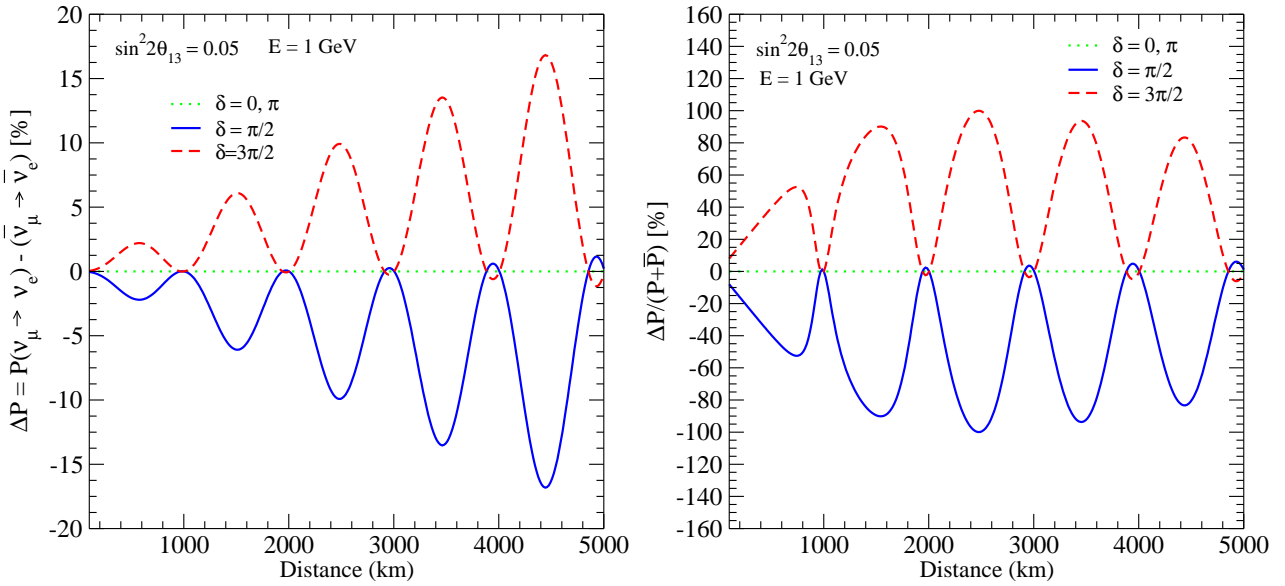


Figure 22: Examples of $\Delta P_{\nu\bar{\nu}} \equiv P(\nu_\mu \rightarrow \nu_e) - P(\bar{\nu}_\mu \rightarrow \bar{\nu}_e)$ (left panel) and the asymmetry $\Delta P/[P(\nu_\mu \rightarrow \nu_e) + P(\bar{\nu}_\mu \rightarrow \bar{\nu}_e)]$ (right panel) in vacuum as a function of distance for fixed value of energy, $E = 1$ GeV and $\sin^2 2\theta_{13} = 0.05$.

as a measure of CP violation. Then, at the vacuum oscillation maxima, $\Delta_{31} = (2n + 1)\frac{\pi}{2}$,

$$\mathcal{A} = \frac{2\sqrt{P_{\text{atm}}}\sqrt{P_{\text{sol}}}\sin\delta}{P_{\text{atm}} + P_{\text{sol}}}. \quad (79)$$

which is maximized when $\sqrt{P_{\text{atm}}} = \sqrt{P_{\text{sol}}}$. This occurs at

$$\sin^2 2\theta_{13} = \cot^2 \theta_{23} \sin^2 2\theta_{12} \sin^2 \Delta_{21} \approx \cot^2 \theta_{23} \sin^2 2\theta_{12} \left(\frac{\Delta m_{21}^2}{\Delta m_{31}^2} \right)^2 \Delta_{31}^2. \quad (80)$$

At the first vacuum oscillation maximum, $\Delta_{31} = \frac{\pi}{2}$, the peak in the asymmetry occurs when $\sin^2 2\theta_{13} \approx 0.002$. In the right panel of Fig. 22 we show the asymmetry in vacuum as a function of L for fixed value of $\sin^2 2\theta_{13} = 0.05$ and energy $E = 1$ GeV. As function of $\sin^2 2\theta_{13}$ the neutrino- anti-neutrino asymmetry is shown in Fig. 23. At the second vacuum oscillation maximum the asymmetry is maximum when $\sin^2 2\theta_{13}$ is 9 times larger.

Another feature of the probability that is important is the existence of zero mimicking solutions [165]. When,

$$\sqrt{P_{\text{atm}}} = -2\sqrt{P_{\text{sol}}}\cos(\Delta_{32} \pm \delta) \quad (81)$$

we have

$$P(\nu_\mu \rightarrow \nu_e) = P_{\text{sol}}. \quad (82)$$

Thus, even if $\sin^2 2\theta_{13} \neq 0$, when this condition is satisfied non-zero θ_{13} is impossible to observe. See Fig. 23 for examples of these “zero mimicking solutions”. The maximum value of $\sin^2 2\theta_{13}$ for which there are zero mimicking solutions is 4 times the value given in Eq. (80). Luckily, the zero mimicking solutions appear at different values of δ if E/L is changed or by switching to anti-neutrinos.

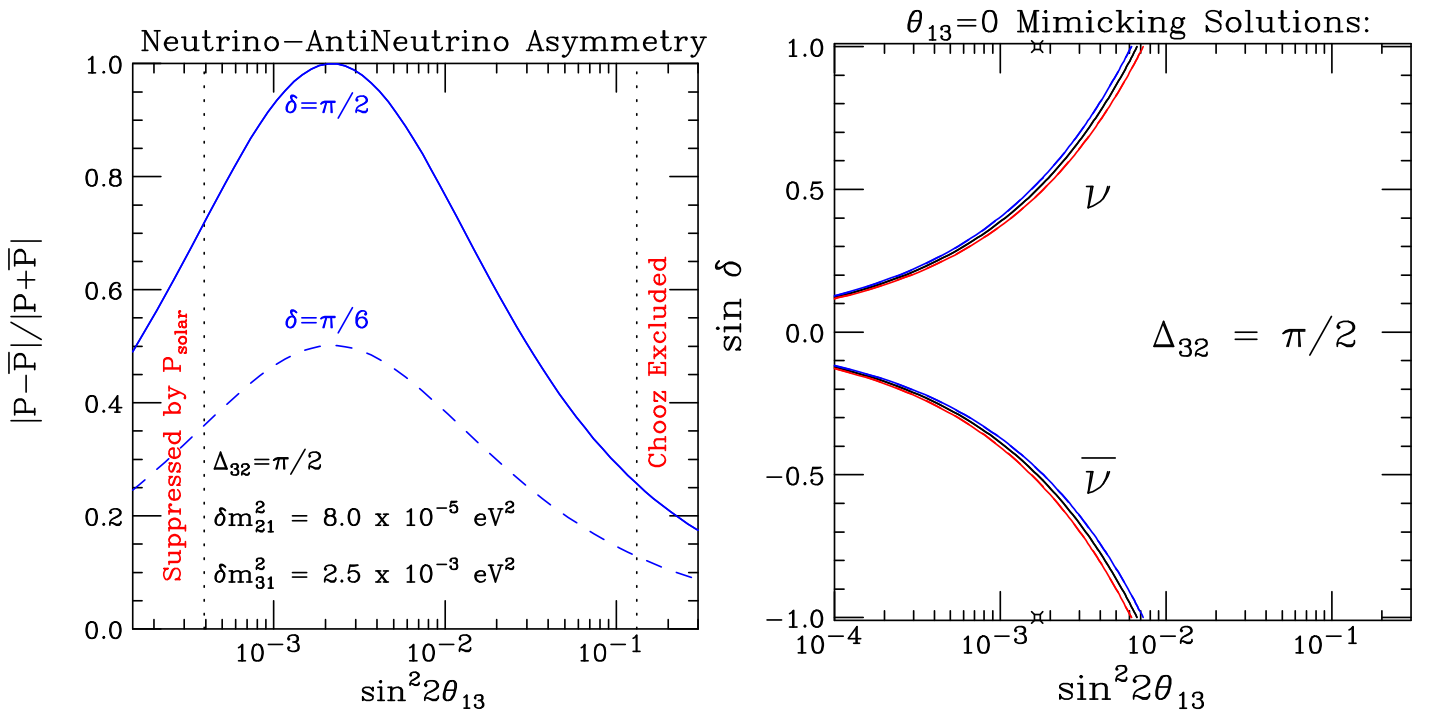


Figure 23: The left panel (a) shows the asymmetry between neutrino and anti-neutrinos as a function of $\sin^2 2\theta_{13}$. The peak occurs when $\sqrt{P_{\text{atm}}} = \sqrt{P_{\text{sol}}}$ at $\sin^2 2\theta_{13} \approx 0.002$. The right panel (b) shows the location of the zero mimicking solutions at the first oscillation maximum.

6.2.2 Matter: $\nu_\mu \rightarrow \nu_e$

In describing neutrino propagation in the Earth it is very important to take into account the effect of matter [18, 143, 19] because it can induce a fake CP violating effect even if the CP phase is zero or π . In matter of constant density, the two component appearance probability, P_{app}^N , using the mixing angle and mass squared difference in matter, θ_N and Δm_N^2 , is given by

$$P_{\text{app}}^N = \sin^2 2\theta_N \sin^2 \Delta_N \quad (83)$$

where $\Delta_N \equiv \Delta m_N^2 L / 4E$. Since $\Delta m_N^2 \sin 2\theta_N$ is independent of the density of matter i.e. it is an invariant, then

$$P_{\text{app}}^N = \sin^2 2\theta_0 \left(\frac{\sin^2 \Delta_N}{\Delta_N^2} \right) \Delta_0^2. \quad (84)$$

Note, that this expression does not depend on the mixing angle in matter, θ_N and that Δm_N^2 is given by

$$\Delta m_N^2 = \sqrt{(\Delta m_0^2 \cos 2\theta_0 - 2\sqrt{2}G_F N_e E)^2 + (\Delta m_0^2 \sin 2\theta_0)^2} \quad (85)$$

where G_F is the Fermi constant and N_e is the number density of electrons. Except near the resonance, $\Delta m_N^2 = \Delta m_0^2 - 2\sqrt{2}G_F N_e E$ is a good approximation. For matter effects to significantly alter the appearance probability the following condition must be satisfied, with the left and right hand side

significantly different

$$\frac{\sin^2 \Delta_N}{\Delta_N^2} \neq \frac{\sin^2 \Delta_0}{\Delta_0^2}. \quad (86)$$

That is, matter must significantly alter the Δm^2 so that $\Delta m_N^2 \neq \Delta m_0^2$ and the baseline of the experiment must be a significant fraction of the oscillation length in matter or vacuum whichever is shorter so that either $\sin \Delta_N \neq \Delta_N$ and/or $\sin \Delta_0 \neq \Delta_0$.

For the three neutrino case, nature has chosen two small parameters, $\sin^2 \theta_{13} \leq 0.04$ and $\Delta m_{21}^2 / \Delta m_{31}^2 \approx 0.03$ [12]; this allows us to factorize the three neutrino case into a product of two neutrino cases and therefore the individual Δm^2 in matter become

$$\begin{aligned} \Delta m_{31}^2|_N &\approx \Delta m_{31}^2 - 2\sqrt{2}G_F N_e E \\ \Delta m_{21}^2|_N &\approx -2\sqrt{2}G_F N_e E \\ \Delta m_{32}^2|_N &\approx \Delta m_{32}^2. \end{aligned} \quad (87)$$

In Fig. 25 we have plotted the exact mass squared differences in matter and the approximation given in Eq. (87) and indeed the approximation is a good one.

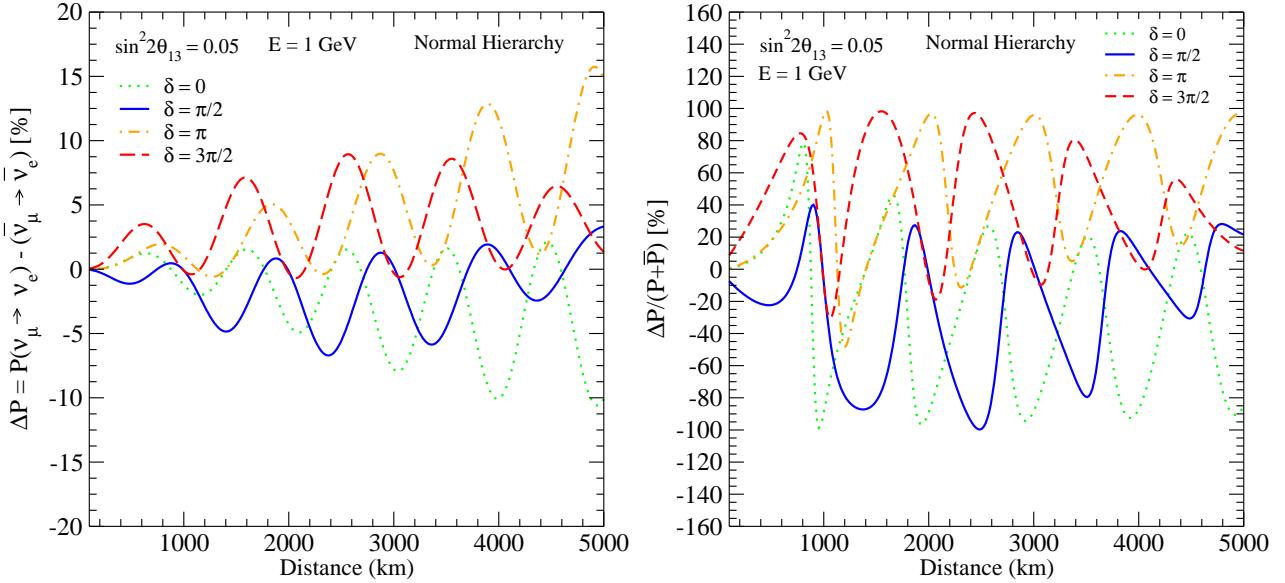


Figure 24: Examples of $\Delta P \equiv P(\nu_e \rightarrow \nu_\mu) - P(\bar{\nu}_e \rightarrow \bar{\nu}_\mu)$ (left panel) and the asymmetry $\Delta P / [P(\nu_e \rightarrow \nu_\mu) + P(\bar{\nu}_e \rightarrow \bar{\nu}_\mu)]$ (right panel) in matter as a function of distance for fixed value of energy, $E = 1$ GeV and $\sin^2 2\theta_{13} = 0.05$. For simplicity, we assume a constant electron number density $N_e = 1.5$ mol/cc.

Thus the $\sqrt{P_{\text{atm}}}$ and $\sqrt{P_{\text{sol}}}$ in matter are simply given by

$$\begin{aligned} \sqrt{P_{\text{atm}}} &= \sin \theta_{23} \sin 2\theta_{13} \frac{\sin(\Delta_{31} - aL)}{(\Delta_{31} - aL)} \Delta_{31}, \\ \sqrt{P_{\text{sol}}} &= \cos \theta_{23} \sin 2\theta_{12} \frac{\sin(aL)}{(aL)} \Delta_{21}, \end{aligned} \quad (88)$$

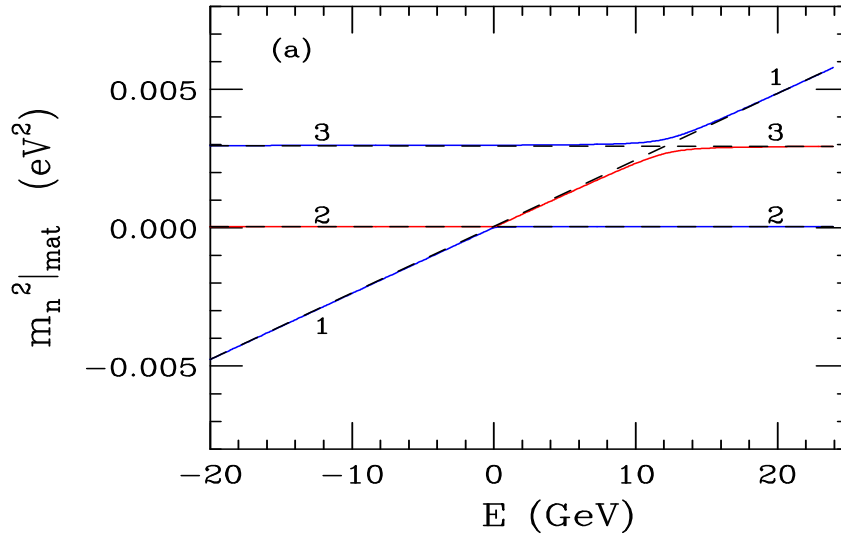


Figure 25: The neutrino mass squared differences in matter as a function of energy (negative energy is anti-neutrinos). The density of matter is $3 \text{ g}\cdot\text{cm}^{-3}$ and m_1^2 at zero energy (vacuum) is arbitrarily chosen to be 0 eV^2 .

where $a \equiv G_F N_e / \sqrt{2}$ which is approximately $(3500 \text{ km})^{-1}$ for $\rho Y_e = 3.0 \text{ g}\cdot\text{cm}^{-3}$. The relative phase $(\Delta_{32} + \delta)$ between $\sqrt{P_{\text{atm}}}$ and $\sqrt{P_{\text{sol}}}$ in Eq. (71) remains unchanged. It is clear from $\sqrt{P_{\text{atm}}}$ that relative size between the kinematic phase Δ_{31} compared to aL determines the effects of matter provided at least one of these is bigger than $\pi/4$. Since L is common to both Δ_{31} and aL provided it is a significant fraction of an oscillation (either in matter or vacuum) then the comparison is between $\Delta m_{31}^2/E$ and $a = G_F N_e / \sqrt{2}$. This implies that the larger the energy of the neutrino, E , the larger the matter effect provided the baseline is the same fraction of an oscillation length.

In Fig. 26 we show the effects of matter on P_{atm} and P_{sol} for fixed energy and varying the baseline and for fixed baseline and varying the energy. For fixed energy, one sees that the amplitude of the matter effect does not increase with distance but the shift in the peaks increases in proportion to the baseline. For fixed baseline, the amplitude of the matter effect gets smaller with lower energy, also proportionally. Thus the biggest matter effect is at the first oscillation peak.

Thus in matter to leading order

$$\begin{aligned}
P(\nu_\mu \rightarrow \nu_e) &= \sin^2 \theta_{23} \sin^2 2\theta_{13} \frac{\sin^2(\Delta_{31} - aL)}{(\Delta_{31} - aL)^2} \Delta_{31}^2 \\
&+ \sin 2\theta_{23} \sin 2\theta_{13} \sin 2\theta_{12} \frac{\sin(\Delta_{31} - aL)}{(\Delta_{31} - aL)} \Delta_{31} \frac{\sin(aL)}{(aL)} \Delta_{21} \cos(\Delta_{31} + \delta) \\
&+ \cos^2 \theta_{23} \sin^2 2\theta_{12} \frac{\sin^2(aL)}{(aL)^2} \Delta_{21}^2, \tag{89}
\end{aligned}$$

where the first (last) term is the atmospheric (solar) probabilities and the middle term is the interference between the atmospheric and solar contributions. The phase of the interference has been written as $(\Delta_{31} + \delta)$ instead of $(\Delta_{32} + \delta)$ since the difference between these two is small. Also, $\sin 2\theta_{13}$ is often written as $2 \sin \theta_{13}$ or even $2\theta_{13}$, again the difference is higher order. We have allowed for Δ_{31} and Δ_{32}

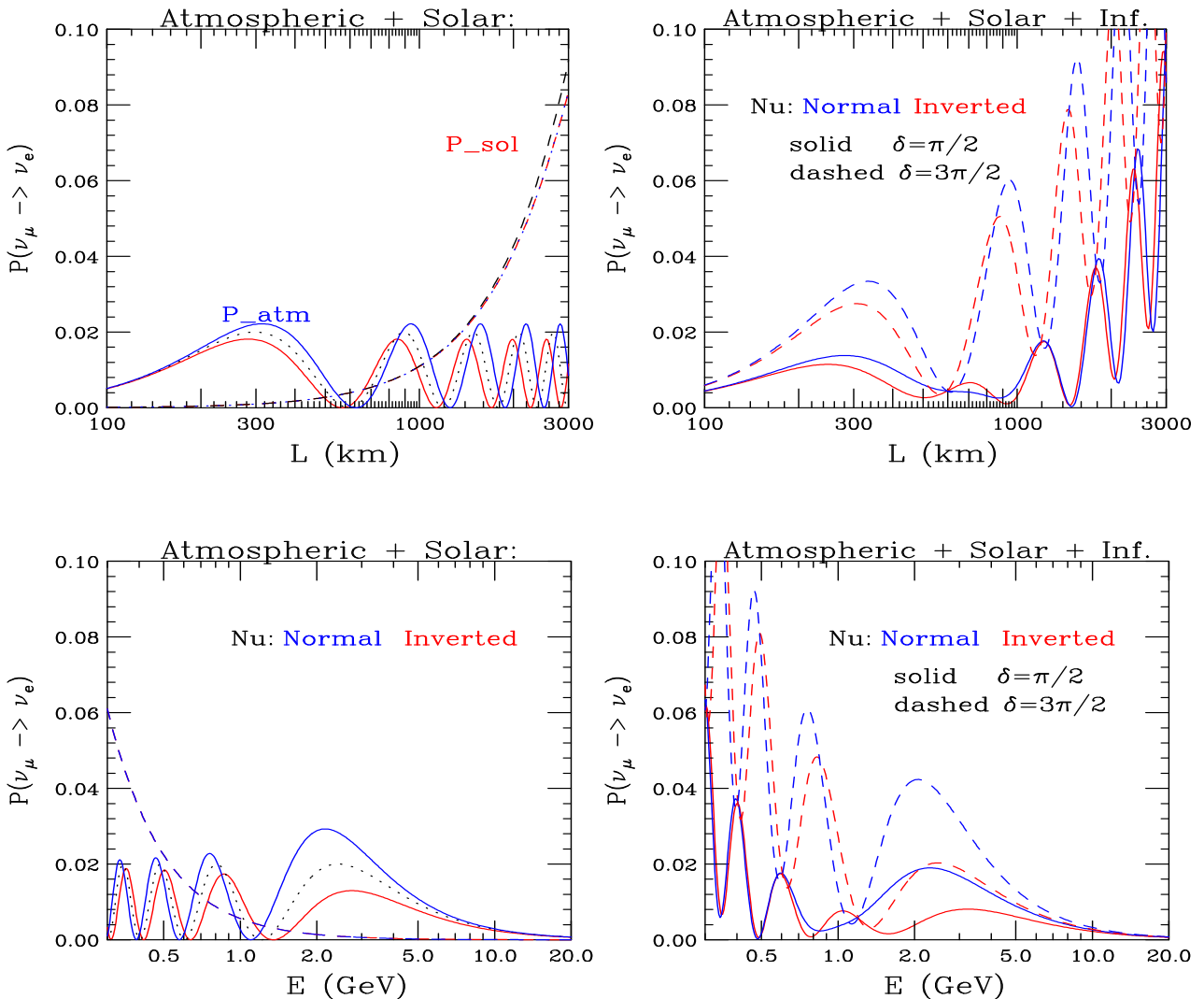


Figure 26: The components of the probability $P(\nu_\mu \rightarrow \nu_e)$ in matter: The left column gives P_{atm} and P_{sol} , whereas the right column gives the full oscillation probability including also the interference term between the atmospheric and solar amplitudes. The first row is for fixed energy, 0.6 GeV, and varying the baseline, whereas the second row is for fixed baseline, 1200 km, and varying the energy.

to be positive or negative in this derivation, thus this expression is valid for both normal, $\Delta m_{31}^2 > 0$ and inverted, $\Delta m_{31}^2 < 0$, hierarchies.

For the CP conjugate process, $\bar{\nu}_\mu \rightarrow \bar{\nu}_e$, in matter both $a \rightarrow -a$ and $\delta \rightarrow -\delta$ is required. Also for the T conjugate process, $\nu_e \rightarrow \nu_\mu$, replacing L with $-L$ including in the kinematic phases, Δ , is necessary. Note also that the CPT conjugate process, $\bar{\nu}_e \rightarrow \bar{\nu}_\mu$, is obtained by changing the sign of a , δ and L . If one changes the sign of a again, since this is equivalent to having propagation in anti-matter, the probability is once again the same as that for $\nu_\mu \rightarrow \nu_e$ as it must from CPT invariance, since

$$P(\nu_\mu \rightarrow \nu_e)|_{\text{matter}} \equiv P(\bar{\nu}_e \rightarrow \bar{\nu}_\mu)|_{\text{anti-matter}}. \quad (90)$$

This CPT relationship is true for any symmetric matter profile, $a(x) = a(L-x)$, where x is the position along the neutrino path and L is the baseline of the experiment.

In fact there are a number of relationships between these probabilities [166, 167]. Here we discuss some, especially those that hold for the case of inverting the hierarchy. The relationship between CP conjugate pairs is given by

$$\begin{aligned} P(\nu_e \rightarrow \nu_\mu; \Delta m_{31}^2, \Delta m_{21}^2, \delta, a) &= P(\bar{\nu}_e \rightarrow \bar{\nu}_\mu; -\Delta m_{31}^2, -\Delta m_{21}^2, \delta, a) \\ &\approx P(\bar{\nu}_e \rightarrow \bar{\nu}_\mu; -\Delta m_{31}^2, +\Delta m_{21}^2, \pi + \delta, a). \end{aligned} \quad (91)$$

The CPT relationship including the effects of switching the hierarchy is

$$\begin{aligned} P(\nu_\mu \rightarrow \nu_e; \Delta m_{31}^2, \Delta m_{21}^2, \delta, a) &= P(\bar{\nu}_e \rightarrow \bar{\nu}_\mu; -\Delta m_{31}^2, -\Delta m_{21}^2, 2\pi - \delta, a) \\ &\approx P(\bar{\nu}_e \rightarrow \bar{\nu}_\mu; -\Delta m_{31}^2, +\Delta m_{21}^2, \pi - \delta, a). \end{aligned} \quad (92)$$

This relationship is demonstrated in Fig. 27 by the dotted horizontal lines. In fact, there are many such relationships, e.g.,

$$\begin{aligned} P(\nu_\mu \rightarrow \nu_e; \Delta m_{31}^2, \Delta m_{21}^2, \delta, a) &= P(\nu_\mu \rightarrow \nu_e; -\Delta m_{31}^2, -\Delta m_{21}^2, 2\pi - \delta, -a) \\ = P(\bar{\nu}_\mu \rightarrow \bar{\nu}_e; -\Delta m_{31}^2, -\Delta m_{21}^2, \delta, a) &= P(\bar{\nu}_\mu \rightarrow \bar{\nu}_e; \Delta m_{31}^2, \Delta m_{21}^2, 2\pi - \delta, -a). \end{aligned} \quad (93)$$

The easiest way to derive such relationships is to look at the evolution equation, Eqs. (56) and (59), and its complex conjugate for neutrinos and anti-neutrinos using a symmetric matter profile and noting that $U^*(2\pi - \delta) = U(\delta)$.

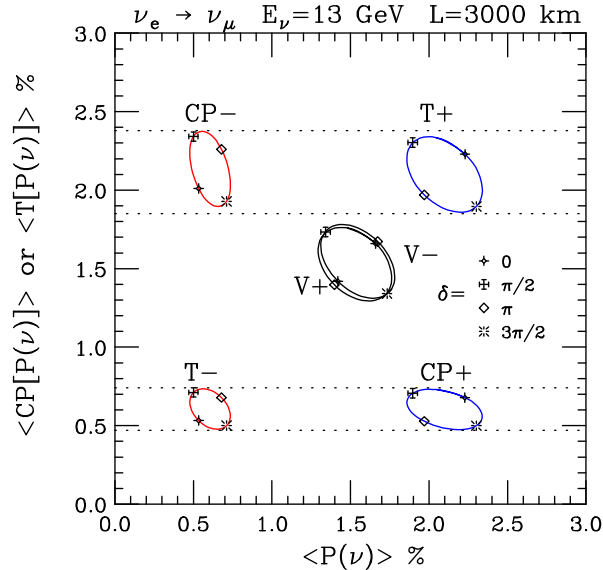


Figure 27: $P(\nu_\mu \rightarrow \nu_e)$ versus $P(\bar{\nu}_\mu \rightarrow \bar{\nu}_e)$ and $P(\nu_\mu \rightarrow \nu_e)$ versus $P(\nu_e \rightarrow \nu_\mu)$ in matter. In vacuum the four ellipse overlap, one for CP conjugate pair plus one for T conjugate pair times two, one for the normal (+) and one for the inverted (-) hierarchies. When matter effects are turned on the four ellipses split to form a baseball diamond with the vacuum ellipse is the pitcher's mound. All the parameters are held fixed except the CP-violating phase, δ and $\sin^2 2\theta_{13} = 0.05$. The dotted lines demonstrate the approximate relationship of Eq. (92).

We show in Fig. 24 the same quantities shown in Fig. 26 but in the presence of the matter effect. As we can see, the matter effect can make $\Delta P_{\nu\bar{\nu}}$ as well as the asymmetry significantly different from zero even if the CP phase is zero or π .

When the matter effect is significant the quantity defined in Eq. (76) is no longer a good measure of the intrinsic CP violation, since the matter effect makes this quantity significantly different from zero even if $\delta = 0$ or π . Therefore we define

$$\delta P_{CP} \equiv \Delta P_{\nu\bar{\nu}}(\delta = \pi/2) - \Delta P_{\nu\bar{\nu}}(\delta = 0), \quad (94)$$

which reduces to Eq. (76) in vacuum. We note that in this quantity the matter effect is approximately canceled so that only the intrinsic CP violation effect remains, to a good approximation.

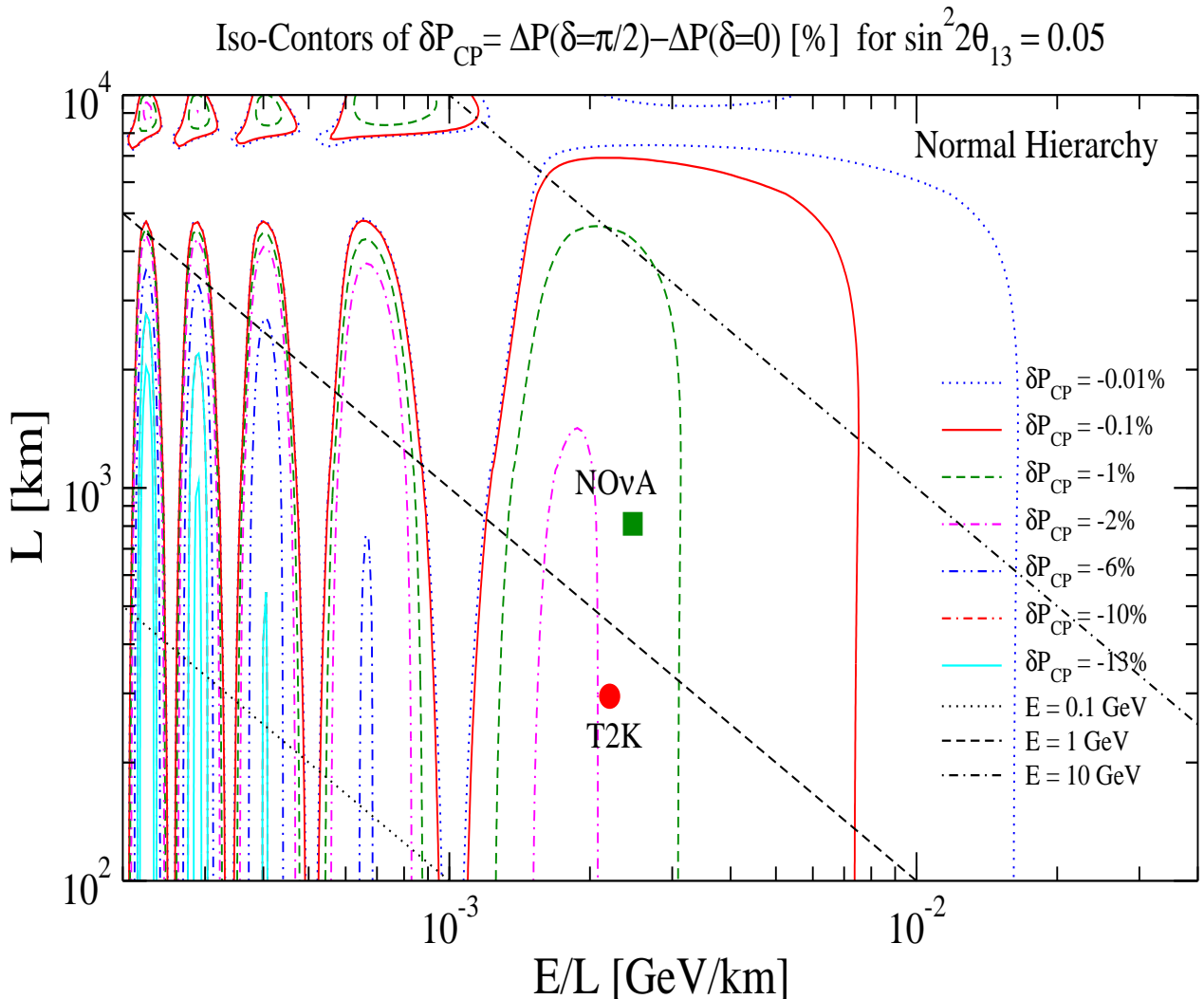


Figure 28: Iso-contours of $\delta P_{CP} \equiv \Delta P_{\nu\bar{\nu}}(\delta = \pi/2) - \Delta P_{\nu\bar{\nu}}(\delta = 0)$ for $\sin^2 \theta_{13} = 0.05$ in the $E/L - L$ plane in matter for normal hierarchy.

In Fig. 28 for a given baseline distance the matter density was assumed constant and estimated from the Preliminary Reference Earth Model (PREM) [168] by taking the average along the neutrino trajectory. The baseline and energy corresponding to T2K and NO ν A are indicated by the solid circle

and square, respectively. The positions of the peaks of the 5 “peninsula” regions correspond to, from right to left, 1st, 2nd, 3rd, 4th and 5th oscillation maxima. The best places to search for CP violation effects in the probabilities are those within the regions with higher δP_{CP} values. Since the neutrino flux decreases as $1/L^2$ as the baseline gets larger one should, in practice, try to measure the first or first few oscillation maxima. We note that in the region with $L \sim 7000 - 8000$ km no significant CP violation is expected: at such “magic” baselines [169] the dependence of the probability on the CP δ and the solar oscillation parameters disappears (see [170] for its physical interpretation).

7 Near Term Experiments

Here we discuss the prospects of observing CP violation by the following two near term experiments⁸, T2K and NO ν A:

- T2K [171]: Initially this experiment will send a beam of ν_μ 's from the JPARC facility to the existing 50 kton Super-Kamiokande (SK) detector. The beam will be aimed 2.5 degrees off the JPARC to SK axis resulting in a mean neutrino energy of 0.63 GeV with an approximate Gaussian spread of 0.13 GeV at SK. The source detector distance is 295 km with a mean matter density of 2.3 g cm^{-3} . The beam power will be ramped over time to 0.75 MW. Only neutrino running is expect during the initial phase, Phase I. In the future, there is a possibility to upgrade the beam power to as high as 4 MW and to include anti-neutrino running.
- NO ν A[172, 173]: The NO ν A detector will be placed 12km off-axis of the existing NUMI neutrino beam line at a distance of 810 km. The mean neutrino energy in this configuration is 2.0 GeV with an approximate Gaussian spread of 0.30 GeV. By the time the 25kton liquid scintillator detector has been completed the NUMI beam power is expected to be greater than or equal to 0.4 MW. This allows for the running in both neutrino or anti-neutrino mode. The mean matter density for this configuration is 2.8 g cm^{-3} . In the future, there is a possibility to upgrade the beam power up to as high as 2 MW.

Given the current best fit value for $\Delta m_{\text{atm}}^2 = 2.5 \times 10^{-3} \text{ eV}^2$ from the global analysis [174] both of these experiments are at a mean energy which is above the first vacuum oscillation maximum (VOM) energy. Also, because of the longer path length for the NO ν A experiment the matter effects are three times larger for NO ν A than the T2K experiment.

⁸At the time of writing this review, the beam line for T2K is under construction with first beam to the existing Super-Kamiokande detector is expected in 2009. The NuMI beam line is operating for the MINOS experiment but the NO ν A detector has still to get final approval from DOE to begin construction and is expected to come on line after T2K by at least one year.

7.1 Dependence of probabilities on θ_{13} and δ

First let us look at the how the oscillation probabilities as well as CP violation (the difference of probabilities) for these two experiments depends on θ_{13} and δ . Fig. 29 shows the iso-probability contours for the T2K experiment for both hierarchies in neutrino and anti-neutrino running. The expected sensitivity for the first phase of running of T2K is approximately equal to the 0.5% contour in neutrino running. There is a small difference between the contours for the two hierarchies due to matter effects

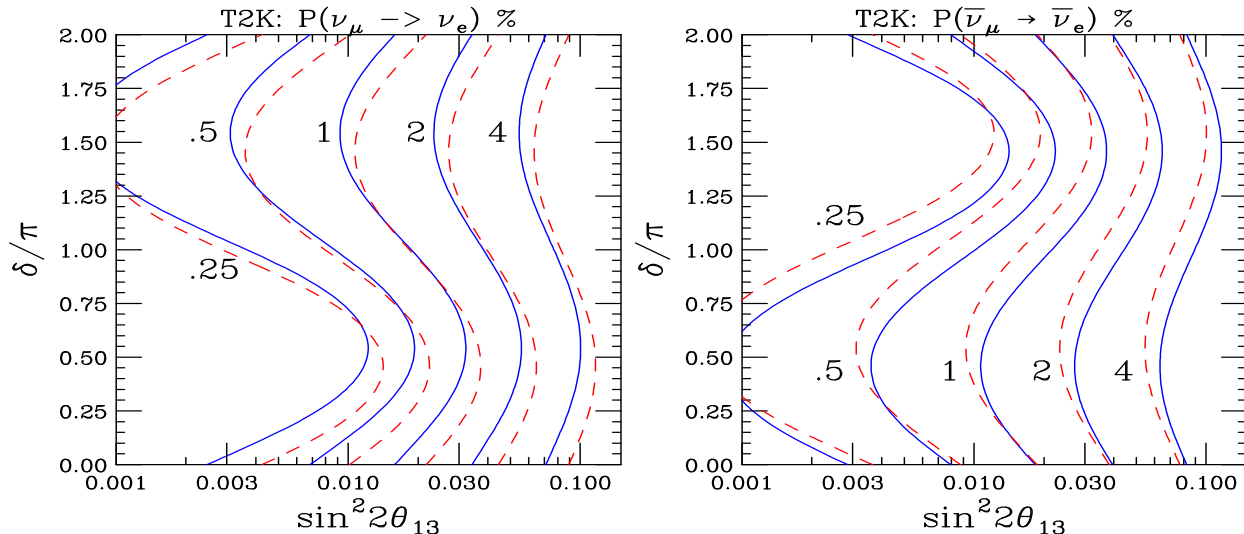


Figure 29: Iso-contours of $P(\nu_\mu \rightarrow \nu_e)$ and $P(\bar{\nu}_\mu \rightarrow \bar{\nu}_e)$ in matter for T2K experiment. The solid (dashed) curves correspond to the normal (inverted) hierarchy. In Phase I, T2K is expected to reach a sensitivity which is close to the 0.5% contour for neutrinos.

and the fact that the mean neutrino energy is above vacuum oscillation maximum. Since the beam and fake backgrounds contribute approximately 1%, further improvement on the sensitivity will be challenging. No anti-neutrino running is expected in the first phase since the event rate is appreciably smaller than in neutrino running. Of course, anti-neutrino will be included as the beam power is ramped up above the initial phase. Due to the increased background and smaller statistics, compared to neutrino running, a reasonable estimate of the sensitivity in anti-neutrino running is the 1% contour of the anti-neutrino plot in Fig. 29. Fig. 30 shows the iso-probability contours for the NO ν A experiment for both hierarchies in neutrino and anti-neutrino running. The expected sensitivity for neutrino running is also approximately 0.5% and approximately 1% for anti-neutrino running. Again, further improvements will be challenging due to backgrounds. Notice the sizable difference in the sensitivity between the two hierarchies [175], primarily due to the matter effects. The combined running of neutrinos and anti-neutrinos will make the combined sensitivity much less dependent on the CP violating phase, δ .

In order to have some idea about the magnitude of the intrinsic CP violation (coming from δ) which can potentially be observed in these two experiments, we show in Fig. 31, the iso-contours of $\Delta P_{\nu\bar{\nu}} \equiv P(\nu_\mu \rightarrow \nu_e) - P(\bar{\nu}_\mu \rightarrow \bar{\nu}_e)$ in the plane of δ and $\sin^2 2\theta_{13}$ by switching off the matter effect. Note, that this quantity is just the CP-invariant factor multiplied by a constant which depends on the

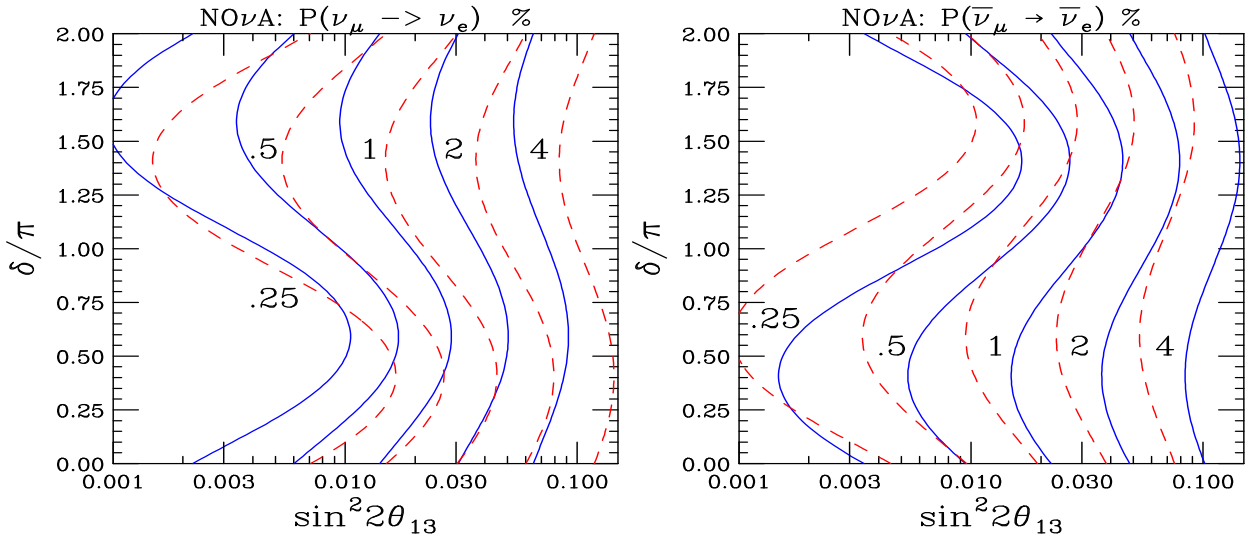


Figure 30: Iso-contours of $P(\nu_\mu \rightarrow \nu_e)$ and $P(\bar{\nu}_\mu \rightarrow \bar{\nu}_e)$ in matter for NO ν A experiment. The solid (dashed) curves correspond to the normal (inverted) hierarchy. The NO ν A experiment in its initial phase is expected to reach a sensitivity close to the 0.5% contour in neutrinos and approximately the 1% contour in anti-neutrinos.

neutrino energy and baseline, see Eq. (64).

Note also that in vacuum this quantity does not depend on mass hierarchy so that the contours are symmetric with respect to the line $\delta = \pi$ except for the sign difference. The positions of the CP conserving solutions in the $(\sin^2 2\theta_{13}, \sin \delta)$ plane are shown in Fig. 32.

However, this quantity is not directly observable as the actual positions of the $\Delta P_{\nu\bar{\nu}}$ contours are modified by matter effects, as shown in Fig. 33 for T2K and Fig. 34 for NO ν A. As expected, the modifications due to the matter effect, which can be seen by the asymmetry of contours with respect the line $\delta = \pi$, are smaller for T2K than for NO ν A.

In Fig. 32 we have show the location of the CP conserving solutions of one hierarchy in the $(\sin^2 2\theta_{13}, \sin \delta)$ plane of the other hierarchy. These locations depend on the matter effect for the experiment and thus differ for T2K and NO ν A. In order to claim the observation of CP violation, one must be sufficiently away (with a required CL) not only from the line $\sin \delta = 0$ but also from the dot-dashed (T2K) and dashed (NO ν A) curves shown in these plots unless the mass hierarchy is known.

For baseline $L < 1500$ km or so, one can expand $\Delta P_{\nu\bar{\nu}}(a)$ in matter as a Taylor series about the vacuum $\Delta P_{\nu\bar{\nu}}(0)$ as follows,

$$\Delta P_{\nu\bar{\nu}}(a) = \Delta P_{\nu\bar{\nu}}(0) \pm 4(aL)G(\Delta_{32})[P_{\text{atm}}(0) + \sqrt{P_{\text{atm}}(0)P_{\text{sol}}} \cos \Delta_{32} \cos \delta], \quad (95)$$

where $G(x) \equiv 1/x - \cot x$ and the + (-) sign is for the normal (inverted) hierarchies. This simple expression gives the relationship of Figs. 33 and 34 to Fig. 31.

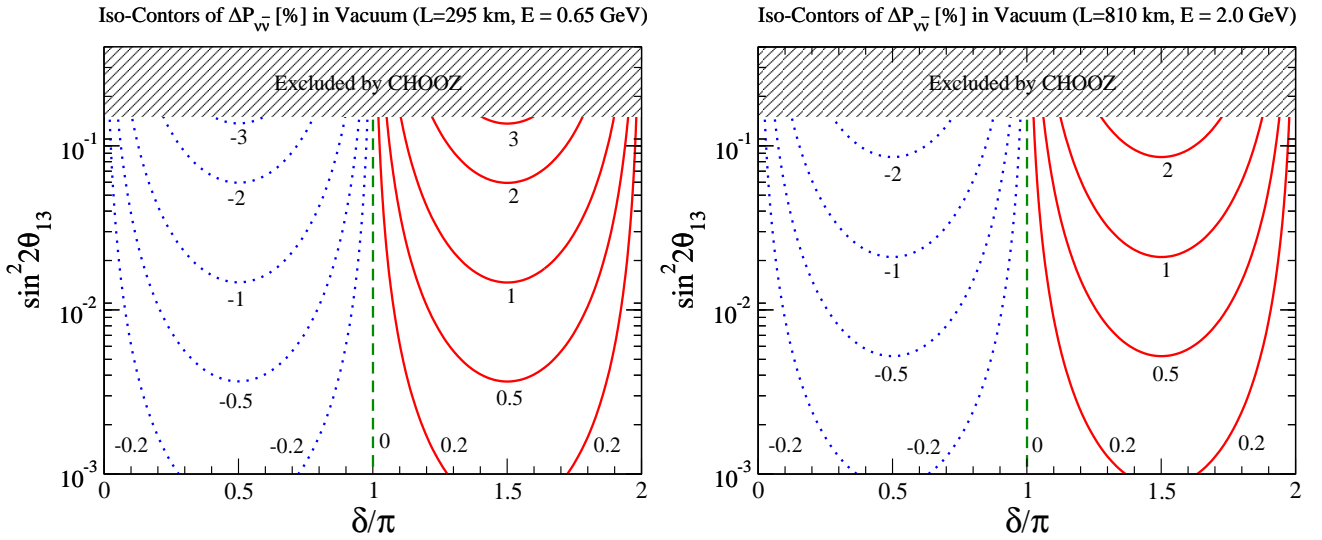


Figure 31: Iso-contours of $\Delta P_{\nu\bar{\nu}} \equiv P(\nu_\mu \rightarrow \nu_e) - P(\bar{\nu}_\mu \rightarrow \bar{\nu}_e)$ in the δ and $\sin^2 2\theta_{13}$ in vacuum for T2K (left panel) and NO ν A (right panel).

7.2 Bi-probability plots

Of course, the neutrino and anti-neutrino probabilities are correlated. This correlation depends on the CP violating phase, δ , and the mass hierarchy. Therefore it is useful to use bi-probability diagrams. In the bi-probability space spanned by $P(\nu_\mu \rightarrow \nu_e)$ and $P(\bar{\nu}_\mu \rightarrow \bar{\nu}_e)$, for a given θ_{13} (fixing all the mixing parameters except for δ), energy and baseline, the variation of δ from 0 to 2π gives a closed trajectory which is an ellipse⁹. In Figs. 35 and 36, we give the bi-probability diagrams for both T2K and NO ν A, respectively. For T2K the separation between the hierarchies is small but non-negligible whereas for NO ν A the separation is much larger with complete separation occurring for $\sin^2 2\theta_{13} = 0.11$. The value of θ_{13} for which the two hierarchies separate is called the critical value, θ_{13}^{crit} . For T2K and NO ν A the bi-probability diagrams are shown for two energies, one such that $\Delta_{31} \approx \pi/2$ which is known as vacuum oscillation maximum (VOM) and at an energy above VOM. At VOM the ellipses in the bi-probability plot are squashed to lines as the probabilities become independent of $\cos \delta$ since $\cos \Delta_{31} = 0$.

7.3 Parameter Degeneracy

Unfortunately the measurement of $P(\nu_\mu \rightarrow \nu_e)$ and $P(\bar{\nu}_\mu \rightarrow \bar{\nu}_e)$ does not determine the values of θ_{13} and δ uniquely due to the possibility of drawing more than one ellipse through any (P, \bar{P}) point. In general four such ellipses can be drawn assuming $\sin^2 \theta_{23}$ is known uniquely. Eight if only $\sin^2 2\theta_{23} (\neq 1)$ is known. Fig. 37 demonstrate this point.

The cross in the left hand panel of these two figure, are the transition probabilities for the normal hierarchy with $\sin^2 2\theta_{13} = 0.05$ and $\delta = \pi/4$ for both T2K and NO ν A. The right hand panels show the four allowed solutions in the $\sin^2 2\theta_{13}$ v $\sin \delta$ plane that are consistent with this point in the (P, \bar{P})

⁹ We note that the trajectory is exactly elliptic as it was shown [176] that even in matter, oscillation probabilities take the form of $P = A \cos \delta + B \sin \delta + C$ where A , B and C are some constants which depend on mixing parameters as well as experimental parameters such as energy and baseline.

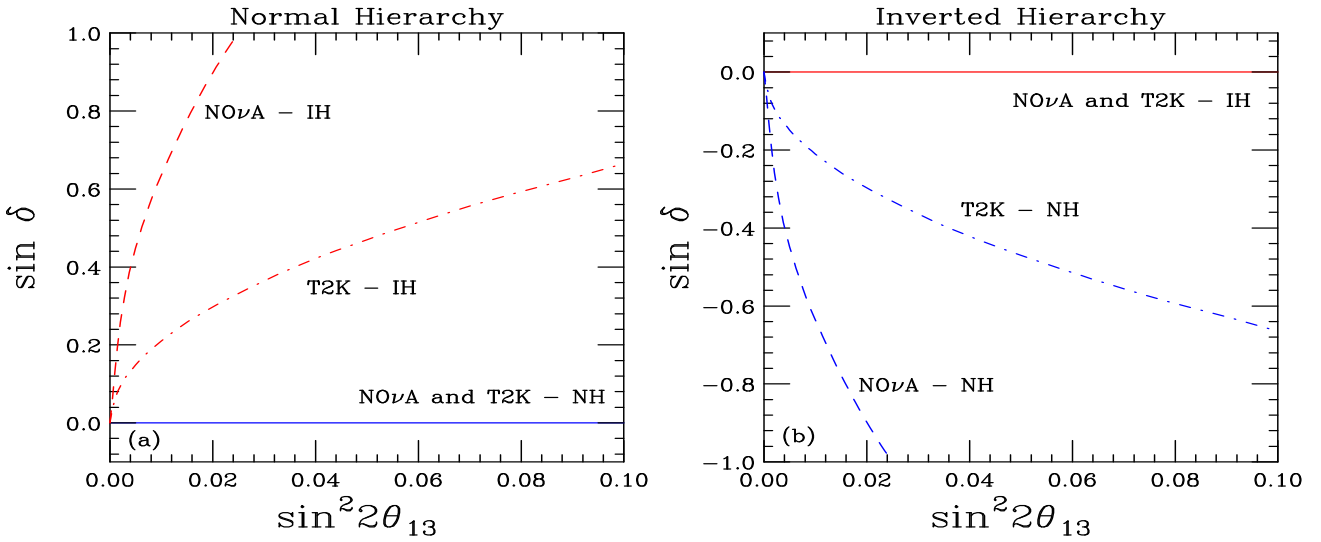


Figure 32: The positions of the CP conserving solutions in the $(\sin^2 2\theta_{13}, \sin \delta)$ plane: (a) for the Normal Hierarchy, the curves above $\sin \delta = 0$ for T2K (dot-dashed) and NO ν A (dashed) are the locations of the CP conserving solutions for the Inverted Hierarchy. (b) is the equivalent plot for the Inverted Hierarchy. Without determining the hierarchy, a given experiment cannot claim the observation of CP violation unless it can exclude both of lines with its label at the required confidence level in one of these plots.

plane. Clearly, the four solutions are related to one another:

- Within the same hierarchy, the intrinsic degeneracy [177].

The two solutions have approximately the same $\sin \delta$, but different signs for $\cos \delta$ i.e. δ and $\pi - \delta$. But the values of θ_{13} differ by

$$\Delta\theta_{13} = \cos \delta \sin 2\theta_{12} \Delta_{21} \cot \Delta_{31}$$

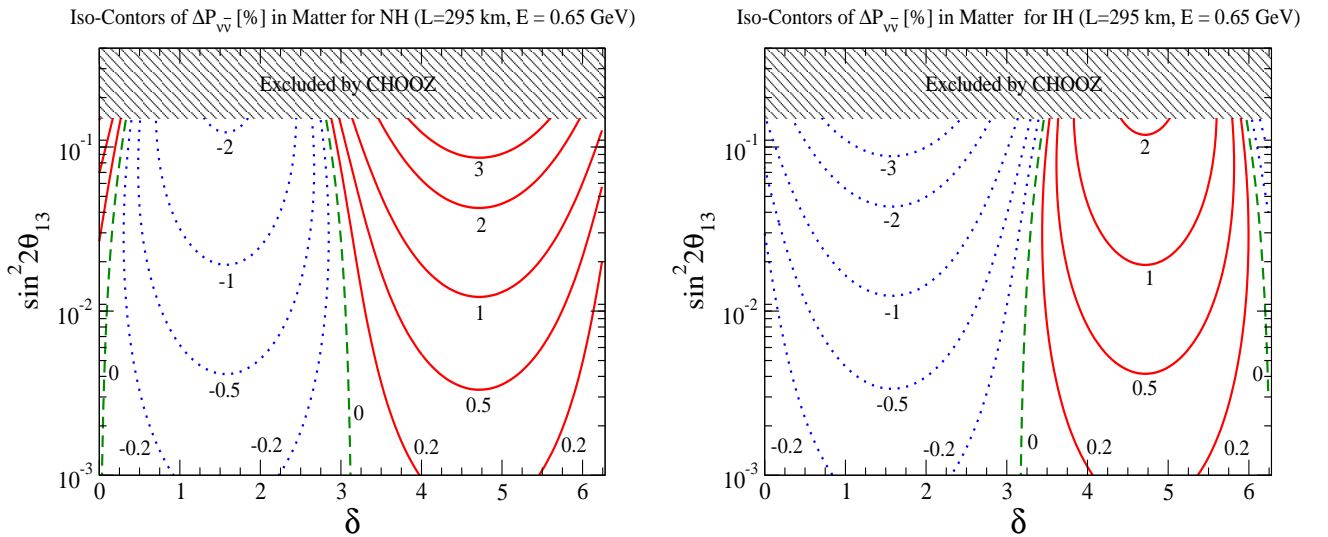


Figure 33: Iso-contours of $\Delta P_{\nu\bar{\nu}} \equiv P(\nu_\mu \rightarrow \nu_e) - P(\bar{\nu}_\mu \rightarrow \bar{\nu}_e)$ in the δ and $\sin^2 2\theta_{13}$ for T2K for the normal (left panel) and the inverted (right panel) mass hierarchy, with the matter effect included.

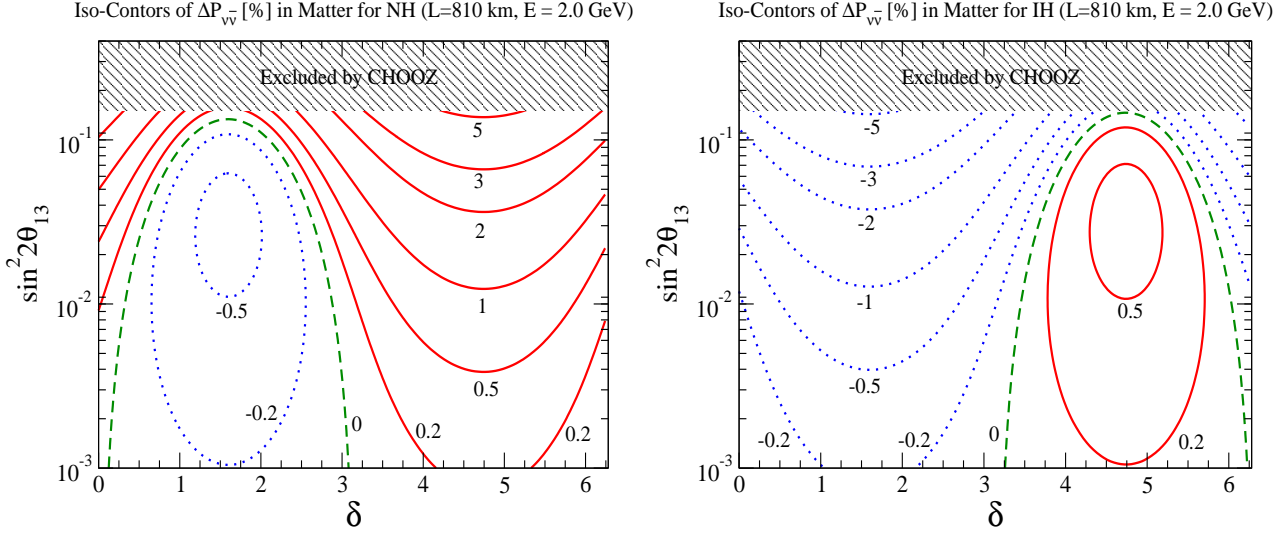


Figure 34: Iso-contours of $\Delta P_{\nu\bar{\nu}} \equiv P(\nu_\mu \rightarrow \nu_e) - P(\bar{\nu}_\mu \rightarrow \bar{\nu}_e)$ in the δ and $\sin^2 2\theta_{13}$ for NO ν A for the normal (left panel) and the inverted (right panel) mass hierarchy, with the matter effect included.

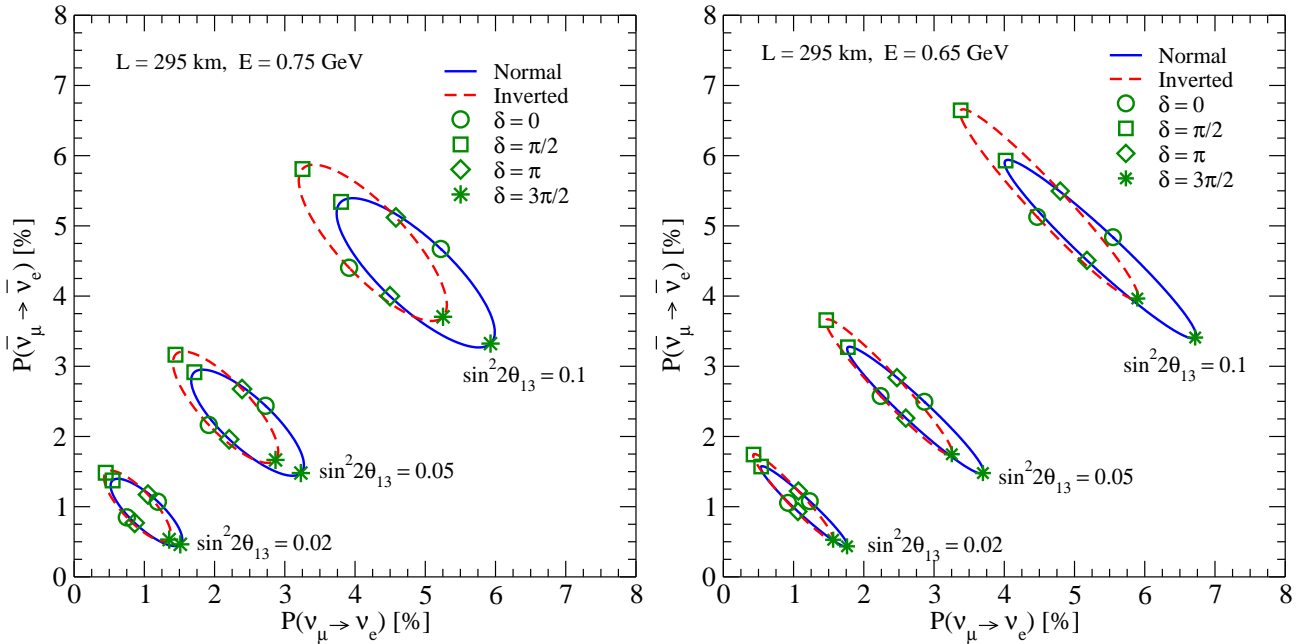


Figure 35: The bi-probability $P(\nu_\mu \rightarrow \nu_e)$ diagram for T2K including matter effects.

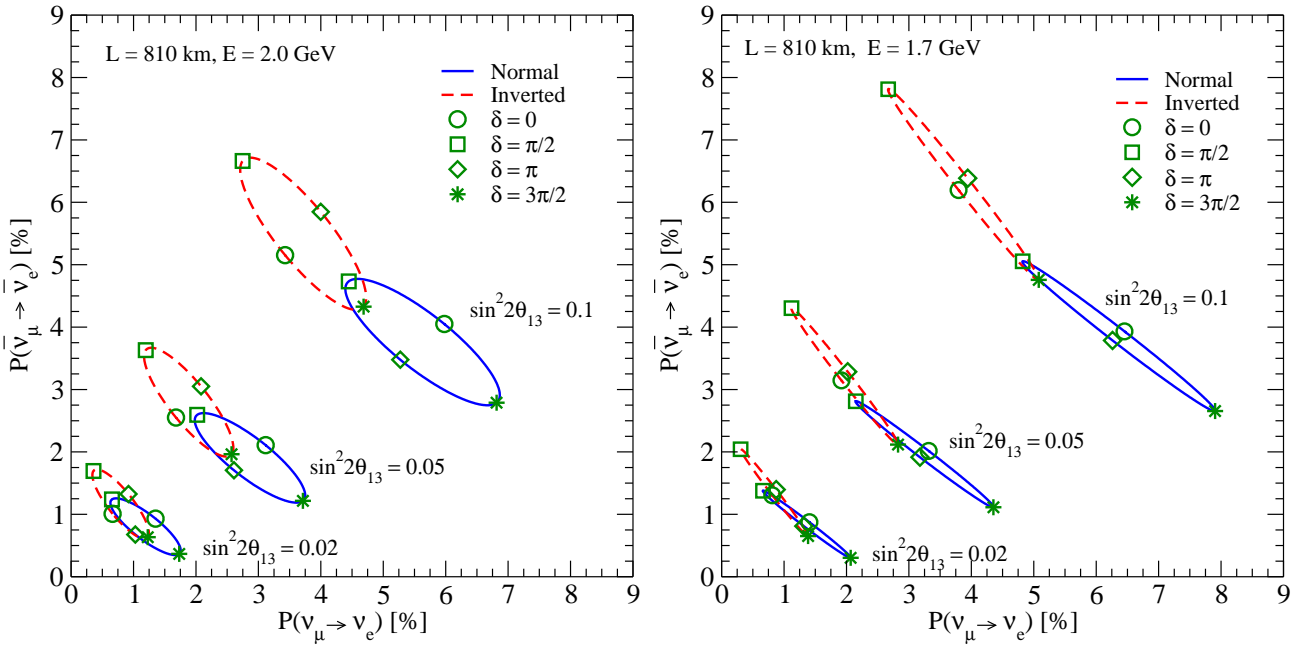


Figure 36: The bi-probability $P(\nu_\mu \rightarrow \nu_e)$ diagram for $\text{NO}\nu\text{A}$ including matter effects.

At vacuum oscillation maximum, $\Delta_{31} = \pi/2$, these two different values of θ_{13} coincide, see Fig. 37.

- Between the two hierarchies[175].

The allowed values for $\sin^2 2\theta_{13}$ are the same for both hierarchies but the $\sin \delta$'s differ between the normal (NH) and inverted (IH) hierarchies as follows, $\sin \delta|_{NH} - \sin \delta|_{IH} = 2\theta_{13}/\theta_{13}^{\text{crit}}$, see [178]. Where $\theta_{13}^{\text{crit}}$ is the largest value of θ_{13} for which the two regions in the bi-probability diagram overlap¹⁰, see Fig. 37. For T2K and $\text{NO}\nu\text{A}$ this corresponds to

$$\sin \delta|_{NH} - \sin \delta|_{IH} = \begin{cases} 0.47 \sqrt{\frac{\sin^2 2\theta_{13}}{0.05}} & \text{T2K} \\ 1.42 \sqrt{\frac{\sin^2 2\theta_{13}}{0.05}} & \text{NO}\nu\text{A} \end{cases} \quad (97)$$

The coefficient is 3 times bigger for $\text{NO}\nu\text{A}$ than T2K primarily because the baseline for $\text{NO}\nu\text{A}$ is approximately 3 times that of T2K so that the matter effects are 3 times larger. Notice that the matter effects are smaller but not negligible for T2K, see Fig. 32. Clearly the combination of T2K and $\text{NO}\nu\text{A}$ can be used to determine the hierarchy at least for large values of θ_{13} .

If $\sin^2 2\theta_{23} \neq 1$ then there is a further degeneracy [179] associated with whether

$$\sin^2 \theta_{23} = \frac{1 \mp \sqrt{1 - \sin^2 2\theta_{23}}}{2}. \quad (98)$$

¹⁰The value of $\theta_{13}^{\text{crit}}$ for any experiment is given by

$$\theta_{13}^{\text{crit}} \approx \frac{\pi^2}{8} \frac{\sin 2\theta_{12}}{\tan \theta_{23}} \frac{\Delta m_{21}^2}{\Delta m_{31}^2} \left(\frac{4\Delta_{31}^2/\pi^2}{1 - \Delta_{31} \cot \Delta_{31}} \right) / (aL). \quad (96)$$

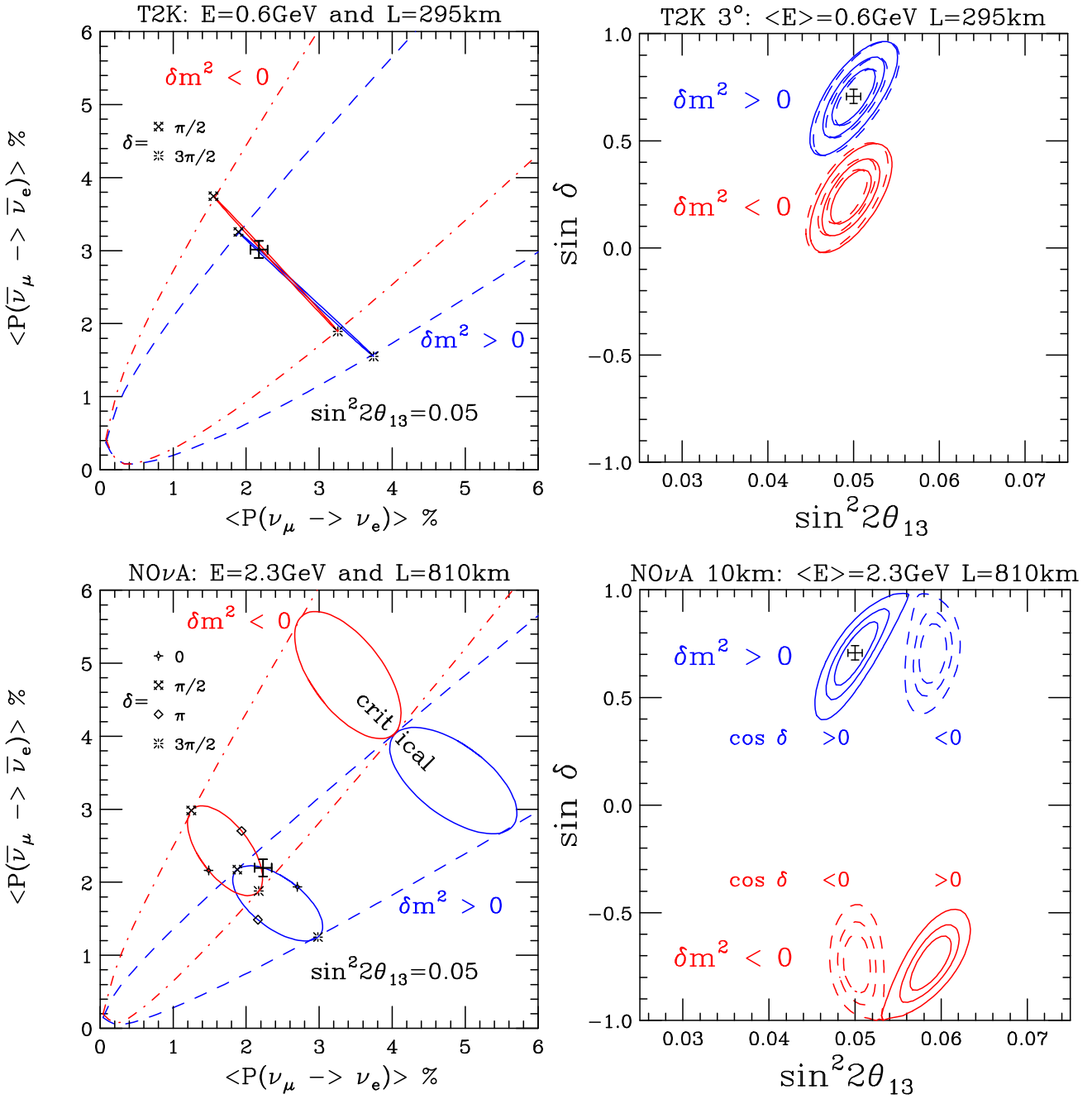


Figure 37: (a) The bi-probability plot for T2K (top) NOνA (bottom), showing the allowed regions for the normal (dashed) and inverted (dot-dashed) hierarchies. The cross is the assumed measured value of (P, \bar{P}) . The value of θ_{13} for which the two hierarchies separate is labeled as the critical value, θ_{13}^{crit} . (b) The four solutions for the assumed point in the $\sin^2 2\theta_{13}$ vs. $\sin \delta$ plane. Since T2K is near vacuum oscillation maximum all four solutions have approximately the same value of $\sin^2 2\theta_{13}$. But the solutions for the normal and inverted hierarchies occur at different values of $\sin \delta$. Since NOνA is above vacuum oscillation maximum, there are two distinct allowed values of $\sin^2 2\theta_{13}$. Again the solutions for the same hierarchy have the same value of $\sin \delta$. But the solutions for the normal and inverted hierarchies occur at different values of $\sin \delta$.

The simultaneous presence of these three independent 2-fold degeneracies leads up to 8-fold degeneracies [180]. Resolving all three of these degeneracies will be challenging but, except for the hierarchy degeneracy, they do not affect much whether or not one can claim the observation of leptonic CP violation.

For the mass hierarchy degeneracy this ambiguity can affect whether or not one can claim CP violation especially for larger values of θ_{13} . At larger values of θ_{13} , NO ν A alone may be able to determine the hierarchy if $\text{sign}(\Delta m_{31}^2) \sin \delta$ is close to one. Otherwise a combination of T2K and NO ν A is our best option for determining the hierarchy with only these two experiments. Even if the hierarchy is not determined there is still a substantial region of (θ_{13}, δ) space where not knowing the hierarchy does not preclude being able to claim the observation of leptonic CP violation. However there is a region in both experiments where one hierarchy is CP violating and the other CP conserving, fortunately these troublesome regions occur in different locations for the two experiments. This makes the combination of T2K and NO ν A a very powerful tool to observe leptonic for large θ_{13} .

7.4 Beyond the First Oscillation Maximum:

To untangle all of the degeneracy associated with the neutrino mass hierarchy, the quadrant of θ_{23} and the sign of $\cos \delta_{CP}$ discussed in the previous subsection, it is probable that experiments beyond the first atmospheric oscillation maximum will be necessary. First, let us discuss what happens in vacuum [181] and then add matter effects. In vacuum, the atmospheric amplitude given by Eq. (72) has the same magnitude at each of the successive maxima whereas the solar amplitude at the n -th peak is $(2n - 1)$ times larger than at the first peak as long as Δ_{21} is less than 1. Thus, the magnitude of the ratio of the solar to atmospheric amplitude grows as $(2n - 1)$. Hence, the relative magnitude of the probabilities associated with the atmospheric and solar δm^2 and their interference in the total $\nu_\mu \rightarrow \nu_e$ transition probability, the three terms in Eq. (71), changes at the successive peaks. At the n -th peak, the interference term, and hence CP violation, grows as $(2n - 1)$ compared to the first peak whereas the term associated with purely the solar δm^2 grows as $(2n - 1)^2$. This change in the relative magnitude of the three terms can be exploited to untangle the degeneracies.

In vacuum, the transition probability $\nu_\mu \rightarrow \nu_e$ is the same if one goes to the successive peaks by lowering the energy or increasing the baseline or some combination of the two (as long as E/L is kept to be the same). However, as we will see shortly, in matter, the $\nu_\mu \rightarrow \nu_e$ transition probability depends on exactly how one goes to the successive peaks. E.g. the transition probability at the second peak is different for lowering the energy by a factor of three at the same baseline than increasing the baseline by a factor of three at the same energy. To understand this we need to understand how matter effects change the atmospheric and solar amplitudes which is most easily done for a constant matter density. The solar amplitude changes little except at very large distances whereas the atmospheric amplitude is substantially modified by matter effects, see Eq. (88). The change in the atmospheric amplitude depends on whether one goes to the successive peaks by varying the baseline holding the energy fixed or varying the energy and holding the baseline fixed.

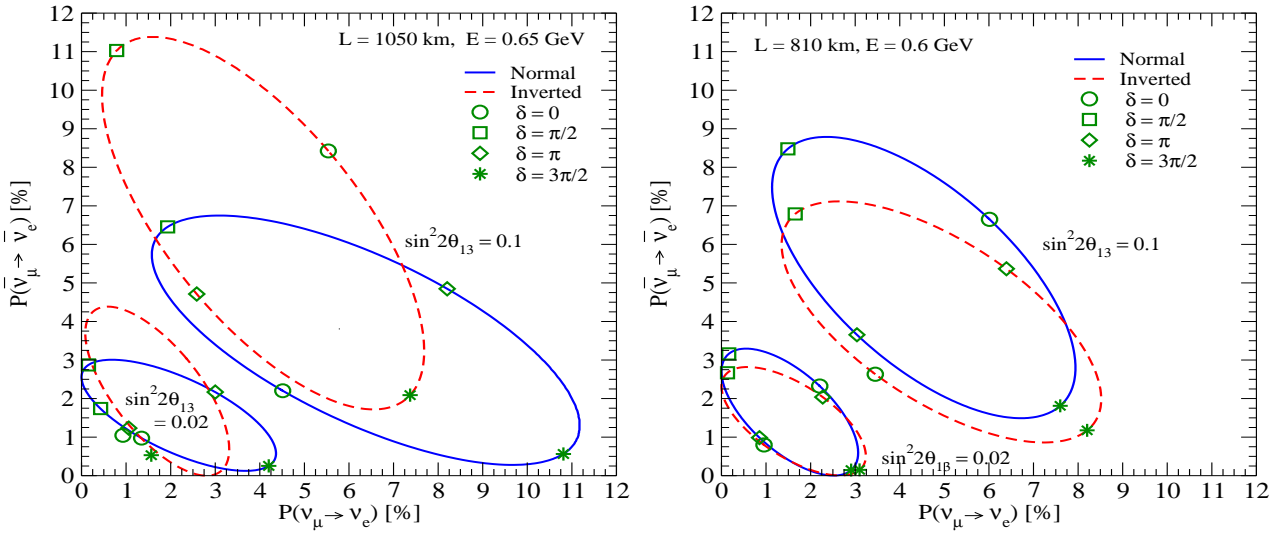


Figure 38: Examples of the bi-probability $P(\nu_\mu \rightarrow \nu_e)$ diagram corresponding to near the second oscillation maximum including matter effects.

For fixed energy and varying baseline, the modification of the atmospheric amplitude can be understood as just a change in the mixing angle and δm^2 which depend on the energy and matter density but are independent of the baseline, see section 6.2.2. So the amplitude of the oscillation is the same at all successive peaks and the position of n -th peak is just $(2n - 1)$ times the distance to the first peak. See top left panel of Fig. 26.

For fixed baseline and varying energy, again one can think of the modification as just changing the mixing angle and δm^2 but these parameters are energy dependent and approach the vacuum values as the energy gets smaller and smaller, see Fig. 25. Again, see the discussion in section 6.2.2. So the matter effects are reduced by $(2n - 1)$ in amplitude at the n -th peak since the energy at the n -th peak is reduced by $(2n - 1)$ compared to the first peak. Therefore, matter effects become increasingly less important at the successive peaks. This can be seen in the bottom left panel of Fig. 26.

7.5 Possible Experiments

A possible extension of the T2K experiment, called T2KK [182, 183] (see also [184, 185]), consists of building two new large detectors, one at the first oscillation peak at Kamioka, Japan and the other in Korea, near the second oscillation peak. Both detectors would be at the same off-axis angle so they would see the same neutrino energy spectrum but the Korean detector would be three times further from the source than the Kamioka detector. This is an example of getting to the second peak by varying the baseline holding the neutrino energy fixed. In the left panel of Fig. 38 we show the examples of bi-probability plots corresponding to such an experimental set up, which should be compared with the right panel of Fig. 35. From these two plots, we confirm that the oscillation probabilities as well as its dependence on δ are significantly enhanced at Korea due to the increase of the solar term. In Fig. 39 we show the iso-contour of $\Delta P_{\nu\bar{\nu}} = P(\nu_\mu \rightarrow \nu_e) - P(\bar{\nu}_\mu \rightarrow \bar{\nu}_e)$ in the $\delta - \sin^2 2\theta_{13}$ plane for the normal (left

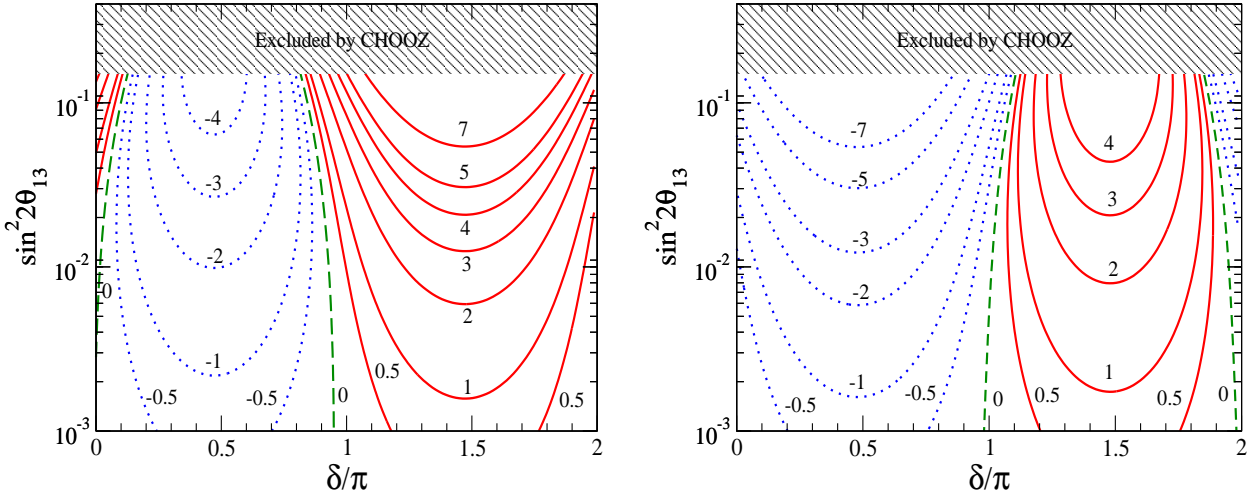


Figure 39: Iso-contours of $\Delta P_{\nu\bar{\nu}} \equiv P(\nu_\mu \rightarrow \nu_e) - P(\bar{\nu}_\mu \rightarrow \bar{\nu}_e)$ in the δ and $\sin^2 2\theta_{13}$ for T2KK (L=1050 km) for the normal (left panel) and the inverted (right panel) mass hierarchy, with the matter effect included.

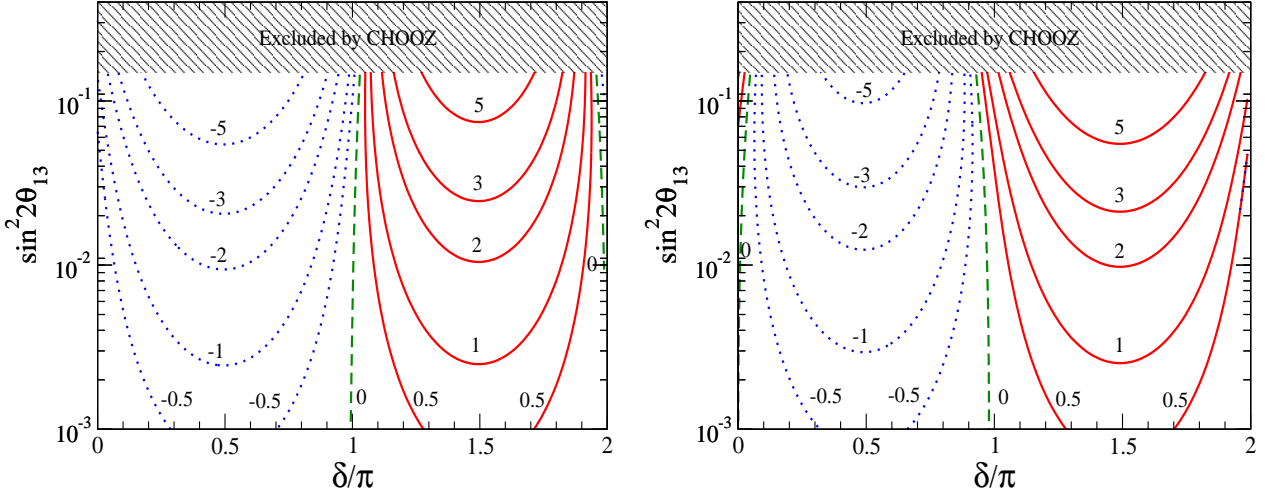


Figure 40: Iso-contours of $\Delta P_{\nu\bar{\nu}} \equiv P(\nu_\mu \rightarrow \nu_e) - P(\bar{\nu}_\mu \rightarrow \bar{\nu}_e)$ in the δ and $\sin^2 2\theta_{13}$ for the NO ν A baseline (L=810 km) but for the neutrino energy $E = 0.6$ GeV for the normal (left panel) and the inverted (right panel) mass hierarchy, with the matter effect included.

panel) and the inverted (right panel) hierarchy, which should be compared with Fig. 33. We observe that the qualitative behaviour of these plots are similar but magnitude of $\Delta P_{\nu\bar{\nu}}$ for larger baseline is significantly greater. By studying the neutrino spectrum at both detectors one could untangle all of the degeneracy [183].

Another possibility is to build a second large off-axis detector near the NO ν A detector such that the energy of the neutrino beam is one third of that seen by the NO ν A detector [186]. Both detectors would be approximately at the same distance so this is an example of getting to the second peak by varying the neutrino energy and holding the baseline fixed. At the second peak, CP violation is three times

larger than at the first peak and matter effects are three times smaller. Therefore, counting experiments at both peaks could resolve the entanglement of the mass hierarchy and CP-violation.

In the right panel of Fig. 38 we show an example of bi-probability plot corresponding to this case which should be compared with Fig. 36. We confirm that the effect of the CP phase (i.e., the size of the ellipses) become larger and the matter effects get smaller. The corresponding iso-contour plots of $\Delta P_{\nu\bar{\nu}}$, shown in Fig. 40, also support this feature.

A third possibility is to build a large detector on-axis at a distance of 1000 - 1500 km from the source and to measure the oscillated neutrino spectrum over a wide neutrino energy covering the first, second and possibly the third atmospheric oscillation peaks [187, 186]. This again is an example of a fixed baseline and varying the neutrino energy. The hierarchy would be determined by studying the first peak and CP-violation from studies of the second peak.

8 CP violation and lepton number violation: $\beta\beta_{0\nu}$

As we have seen, neutrino oscillations are insensitive to the absolute scale of neutrino masses. While the origin of the latter remains a theoretical mystery, one expects on general grounds that neutrinos are Majorana fermions, and that this accounts for their relative lightness with respect to the other fundamental fermions.

The search for lepton number violating processes such as $\beta\beta_{0\nu}$ opens the way to probe the basic nature - Dirac or Majorana - of neutrinos, and also to probe the CP violation induced by so-called Majorana phases [7]. As already mentioned, the latter does not show up in conventional neutrino oscillation experiments [24, 25, 26] but can affect neutrinoless double beta decays and electromagnetic properties of neutrinos [23, 28, 32] [188, 189].

The most direct mechanism engendering $\beta\beta_{0\nu}$ is the so-called “mass mechanism” involving the exchange of massive Majorana neutrinos. The associated amplitude is proportional to

$$m_{\beta\beta} = \sum_i K_{ei} m_i K_{ei} ,$$

where the K_{ei} are the first row in the lepton mixing matrix. An important feature of this amplitude is that it involves the lepton-number-violating propagator in Eq. 21 and, as a result, none of the K_{ei} factors appear with complex conjugation, hence the effect of Majorana phases and the possibility of destructive interference among amplitudes arising from different neutrino types.

Such destructive interferences may also take place without CP violation. This is what happens for example in the case of a pure Dirac neutrino, the exact cancellation coming in this case from the phase present in Eq. (15). Related concepts are those of partial cancellations due to symmetry. One example is the case of a Quasi-Dirac neutrino, made up of one active and one sterile neutrino, almost degenerate in mass due to the nearly exact conservation of standard lepton number [29]. Mass splittings between the two neutrinos may be radiatively calculable in some gauge models [30] and lead to active-sterile neutrino oscillations. Depending on the size of the mass splitting, these active-to-sterile conversions

may affect primordial Big Bang Nucleosynthesis [190, 191]. A different concept is that of a pseudo-Dirac neutrino made up of two active neutrinos, nearly degenerate due to the approximate conservation of some non-standard combination of lepton numbers [31].

The significance of neutrinoless double beta decay stems from the fact that, in a gauge theory, *irrespective of which is the mechanism* that induces $\beta\beta_{0\nu}$, it necessarily implies a Majorana neutrino mass [23], as illustrated in Fig. 41¹¹. This is specially relevant given the fact that gauge theories bring in other possible ways of inducing $\beta\beta_{0\nu}$ and it is conceivable that one of such mechanisms might, perhaps, give the leading contribution. Hence the importance of searching for neutrinoless double beta decay. Quantitative implications of the “black-box” argument are strongly model-dependent, but the

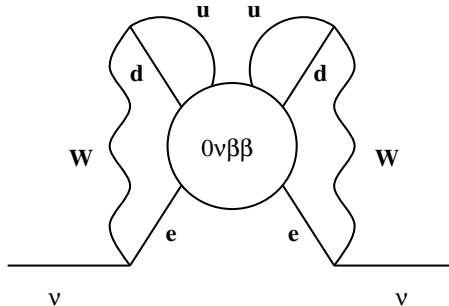


Figure 41: Neutrinoless double beta decay and Majorana mass are theoretically equivalent [23].

theorem itself holds in any “natural” gauge theory.

Now that oscillations are experimentally confirmed we know that there is a contribution to $\beta\beta_{0\nu}$ involving the exchange of light Majorana neutrinos, the “mass-mechanism”. The corresponding amplitude is sensitive both to the absolute scale of neutrino mass as well as the two Majorana CP phases that characterize the minimal 3-neutrino mixing matrix [7], none of which can be probed in oscillations.

Fig. 42 shows the estimated average mass parameter characterizing the neutrino exchange contribution to $\beta\beta_{0\nu}$ versus the lightest neutrino mass. The calculation takes into account the current neutrino oscillation parameters in [12] and latest nuclear matrix elements of [192] and compares with experimental sensitivities.

The most stringent lower bounds on the half-life of $\beta\beta_{0\nu}$ decay were obtained in the Heidelberg-Moscow ^{76}Ge [193] and CUORICINO ^{130}Te [194] experiments:

$$T_{1/2}^{0\nu}(^{76}\text{Ge}) \geq 1.9 \cdot 10^{25} \text{ years}, \quad T_{1/2}^{0\nu}(^{130}\text{Te}) \geq 1.8 \cdot 10^{24} \text{ years}. \quad (99)$$

Using recently calculated nuclear matrix elements with significantly reduced theoretical uncertainties [192] from these data the following upper bounds for the effective Majorana mass $m_{\beta\beta} \equiv \langle m_{\nu} \rangle$ can be

¹¹Such black-box theorem does *not* exist for the case of lepton flavour violation, which may proceed in the absence of neutrino mass [80].

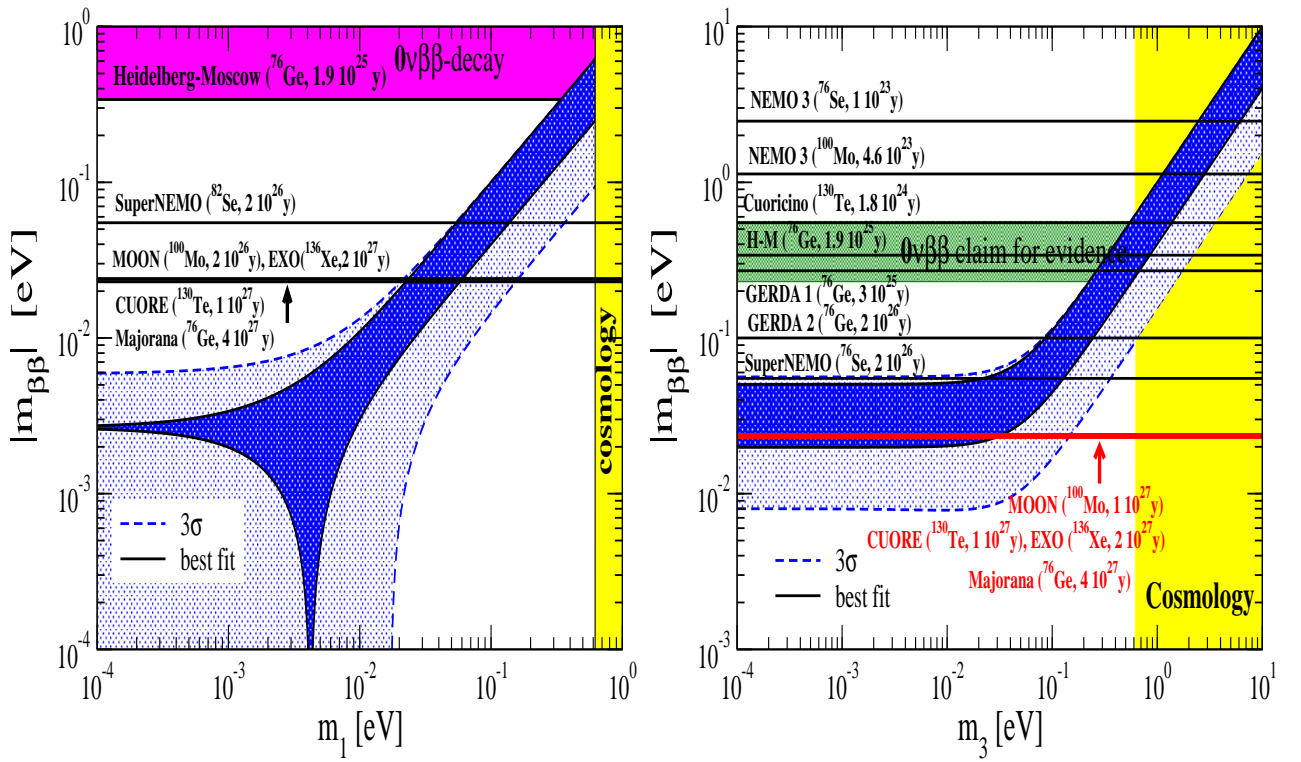


Figure 42: Neutrinoless double beta decay amplitude versus current oscillation data [192].

inferred

$$\begin{aligned}
 |m_{\beta\beta}| &\leq 0.34 \text{ eV} \quad (\text{Heidelberg} - \text{Moscow}) \\
 |m_{\beta\beta}| &\leq 0.55 \text{ eV} \quad (\text{CUORICINO}).
 \end{aligned}
 \tag{100}$$

The Heidelberg group, which includes a few authors of the Heidelberg-Moscow collaboration, recently claimed [199] evidence for the $\beta\beta_{0\nu}$ decay of ^{76}Ge with $T_{1/2}^{0\nu} = (0.69 - 4.18) \cdot 10^{25}$ years at the 4.2σ confidence level. Using the nuclear matrix element obtained in Ref. [192], from this data one finds for the effective Majorana mass the range $0.23 \text{ eV} \leq |m_{\beta\beta}| \leq 0.56 \text{ eV}$. Future experiments will extend the sensitivity of current $\beta\beta_{0\nu}$ searches and provide an independent check of this claim and even go further in sensitivity, as seen in the figure [201].

The left (right) panel in Fig. 42 corresponds to the cases of normal (inverted) neutrino mass spectra. In these plots the “diagonals” correspond to the case of quasi-degenerate neutrinos [70], which give the largest $\beta\beta_{0\nu}$ amplitude. In the normal hierarchy case there is in general no lower bound on the $\beta\beta_{0\nu}$ rate since there can be a destructive interference amongst the neutrino amplitudes. In contrast, the inverted neutrino mass hierarchy implies a “lower” bound for the $\beta\beta_{0\nu}$ amplitude.

A normal hierarchy model with a lower bound on $\beta\beta_{0\nu}$ is given in Ref. [132]. An interesting feature is that the lower bound obtained depends on the value of the Majorana violating phase ϕ_1 , as indicated in Fig. 43. Note that the lines in dark (red) and grey (green) of the left panel correspond to normal and inverse hierarchy, respectively. An alternative model based on the A_4 flavour symmetry has been suggested [133] which implies a lower bound on the neutrinoless double beta decay rate, corresponding

Table 2: Sensitivities of future $0\nu\beta\beta$ -decay experiments to the effective Majorana neutrino mass calculated with the RQRPA nuclear matrix elements $M^{0\nu}(A, Z)$ of Ref. [192]. For the axial coupling constant g_A the value $g_A = 1.25$ was assumed. $T_{1/2}^{0\nu-exp}$ is the maximal half-life, which can be reached in the experiment and $m_{\beta\beta} \equiv \langle m_\nu \rangle$ is the corresponding upper limit of the effective Majorana neutrino mass.

Nucleus	Experiment	Source	$T_{1/2}^{0\nu-exp}$ [yr]	Ref.	$M^{0\nu}(A, Z)$	$ m_{\beta\beta} $ [eV]
^{76}Ge	GERDA(I)	15 kg of ^{enr}Ge	$3 \cdot 10^{25}$	[200]	3.92	0.27
	GERDA(II)	100 kg of ^{enr}Ge	$2 \cdot 10^{26}$	[200]	3.92	0.10
	Majorana	0.5 t of ^{enr}Ge	$4 \cdot 10^{27}$	[195]	3.92	0.023
^{82}Se	SuperNEMO	100 kg of ^{enr}Se	$2 \cdot 10^{26}$	[196]	3.49	0.055
^{100}Mo	MOON	3.4 t of ^{nat}Mo	$1 \cdot 10^{27}$	[21]	2.78	0.024
^{116}Cd	CAMEO	1 t of CdWO_4 crystals	$\approx 10^{26}$	[21]	2.42	0.085
^{130}Te	CUORE	750 kg of TeO_2	$\approx 10^{27}$	[197]	2.95	0.023
^{136}Xe	XMASS	10 t of liq. Xe	$3 \cdot 10^{26}$	[21]	1.67	0.073
					1.97	0.024
	EXO	1 t ^{enr}Xe	$2 \cdot 10^{27}$	[198]	1.67	0.028

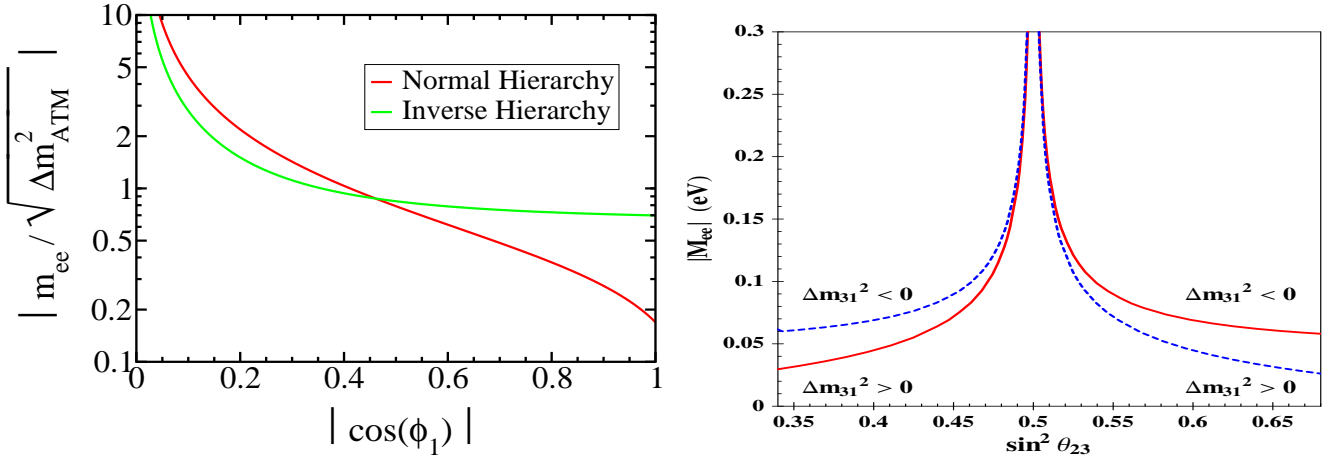


Figure 43: Lower bound on neutrinoless double beta decay in the models of Refs. [132] (left) and [133] (right). In first model the lower bound depends on the Majorana phase ϕ_1 , while in the second one has a strong dependence of the lower bound on the value of the atmospheric angle.

to an effective mass parameter $M_{ee} \gtrsim 0.03$ eV, as illustrated in the right panel of the same figure.

Complementary information on the absolute scale of neutrino mass is expected to come from future beta decays searches such as in the KATRIN experiment [202]. Altogether beta and $\beta\beta_{0\nu}$ sensitivities should be confronted with information coming from cosmology [68, 69].

9 Beyond neutrino oscillations

How robust is the current oscillation picture of neutrino data? For example, how well do we know the astrophysics of the Sun, neutrino propagation and/or neutrino detection to be confident that there are no loop holes in our understanding of neutrinos?

9.1 Solar magnetic fields

Here we give two examples of how solar magnetic fields can affect the neutrino oscillation interpretation of solar neutrino data.

9.1.1 Radiative zone magnetic fields and density noise

The Sun can harbor magnetic fields in its radiative zone as well as in its convective zone. It has been shown [218] that magnetic fields deep within the solar radiative zone can produce density fluctuations that could affect solar neutrino fluxes in an important way [219]. However it has been shown that consistency with KamLAND reactor data restores robustness of the determination of neutrino oscillation parameters [217].

9.1.2 Convective zone magnetic fields and spin flavour precession

Convective zone magnetic fields can lead to spin flavour precession if neutrinos have non-zero transition magnetic moments [28] that may affect neutrino propagation both in *vacuo* and in matter [220, 221]. A global analysis of spin-flavour precession (SFP) solutions to the solar neutrino problem is characterized by three effective parameters: $\Delta m_{\text{SOL}}^2 \equiv \Delta m^2$, the neutrino mixing angle $\theta_{\text{SOL}} \equiv \theta$ and the magnetic field parameter μB_{\perp} [222, 223]. For $\mu = 10^{-11}$ Bohr magneton, and an optimum self-consistent magneto-hydrodynamics magnetic field profile with maximum strength $B_{\perp} \sim 80$ KGauss in the convective zone [224] one finds an excellent description of the solar neutrino data in terms of spin flavor precession. However, after combining with data from the KamLAND reactor experiment, one finds that such solutions to the solar neutrino problem are ruled out, as they can not account for the deficit and spectral distortion observed at KamLAND.

9.1.3 Probing for neutrino magnetic moments

Even though by themselves Majorana neutrino transition moments can not provide an acceptable explanation of the solar plus KamLAND data, they can still be present at a sub-leading level and be studied using existing solar and reactor neutrino data. They would contribute to the neutrino–electron scattering cross section and hence alter the signal observed in Super-Kamiokande and at Borexino. In ref. [225] constraints were placed on the neutrino transition moments by using the solar neutrino data. It was found that all transition elements can be bounded at the same time. Furthermore, improved reactor data play a complementary role to the solar neutrino data in further improving the sensitivity,

which is currently at $2 \times 10^{-10} \mu_B$ at the 90% C.L. for the combined solar + reactor data. The upcoming Borexino experiment will improve the bounds from today's data by roughly one order of magnitude, thanks to the lower energy.

9.2 Non-standard neutrino interactions

It is hard to find a neutrino mass generation scheme that does not bring in dimension-6 non-standard neutrino interaction (NSI) terms. Such sub-weak strength εG_F operators are illustrated in Fig. 44. They can be of two types: flavour-changing (FC) and non-universal (NU) and may arise in several ways. One is from the non-trivial structure of charged and neutral current weak interactions characterizing the broad class of seesaw-type models [7]. If present, these interactions would in general bring additional

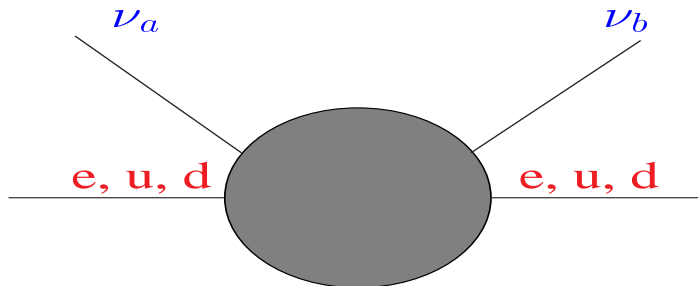


Figure 44: Flavour-changing effective operator for non-standard neutrino interaction.

sources of CP violation. While the expected magnitude of the non-standard interactions is rather model dependent, it may well fall in the range that can be tested in the precision neutrino oscillation studies discussed in Sec. 6. The first manifestation non-standard interactions can have is through the violation of unitarity in the lepton mixing matrix [7]. The non-unitary piece of the lepton mixing matrix can be sizable in inverse seesaw-type models [43] and hence can be phenomenologically important [80, 81, 82]. With neutrino physics entering the precision age it becomes an important challenge to scrutinize how good is the unitary approximation of the lepton mixing matrix in future experiments, given its theoretical fragility.

Relatively sizable NSI strengths may also be induced through the exchange of new scalar bosons, as present in models with radiatively induced neutrino masses. These typically contain new relatively light scalar states such as Higgs bosons [50], scalar leptoquarks, etc. NSI terms may also arise from renormalization group evolution in supersymmetric unified models [71].

Non-standard physics may affect neutrino production and detection cross sections, as well as propagation properties. In their presence, the Hamiltonian describing neutrino propagation has, in addition to the standard oscillation part, another term H_{NSI} ,

$$H_{\text{NSI}} = \pm \sqrt{2} G_F N_f \begin{pmatrix} 0 & \varepsilon \\ \varepsilon & \varepsilon' \end{pmatrix}. \quad (101)$$

Here $+$ ($-$) holds for neutrinos (anti-neutrinos) and ε and ε' parametrize the NSI: $\sqrt{2} G_F N_f \varepsilon$ is the forward scattering amplitude for the FC process $\nu_\mu + f \rightarrow \nu_\tau + f$ and $\sqrt{2} G_F N_f \varepsilon'$ represents the difference

between $\nu_\mu + f$ and $\nu_\tau + f$ elastic forward scattering. Here N_f is the number density of the fermion f along the neutrino path. A remarkable fact is that, in the presence of non-standard interactions resonant neutrino conversions can take place even in the absence of neutrino masses [203].

Solar neutrino oscillations

Although non-standard interaction effects may provide an alternative way to account for the current solar neutrino data [204], consistency with KamLAND reactor neutrino data requires them to be sub-leading [113]. However the oscillation interpretation of solar neutrino data is still “fragile” against the presence of non-standard interactions in the $e - \tau$ sector, opening another degenerate solution in the second octant of the solar mixing angle [205]. Indeed, as seen in Fig. 45, in the presence of NSI, there appear new solar neutrino oscillation solutions in addition to the standard one. The two degenerate solutions are denoted LMA-I or “normal” and LMA-D “degenerate or dark-side” solution. Although

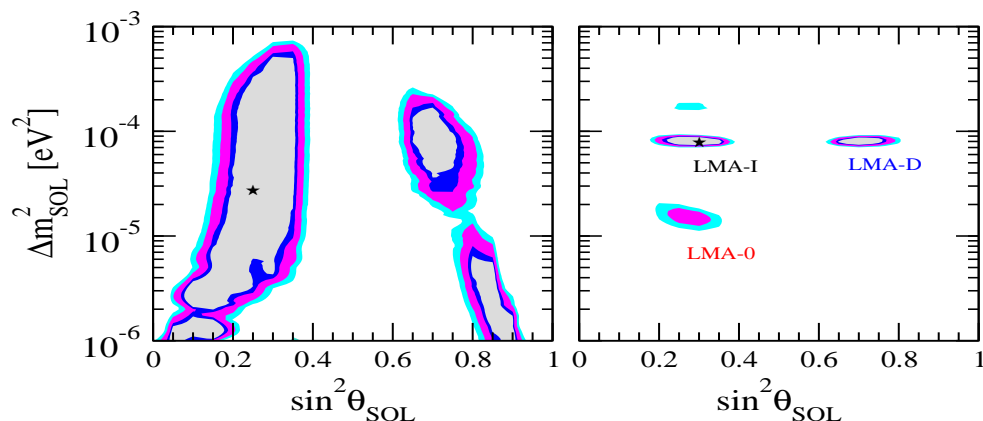


Figure 45: New solar neutrino oscillation solutions in the presence of NSI [205].

some ways of inducing the new LMA-D solution, for example via NSI between neutrinos and down-type-quarks-only, are already in conflict with the combination of current atmospheric data and accelerator neutrino oscillation data of the CHARM experiment, the general form of these solutions is not yet ruled out. Moreover, further precision KamLAND reactor measurements will not resolve the ambiguity in the determination of the solar neutrino mixing angle, since they are expected to constrain mainly Δm_{SOL}^2 .

However, as can be seen from Fig. 46, the “normal” LMA-I solutions have quite different predicted neutrino survival probabilities for low energy neutrinos (left panel) and boron neutrinos (right panel). Thus future precision low energy solar neutrino experiments will help in lifting the degeneracy between the “normal” and the new degenerate solution.

On the other hand, even if very small, non-standard interaction effects may play an important role in supernova astrophysics, opening the possibility of new resonances that could take place in the internal neutron-rich regime [206, 207, 208, 209].

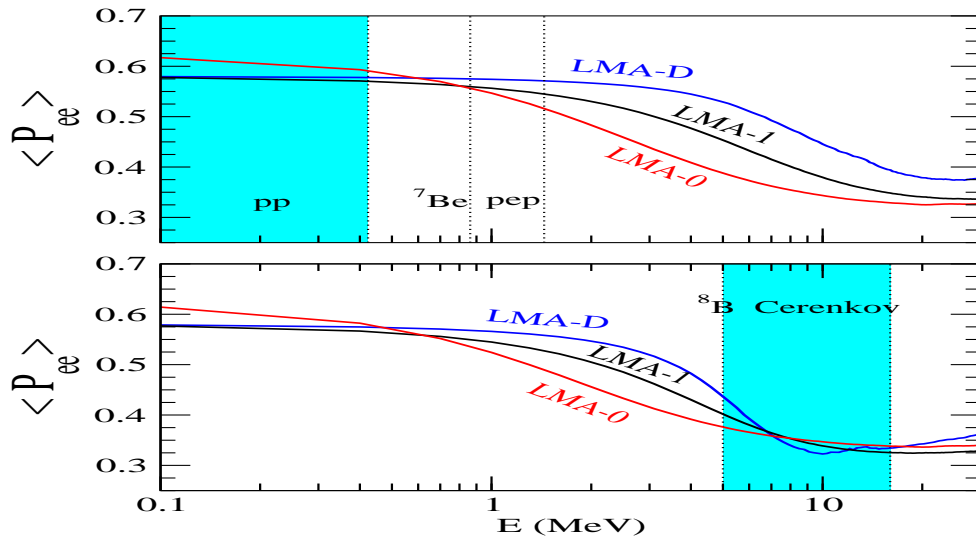


Figure 46: Probing for NSI in future low energy solar neutrino experiments [205].

Atmospheric neutrino oscillations

In contrast to the solar case, it has been shown [210] that, within the 2-neutrino approximation, the determination of atmospheric neutrino parameters Δm_{ATM}^2 and $\sin^2 \theta_{\text{ATM}}$ has been shown to be practically unaffected by the presence of NSI on down-type quarks ($f = d$). There are however loop-holes in the three neutrino case [211]. Let us also mention here that future neutrino factories will have good potential for probing non-standard neutrino in the mu-tau channel [212].

NSI-oscillation confusion theorem

For the coming generation of experiments we note that even a small residual non-standard interaction of neutrinos in the $e - \tau$ channel characterized by a parameter $\epsilon_{e\tau}$ can have dramatic consequences for the prospects of probing neutrino oscillations at neutrino factories. For example, it has been shown [213] that the presence of such NSI leads to a drastic loss in sensitivity in the θ_{13} determination at a neutrino factory. It is therefore important to improve the sensitivities on NSI, another window of opportunity for neutrino physics in the precision age.

10 Summary

We have reviewed the basic mechanisms to generate neutrino mass, analysing the corresponding structure of the lepton mixing matrix. After an overview of the status of neutrino oscillation parameters as determined from current data, we have focused on the next neutrino oscillation experiments using accelerator neutrinos, and discussed the prospects for probing the strength of CP violation in two of them, T2K and NO ν A. Intermediate term experiments using wide band beams and capable of probing

also the second Oscillation Maximum, such as T2KK, have also been discussed [182, 184, 185, 183].

Farther in the future are experiments with novel neutrino beams, such as neutrino factories and beta beams. One of the advantages of the neutrino beam coming from a muon storage ring is that the energy spectrum is accurately known, in contrast with conventional muon neutrino beam from pion decay, where the energy spectrum is not very well determined. It was suggested in [214] that pure ν_e or $\bar{\nu}_e$ beams can be obtained by using β unstable isotopes. The idea is to produce first a huge number of β unstable ions and then accelerate them in a storage ring to some reference energy, and let them to decay in the straight section of a storage ring in order to get an intense ν_e or $\bar{\nu}_e$ beam. The advantage of this method is that the energy spectrum is precisely known (as in the case of neutrino beam from muon decay) and there is no contamination of the other neutrino species unlike the case of neutrino beam from muon decay. None of these possibilities were considered here, but they are discussed in a recent review by Geer and Zisman in this same series [215] for neutrino factories, and e.g., in Ref. [216] for the case of beta beam. Another extensive review is being prepared for the International scoping study of a future Neutrino Factory and super-beam facility. We have also briefly commented on the possibility of probing CP violation effects induced by Majorana phases in neutrinoless double beta decay.

Acknowledgements

We thank Martin Hirsch, Filipe Joaquim, Stefano Morisi, Jorge Romão, Joe Schechter and M. Tortola for useful comments. We thank Fedor Simkovic for the updated results on nuclear matrix elements. This work has been supported by Spanish grants FPA2005-01269 and FPA2005-25348-E, by the European Commission RTN Contract MRTN-CT-2004-503369 and ILIAS/N6 Contract RII3-CT-2004-506222, and also by a Humboldt Research Award (JWFV). Fermilab is operated under DOE Contract No. DE-AC02-76CH03000.

References

- [1] M. Kobayashi and T. Maskawa, Prog. Theor. Phys. **49**, 652 (1973).
- [2] Super-Kamiokande collaboration, S. Fukuda *et al.*, Phys. Lett. **B539**, 179 (2002), [hep-ex/0205075].
- [3] SNO collaboration, Q. R. Ahmad *et al.*, Phys. Rev. Lett. **89**, 011301 (2002), [nucl-ex/0204008]; Phys. Rev. Lett. **89**, 011302 (2002), [nucl-ex/0204009].
- [4] KamLAND collaboration, T. Araki *et al.*, Phys. Rev. Lett. **94**, 081801 (2004).
- [5] For a review on atmospheric neutrinos see T. Kajita, New J. Phys. **6**, 194 (2004).
- [6] K2K collaboration, M. H. Ahn *et al.*, Phys. Rev. Lett. **90**, 041801 (2003), [hep-ex/0212007].

- [7] J. Schechter and J. W. F. Valle, Phys. Rev. **D22**, 2227 (1980).
- [8] J. Schechter and J. W. F. Valle, Phys. Rev. **D25**, 774 (1982).
- [9] BooNE collaboration, E. D. Zimmerman, eConf **C0209101**, TH05 (2002), [hep-ex/0211039].
- [10] LSND collaboration, A. Aguilar *et al.*, Phys. Rev. **D64**, 112007 (2001), [hep-ex/0104049].
- [11] The MiniBooNE collaboration, A. A. Aguilar-Arevalo *et al.*, arXiv:0704.1500 [hep-ex].
- [12] Global fits to neutrino oscillations are reviewed in M. Maltoni, T. Schwetz, M. A. Tortola and J. W. F. Valle, New J. Phys. **6**, 122 (2004); the latest update is given in version 6 of hep-ph/0405172; for previous works by other groups, e. g. Ref. [13] and references therein.
- [13] G. L. Fogli, E. Lisi, A. Marrone and A. Palazzo, Prog. Part. Nucl. Phys. **57** (2006) 742 [hep-ph/0506083].
- [14] CHOOZ collaboration, M. Apollonio *et al.*, Phys. Lett. **B466**, 415 (1999), [hep-ex/9907037].
- [15] Palo Verde collaboration, F. Boehm *et al.*, Phys. Rev. **D64**, 112001 (2001), [hep-ex/0107009].
- [16] J. N. Bahcall and M. H. Pinsonneault, Phys. Rev. Lett. **93**, 121301 (2004), [astro-ph/0402114].
- [17] M. Honda, T. Kajita, K. Kasahara and S. Midorikawa, astro-ph/0404457.
- [18] L. Wolfenstein, Phys. Rev. **D17**, 2369 (1978).
- [19] S. P. Mikheev and A. Y. Smirnov, Sov. J. Nucl. Phys. **42**, 913 (1985).
- [20] N. Cabibbo, Phys. Lett. **B72**, 333 (1978).
- [21] S. R. Elliott and P. Vogel, Ann. Rev. Nucl. Part. Sci. **52**, 115 (2002), [hep-ph/0202264]; S. R. Elliott, Nucl. Phys. Proc. Suppl. **138** (2005) 275 [nucl-ex/0312013].
- [22] M. Doi, T. Kotani and E. Takasugi, Prog. Theor. Phys. Suppl. **83**, 1 (1985).
- [23] J. Schechter and J. W. F. Valle, Phys. Rev. **D25**, 2951 (1982). For a recent extension of the black box theorem for lepton number and flavor violating processes see M. Hirsch, S. Kovalenko and I. Schmidt, Phys. Lett. B **642** (2006) 106 [hep-ph/0608207].
- [24] S. M. Bilenky, J. Hosek and S. T. Petcov, Phys. Lett. **B94**, 49 (1980).
- [25] J. Schechter and J. W. F. Valle, Phys. Rev. **D23**, 1666 (1981).
- [26] M. Doi, T. Kotani, H. Nishiura, K. Okuda and E. Takasugi, Phys. Lett. **B102**, 323 (1981).
- [27] A. de Gouvea, B. Kayser and R. N. Mohapatra, Phys. Rev. **D67**, 053004 (2003), [hep-ph/0211394].

- [28] J. Schechter and J. W. F. Valle, Phys. Rev. **D24**, 1883 (1981), Err. D25, 283 (1982).
- [29] J. W. F. Valle, Phys. Rev. **D27**, 1672 (1983).
- [30] J. W. F. Valle and M. Singer, Phys. Rev. **D28**, 540 (1983).
- [31] L. Wolfenstein, Nucl. Phys. **B186**, 147 (1981).
- [32] L. Wolfenstein, Phys. Lett. **B107**, 77 (1981).
- [33] S. Weinberg, Phys. Rev. **D22**, 1694 (1980).
- [34] K. R. Dienes, E. Dudas and T. Gherghetta, Nucl. Phys. **B557**, 25 (1999), [hep-ph/9811428].
- [35] N. Arkani-Hamed, S. Dimopoulos, G. R. Dvali and J. March-Russell, Phys. Rev. **D65**, 024032 (2002), [hep-ph/9811448].
- [36] A. Ioannisian and J. W. F. Valle, Phys. Rev. **D63**, 073002 (2001), [hep-ph/9911349].
- [37] Round table discussion and articles in Proc. of Int. Conf. on the Seesaw Mechanism and the Neutrino Mass, Paris, France, 10-11 June 2004. Edited by J. Orloff, S. Lavignac and M. Cribier.
- [38] For a recent overview on the seesaw see J. W. F. Valle, J. Phys. Conf. Ser. **53**, 473 (2006), [hep-ph/0608101], based on lectures given at the Corfu Summer Institute on Elementary Particle Physics in September 2005.
- [39] Y. Chikashige, R. N. Mohapatra and R. D. Peccei, Phys. Lett. **B98**, 265 (1981).
- [40] M. Lattanzi and J. W. F. Valle, arXiv:0705.2406 [astro-ph], Phys. Rev. Lett. in press
- [41] P. Minkowski, Phys. Lett. **B67**, 421 (1977).
- [42] G. Lazarides, Q. Shafi and C. Wetterich, Nucl. Phys. **B181**, 287 (1981).
- [43] R. N. Mohapatra and J. W. F. Valle, Phys. Rev. **D34**, 1642 (1986).
- [44] E. Witten, Nucl. Phys. **B258**, 75 (1985).
- [45] E. Akhmedov, M. Lindner, E. Schnapka and J. W. F. Valle, Phys. Rev. **D53**, 2752 (1996) and Phys. Lett. B **368** (1996) 270
- [46] S. M. Barr and I. Dorsner, Phys. Lett. **B632**, 527 (2006), [hep-ph/0507067].
- [47] T. Fukuyama, A. Ilakovac, T. Kikuchi and K. Matsuda, JHEP **06**, 016 (2005), [hep-ph/0503114].
- [48] M. Malinsky, J. C. Romao and J. W. F. Valle, Phys. Rev. Lett. **95**, 161801 (2005).
- [49] G. 't Hooft, Lecture given at Cargese Summer Inst., Cargese, France, Aug 26 - Sep 8, 1979.

- [50] A. Zee, Phys. Lett. **B93**, 389 (1980).
- [51] K. S. Babu, Phys. Lett. **B203**, 132 (1988).
- [52] J. T. Peltoniemi and J. W. F. Valle, Phys. Lett. **B304**, 147 (1993), [hep-ph/9301231].
- [53] M. Hirsch and J. W. F. Valle, New J. Phys. **6**, 76 (2004), [hep-ph/0405015].
- [54] A. Masiero and J. W. F. Valle, Phys. Lett. **B251**, 273 (1990).
- [55] J. C. Romao, C. A. Santos and J. W. F. Valle, Phys. Lett. **B288**, 311 (1992).
- [56] J. C. Romao, A. Ioannisian and J. W. F. Valle, Phys. Rev. **D55**, 427 (1997), [hep-ph/9607401].
- [57] M. A. Diaz, J. C. Romao and J. W. F. Valle, Nucl. Phys. **B524**, 23 (1998), [hep-ph/9706315].
- [58] M. Hirsch *et al.*, Phys. Rev. **D62**, 113008 (2000), [hep-ph/0004115], Err-ibid. **D65**:119901,2002.
- [59] M. C. Gonzalez-Garcia and J. W. F. Valle, Phys. Lett. **B216**, 360 (1989).
- [60] A. S. Joshipura and J. W. F. Valle, Nucl. Phys. **B397**, 105 (1993).
- [61] J. C. Romao, F. de Campos and J. W. F. Valle, Phys. Lett. **B292**, 329 (1992), [hep-ph/9207269].
- [62] M. Hirsch, J. C. Romao, J. W. F. Valle and A. Villanova del Moral, Phys. Rev. **D70**, 073012 (2004), [hep-ph/0407269]; Phys. Rev. **D73**, 055007 (2006), [hep-ph/0512257].
- [63] F. de Campos, O. J. P. Eboli, J. Rosiek and J. W. F. Valle, Phys. Rev. **D55**, 1316 (1997), [hep-ph/9601269].
- [64] DELPHI collaboration, J. Abdallah *et al.*, Eur. Phys. J. **C32**, 475 (2004), [hep-ex/0401022].
- [65] M. Kachelriess, R. Tomas and J. W. F. Valle, Phys. Rev. **D62**, 023004 (2000), [hep-ph/0001039].
- [66] KATRIN collaboration, G. Drexlin, Nucl. Phys. Proc. Suppl. **145**, 263 (2005).
- [67] S. S. Masood *et al.*, arXiv:0706.0897 [hep-ph], in press, Physical Review C.
- [68] J. Lesgourgues and S. Pastor, Phys. Rep. **429**, 307 (2006), [astro-ph/0603494].
- [69] S. Hannestad, Ann. Rev. Nucl. Part. Sci. **56**, 137 (2006), [hep-ph/0602058].
- [70] K. S. Babu, E. Ma and J. W. F. Valle, Phys. Lett. **B552**, 207 (2003), [hep-ph/0206292].
- [71] L. J. Hall, V. A. Kostelecky and S. Raby, Nucl. Phys. **B267**, 415 (1986).
- [72] F. Borzumati and A. Masiero, Phys. Rev. Lett. **57**, 961 (1986).
- [73] J. Hisano and K. Tobe, Phys. Lett. **B510**, 197 (2001), [hep-ph/0102315].

- [74] J. A. Casas and A. Ibarra, Nucl. Phys. **B618**, 171 (2001), [hep-ph/0103065].
- [75] S. Antusch, E. Arganda, M. J. Herrero and A. M. Teixeira, JHEP **11**, 090 (2006).
- [76] L. Calibbi, A. Faccia, A. Masiero and S. K. Vempati, Phys. Rev. D **74** (2006) 116002 [hep-ph/0605139].
- [77] F. R. Joaquim and A. Rossi, Phys. Rev. Lett. **97**, 181801 (2006), [hep-ph/0604083]; Nucl. Phys. **B765**, 71 (2007), [hep-ph/0607298].
- [78] F. Deppisch and J. W. F. Valle, Phys. Rev. **D72**, 036001 (2005), [hep-ph/0406040].
- [79] F. Deppisch, T. S. Kosmas and J. W. F. Valle, Nucl. Phys. **B752**, 80 (2006), [hep-ph/0512360].
- [80] J. Bernabeu *et al.*, Phys. Lett. **B187**, 303 (1987).
- [81] G. C. Branco, M. N. Rebelo and J. W. F. Valle, Phys. Lett. **B225**, 385 (1989).
- [82] N. Rius and J. W. F. Valle, Phys. Lett. **B246**, 249 (1990).
- [83] M. C. Gonzalez-Garcia and J. W. F. Valle, Mod. Phys. Lett. **A7**, 477 (1992).
- [84] A. Ilakovac and A. Pilaftsis, Nucl. Phys. **B437**, 491 (1995), [hep-ph/9403398].
- [85] Y. Kuno, AIP Conf. Proc. **542**, 220 (2000).
- [86] M. Dittmar *et al.*, Nucl. Phys. **B332**, 1 (1990).
- [87] DELPHI collaboration, P. Abreu *et al.*, Z. Phys. **C74**, 57 (1997).
- [88] W. Porod, M. Hirsch, J. Romao and J. W. F. Valle, Phys. Rev. **D63**, 115004 (2001), [hep-ph/0011248].
- [89] J. C. Romao *et al.*, Phys. Rev. **D61**, 071703 (2000), [hep-ph/9907499].
- [90] B. Mukhopadhyaya, S. Roy and F. Vissani, Phys. Lett. **B443**, 191 (1998), [hep-ph/9808265].
- [91] J. W. F. Valle, Phys. Lett. **B131**, 87 (1983).
- [92] G. B. Gelmini and J. W. F. Valle, Phys. Lett. **B142**, 181 (1984).
- [93] Particle Data Group, W. M. Yao *et al.*, J. Phys. **G33**, 1 (2006).
- [94] S. S. Masood, S. Nasri and J. Schechter, Phys. Rev. **D71**, 093005 (2005), [hep-ph/0412401].
- [95] M. Fukugita and T. Yanagida, Phys. Lett. **B174**, 45 (1986).
- [96] For a review see W. Buchmuller, R. D. Peccei and T. Yanagida, Ann. Rev. Nucl. Part. Sci. **55**, 311 (2005), [hep-ph/0502169].

- [97] V. A. Kuzmin, V. A. Rubakov and M. E. Shaposhnikov, Phys. Lett. **B155**, 36 (1985).
- [98] M. Kawasaki, K. Kohri and T. Moroi, Phys. Rev. **D71**, 083502 (2005), [astro-ph/0408426].
- [99] W. Buchmuller, P. Di Bari and M. Plumacher, hep-ph/0401240.
- [100] A. Pilaftsis and T. E. J. Underwood, Nucl. Phys. B **692** (2004) 303 [hep-ph/0309342].
- [101] M. Hirsch, J. W. F. Valle, M. Malinsky, J. C. Romao and U. Sarkar, Phys. Rev. **D75**, 011701 (2007), [hep-ph/0608006].
- [102] J. C. Romao, M. A. Tortola, M. Hirsch and J. W. F. Valle, arXiv:0707.2942 [hep-ph].
- [103] Y. Farzan and J. W. F. Valle, Phys. Rev. Lett. **96**, 011601 (2006), [hep-ph/0509280].
- [104] E. Ma and U. Sarkar, Phys. Rev. Lett. **80**, 5716 (1998).
- [105] G. D'Ambrosio, T. Hambye, A. Hektor, M. Raidal and A. Rossi, Phys. Lett. **B604**, 199 (2004), [hep-ph/0407312].
- [106] C. Giunti and M. Laveder, hep-ph/0310238.
- [107] H. Nunokawa, V. B. Semikoz, A. Y. Smirnov and J. W. F. Valle, Nucl. Phys. **B501**, 17 (1997), [hep-ph/9701420].
- [108] SNO collaboration, B. Aharmim *et al.*, Phys. Rev. **C72**, 055502 (2005), [nucl-ex/0502021].
- [109] KamLAND collaboration, K. Eguchi *et al.*, Phys. Rev. Lett. **90**, 021802 (2003), [hep-ex/0212021].
- [110] Talk given by I. Shimizu at the 10th International Conference on Topics in Astroparticle and Underground Physics, TAUP 2007.
- [111] M. Maltoni, T. Schwetz, M. A. Tortola and J. W. F. Valle, Phys. Rev. **D68**, 113010 (2003), [hep-ph/0309130].
- [112] For analysis of first KamLAND date see, e. g. M. Maltoni, T. Schwetz and J. W. F. Valle, Phys. Rev. D **67** (2003) 093003 hep-ph/0212129]; A. Bandyopadhyay, S. Choubey, R. Gandhi, S. Goswami and D. P. Roy, Phys. Lett. B **559** (2003) 121 [hep-ph/0212146].
- [113] For a review on the impact of KamLAND on the determination of neutrino properties see S. Pakvasa and J. W. F. Valle, hep-ph/0301061, Proc. of the Indian National Acad. of Sciences on Neutrinos, Vol. 70A, No.1, p.189 - 222 (2004), Eds. D. Indumathi, M. Murthy and G. Rajasekaran.
- [114] Borexino Collaboration, C. Arpesella *et al.*, arXiv:0708.2251 [astro-ph].
- [115] M. C. Gonzalez-Garcia *et al.*, Phys. Rev. Lett. **82**, 3202 (1999), [hep-ph/9809531].

- [116] T. Nakaya, Neutrino 2004 proceedings, neutrino.kek.jp/news/2004.06.10/index-e.html.
- [117] MINOS collaboration, N. Tagg, [hep-ex/0605058 http://www-numi.fnal.gov/talks/results06.html](http://www-numi.fnal.gov/talks/results06.html).
- [118] MINOS Collaboration, arXiv:0708.1495 [hep-ex].
- [119] K2K collaboration, M. H. Ahn, hep-ex/0606032.
- [120] M. Raidal, Phys. Rev. Lett. **93**, 161801 (2004), [hep-ph/0404046].
- [121] H. Minakata and A. Y. Smirnov, Phys. Rev. **D70**, 073009 (2004), [hep-ph/0405088].
- [122] J. Ferrandis and S. Pakvasa, Phys. Rev. **D71**, 033004 (2005), [hep-ph/0412038].
- [123] A. Dighe, S. Goswami and P. Roy, Phys. Rev. **D73**, 071301 (2006), [hep-ph/0602062].
- [124] C. S. Lam, Phys. Lett. B **507** (2001) 214 [hep-ph/0104116];
- [125] W. Grimus, S. Kaneko, L. Lavoura, H. Sawanaka and M. Tanimoto, JHEP **0601** (2006) 110.
- [126] W. Grimus, A. S. Joshipura, S. Kaneko, L. Lavoura, H. Sawanaka and M. Tanimoto, Nucl. Phys. B **713** (2005) 151 [hep-ph/0408123].
- [127] P. F. Harrison and W. G. Scott, Phys. Lett. **B535**, 163 (2002), [hep-ph/0203209].
- [128] P. F. Harrison, D. H. Perkins and W. G. Scott, Phys. Lett. **B530**, 167 (2002), [hep-ph/0202074].
- [129] P. Chankowski, A. Ioannisian, S. Pokorski and J. W. F. Valle, Phys. Rev. Lett. **86**, 3488 (2001).
- [130] U. Amaldi, W. de Boer and H. Furstenau, Phys. Lett. **B260**, 447 (1991).
- [131] W. Grimus and L. Lavoura, Phys. Lett. **B579**, 113 (2004), [hep-ph/0305309].
- [132] M. Hirsch, A. Villanova del Moral, J. W. F. Valle and E. Ma, Phys. Rev. **D72**, 091301 (2005), [hep-ph/0507148].
- [133] M. Hirsch, A. S. Joshipura, S. Kaneko and J. W. F. Valle, hep-ph/0703046, in press, Physical Review Letters.
- [134] A. Zee, Phys. Lett. B **630** (2005) 58 [hep-ph/0508278].
- [135] W. Grimus, A. S. Joshipura, S. Kaneko, L. Lavoura and M. Tanimoto, JHEP **0407** (2004) 078 [hep-ph/0407112]; W. Grimus and L. Lavoura, JHEP **0508** (2005) 013 [hep-ph/0504153]; R. N. Mohapatra, S. Nasri and H. B. Yu, Phys. Lett. B **639** (2006) 318 [hep-ph/0605020].
- [136] C. Luhn, S. Nasri and P. Ramond, arXiv:0706.2341 [hep-ph]; I. de Medeiros Varzielas, S. F. King and G. G. Ross, Phys. Lett. B **648** (2007) 201 [hep-ph/0607045] E. Ma, Mod. Phys. Lett. A **21** (2006) 1917 [hep-ph/0607056]; F. Feruglio, C. Hagedorn, Y. Lin and L. Merlo, Nucl. Phys. B **775** (2007) 120 [hep-ph/0702194]

- [137] P. D. Carr and P. H. Frampton, hep-ph/0701034; P. H. Frampton and T. W. Kephart, arXiv:0706.1186 [hep-ph]; M.-C. Chen and K. T. Mahanthappa, arXiv:0705.0714 [hep-ph]; A. Aranda arXiv:0707.3661 [hep-ph]
- [138] S. Luo and Z. z. Xing, Phys. Lett. B **632** (2006) 341 [hep-ph/0509065]; F. Plentinger and W. Rodejohann, Phys. Lett. B **625** (2005) 264 [hep-ph/0507143]; M. Hirsch, E. Ma, J. C. Romao, J. W. F. Valle and A. Villanova del Moral, Phys. Rev. D **75** (2007) 053006 [hep-ph/0606082].
- [139] G. Altarelli and F. Feruglio, Nucl. Phys. **B720**, 64 (2005), [hep-ph/0504165].
- [140] For a recent review on neutrino models see G. Altarelli and F. Feruglio, New J. Phys. **6**, 106 (2004), [hep-ph/0405048].
- [141] V. A. Kostelecky and M. Mewes, Phys. Rev. **D69**, 016005 (2004), [hep-ph/0309025].
- [142] M. C. Gonzalez-Garcia, M. Maltoni and T. Schwetz, Phys. Rev. **D68**, 053007 (2003), [hep-ph/0306226].
- [143] V. D. Barger, K. Whisnant and R. J. N. Phillips, Phys. Rev. Lett. **45**, 2084 (1980).
- [144] S. Pakvasa, AIP Conf. Proc. **68**, 1164 (1980).
- [145] C. Jarlskog, Phys. Rev. Lett. **55**, 1039 (1985).
- [146] J. Arafune and J. Sato, Phys. Rev. **D55**, 1653 (1997), [hep-ph/9607437].
- [147] M. Tanimoto, Phys. Rev. **D55**, 322 (1997), [hep-ph/9605413].
- [148] M. Tanimoto, Prog. Theor. Phys. **97**, 901 (1997), [hep-ph/9612444].
- [149] J. Arafune, M. Koike and J. Sato, Phys. Rev. **D56**, 3093 (1997), [hep-ph/9703351].
- [150] H. Minakata and H. Nunokawa, Phys. Rev. **D57**, 4403 (1998), [hep-ph/9705208].
- [151] H. Minakata and H. Nunokawa, Phys. Lett. **B413**, 369 (1997), [hep-ph/9706281].
- [152] S. M. Bilenky, C. Giunti and W. Grimus, Phys. Rev. **D58**, 033001 (1998), [hep-ph/9712537].
- [153] T.-K. Kuo and J. T. Pantaleone, Phys. Lett. **B198**, 406 (1987).
- [154] P. I. Krastev and S. T. Petcov, Phys. Lett. **B205**, 84 (1988).
- [155] H. Minakata and H. Nunokawa, Phys. Lett. **B495**, 369 (2000), [hep-ph/0004114].
- [156] A. Donini, M. B. Gavela, P. Hernandez and S. Rigolin, Nucl. Phys. **B574**, 23 (2000), [hep-ph/9909254].
- [157] A. Romanino, Nucl. Phys. **B574**, 675 (2000), [hep-ph/9909425].

- [158] J. T. Peltoniemi and J. W. F. Valle, Nucl. Phys. **B406**, 409 (1993), [hep-ph/9302316].
- [159] J. T. Peltoniemi, D. Tommasini and J. W. F. Valle, Phys. Lett. **B298**, 383 (1993).
- [160] D. O. Caldwell and R. N. Mohapatra, Phys. Rev. **D48**, 3259 (1993).
- [161] O. Mena and S. J. Parke, Phys. Rev. **D69**, 117301 (2004), [hep-ph/0312131].
- [162] H. Nunokawa, S. J. Parke and R. Zukanovich Funchal, Phys. Rev. **D72**, 013009 (2005).
- [163] P. F. Harrison and W. G. Scott, Phys. Lett. **B476**, 349 (2000), [hep-ph/9912435].
- [164] A. Cervera *et al.*, Nucl. Phys. **B579**, 17 (2000), [hep-ph/0002108].
- [165] O. Mena and S. J. Parke, Phys. Rev. **D72**, 053003 (2005), [hep-ph/0505202].
- [166] H. Minakata, H. Nunokawa and S. J. Parke, Phys. Lett. **B537**, 249 (2002), [hep-ph/0204171].
- [167] M. Blom and H. Minakata, New J. Phys. **6**, 130 (2004), [hep-ph/0404142].
- [168] A. M. Dziewonski and D. L. Anderson, Phys. Earth Planet. Interiors **25**, 297 (1981).
- [169] P. Huber and W. Winter, Phys. Rev. **D68**, 037301 (2003), [hep-ph/0301257].
- [170] A. Y. Smirnov, hep-ph/0610198.
- [171] Y. Itow *et al.*, hep-ex/0106019.
- [172] NOvA collaboration, D. S. Ayres *et al.*, hep-ex/0503053.
- [173] NOvA collaboration, D. Ayres *et al.*, hep-ex/0210005.
- [174] T. Schwetz, Phys. Scripta **T127**, 1 (2006), [hep-ph/0606060].
- [175] H. Minakata and H. Nunokawa, JHEP **10**, 001 (2001), [hep-ph/0108085].
- [176] K. Kimura, A. Takamura and H. Yokomakura, Phys. Lett. **B537**, 86 (2002), [hep-ph/0203099].
- [177] J. Burguet-Castell, M. B. Gavela, J. J. Gomez-Cadenas, P. Hernandez and O. Mena, Nucl. Phys. **B608**, 301 (2001), [hep-ph/0103258].
- [178] O. Mena and S. J. Parke, Phys. Rev. **D70**, 093011 (2004), [hep-ph/0408070].
- [179] G. L. Fogli and E. Lisi, Phys. Rev. **D54**, 3667 (1996), [hep-ph/9604415].
- [180] V. Barger, D. Marfatia and K. Whisnant, Phys. Rev. **D65**, 073023 (2002), [hep-ph/0112119].
- [181] W. J. Marciano, hep-ph/0108181.
- [182] M. Ishitsuka, T. Kajita, H. Minakata and H. Nunokawa, Phys. Rev. **D72**, 033003 (2005).

- [183] T. Kajita, H. Minakata, S. Nakayama and H. Nunokawa, hep-ph/0609286.
- [184] K. Hagiwara, N. Okamura and K.-i. Senda, Phys. Lett. **B637**, 266 (2006), [hep-ph/0504061].
- [185] K. Hagiwara, N. Okamura and K.-i. Senda, hep-ph/0607255.
- [186] V. Barger *et al.*, arXiv:0705.4396 [hep-ph].
- [187] M. V. Diwan *et al.*, Phys. Rev. **D68**, 012002 (2003), [hep-ph/0303081].
- [188] P. B. Pal and L. Wolfenstein, Phys. Rev. **D25**, 766 (1982).
- [189] B. Kayser, Phys. Rev. **D26**, 1662 (1982).
- [190] K. Enqvist, K. Kainulainen and M. J. Thomson, Nucl. Phys. **B373**, 498 (1992).
- [191] For a review see A. D. Dolgov, Phys. Rept. **370**, 333 (2002), [hep-ph/0202122].
- [192] V. A. Rodin, A. Faessler, F. Simkovic and P. Vogel, Nucl. Phys. **A766**, 107 (2006); Erratum in arXiv:0706.4304
- [193] L. Baudis *et. al.*, Phys. Rev. Lett. **83** (1999) 41 [hep-ex/9902014].
- [194] C. Arnaboldi *et. al.*, Phys. Rev. Lett. **95** (2005) 142501 [hep-ex/0501034]; Phys. Lett. B **584** (2004) 260; S.Capelli on behalf of CUORE Collaboration, hep-ex/0505045v1
- [195] C. E. Aalseth *et. al.* [Majorana Collaboration], Nucl. Phys. Proc. Suppl. **138** (2005) 217.
- [196] A. S. Barabash, Phys. Atom. Nucl. **67** (2004) 438 [Yad. Fiz. **67** (2004) 458].
- [197] A. Giuliani, Nucl. Phys. Proc. Suppl. **138** (2005) 267.
- [198] M. Danilov *et. al.*, Phys. Lett. B **480** (2000) 12, S. Gratta, SAGANET meeting, April 2004
- [199] H. V. Klapdor-Kleingrothaus, I. V. Krivosheina, A. Dietz and O. Chkvorets, Phys. Lett. **B586**, 198 (2004), [hep-ph/0404088].
- [200] GERDA collaboration I. Abt *et. al.*, hep-ex/0404039.
- [201] For additional discussion on prospects for $\beta\beta_{0\nu}$ experiments see talks at DBD06 - ILIAS/N6 WG1 Collaboration meeting, April, 2006, accessible from <http://ahep.uv.es/dbd06/index.php> and at the Joint Annual Meeting of N4 IDEA and N6/WP1 ENTApP, accessible from <http://www.uni-tuebingen.de/ilias-dbd/PMN07/>
- [202] KATRIN collaboration, A. Osipowicz *et al.*, hep-ex/0109033.
- [203] J. W. F. Valle, Phys. Lett. **B199**, 432 (1987).

- [204] M. Guzzo *et al.*, Nucl. Phys. **B629**, 479 (2002), [hep-ph/0112310 v3 KamLAND-updated version].
- [205] O. G. Miranda, M. A. Tortola and J. W. F. Valle, JHEP **10**, 008 (2006), [hep-ph/0406280].
- [206] H. Nunokawa, Y. Z. Qian, A. Rossi and J. W. F. Valle, Phys. Rev. **D54**, 4356 (1996), [hep-ph/9605301].
- [207] H. Nunokawa, A. Rossi and J. W. F. Valle, Nucl. Phys. **B482**, 481 (1996), [hep-ph/9606445].
- [208] D. Grasso, H. Nunokawa and J. W. F. Valle, Phys. Rev. Lett. **81**, 2412 (1998), [astro-ph/9803002].
- [209] A. Esteban-Pretel, R. Tomas and J. W. F. Valle, Phys. Rev. D **76** (2007) 053001 [arXiv:0704.0032 [hep-ph]].
- [210] N. Fornengo *et al.*, Phys. Rev. **D65**, 013010 (2002), [hep-ph/0108043].
- [211] A. Friedland, C. Lunardini and M. Maltoni, Phys. Rev. **D70**, 111301 (2004), [hep-ph/0408264].
- [212] P. Huber and J. W. F. Valle, Phys. Lett. **B523**, 151 (2001), [hep-ph/0108193].
- [213] P. Huber, T. Schwetz and J. W. F. Valle, Phys. Rev. Lett. **88**, 101804 (2002) [hep-ph/0111224]; Phys. Rev. **D66**, 013006 (2002), [hep-ph/0202048].
- [214] P. Zucchelli, Phys. Lett. **B532**, 166 (2002).
- [215] S. Geer and M. S. Zisman, FERMILAB-PUB-06-454-E.
- [216] J. Burguet-Castell, D. Casper, E. Couce, J. J. Gomez-Cadenas and P. Hernandez, Nucl. Phys. **B725**, 306 (2005), [hep-ph/0503021].
- [217] C. P. Burgess, *et. al.* JCAP **0401** (2004) 007 [hep-ph/0310366].
- [218] C. P. Burgess, *et. al.* Mon. Not. Roy. Astron. Soc. **348** (2004) 609 [astro-ph/0304462].
- [219] C. Burgess, *et. al.* Astrophys. J. **588** (2003) L65 [hep-ph/0209094].
- [220] C. S. Lim and W. J. Marciano, Phys. Rev. D **37**, 1368 (1988).
- [221] E. K. Akhmedov, Phys. Lett. B **213** (1988) 64.
- [222] O. G. Miranda *et. al.* Nucl. Phys. **B595**, 360 (2001), [hep-ph/0005259].
- [223] O. G. Miranda, *et. al.* Phys. Lett. **B521**, 299 (2001), [hep-ph/0108145].
- [224] J. Barranco, *et. al.* Phys. Rev. **D66**, 093009 (2002), KamLAND-update at hep-ph/0207326 v3
- [225] W. Grimus, *et. al.* Nucl. Phys. B **648** (2003) 376 [hep-ph/0208132].